A STUDY ON ENERGY TRAPPING PARAMETERS OF A MULTISTABLE ELASTIC BEAM

A THESIS SUBMITTED TO
THE GRADUATE SCHOOL OF NATURAL AND APPLIED SCIENCES
OF
MIDDLE EAST TECHNICAL UNIVERSITY

BY

AHMET ZEMBİLÖREN

IN PARTIAL FULFILLMENT OF THE REQUIREMENTS
FOR
THE DEGREE OF MASTER OF SCIENCE
IN
AEROSPACE ENGINEERING

FEBRUARY 2018

Approval of the thesis:

A STUDY ON ENERGY TRAPPING PARAMETERS OF A MULTISTABLE ELASTIC BEAM

submitted by **AHMET ZEMBİLÖREN** in partial fulfillment of the requirements for the degree of **Master of Science in Aerospace Engineering Department, Middle East Technical University** by,

Prof. Dr. Gülbin Dural Ünver
Dean, Graduate School of **Natural and Applied Sciences** _____

Prof. Dr. Ozan Tekinalp
Head of Department, **Aerospace Engineering** _____

Assoc. Prof. Dr. Ercan Gürses
Supervisor, **Aerospace Engineering Department, METU** _____

Examining Committee Members:

Prof. Dr. Altan KAYRAN
Aerospace Engineering, METU _____

Assoc. Prof. Dr. Ercan GÜRSES
Aerospace Engineering, METU _____

Assist. Prof. Dr. Tuncay YALÇINKAYA
Aerospace Engineering, METU _____

Assist. Prof. Dr. Mustafa PERÇİN
Aerospace Engineering, METU _____

Assoc. Prof. Dr. Cihan TEKOĞLU
Mechanical Engineering, TOBB Economy&Tech. University _____

Date: February 2, 2018

I hereby declare that all information in this document has been obtained and presented in accordance with academic rules and ethical conduct. I also declare that, as required by these rules and conduct, I have fully cited and referenced all material and results that are not original to this work.

Name, Last Name: AHMET ZEMBİLÖREN

Signature :

ABSTRACT

A STUDY ON ENERGY TRAPPING PARAMETERS OF A MULTISTABLE ELASTIC BEAM

ZEMBİLÖREN, Ahmet
M.S., Department of Aerospace Engineering
Supervisor : Assoc. Prof. Dr. Ercan Gürses

February 2018, 94 pages

Energy absorbing systems are being widely used in personnel protection, packaging of special products, aircraft and land vehicles and in many other industries as impact absorbers. Conventional energy absorbing systems absorb impact energy usually by undergoing plastic deformation and thus cannot be reused. A multistable elastic tilted beam can lock in (trap) strain energy when exposed to an impact and can fully recover after unloading. This fully reversible cycle allows repetitive usage of the system for many times. In this study, factors effecting energy-trapping capacity of an elastic tilted beam are determined by using finite element method (FEM). A 2D planar beam is modeled with the commercial finite element program ABAQUS. Geometrical and topological parameters defining the model are varied and many finite element runs are conducted to determine the energy trapping capacity of the beam while keeping the volume of the beam constant. Optimum beam dimensions, tilt angle and geometry are found. The objective of this study is to determine the parameters of the tilted beam yielding to the maximum energy trapping while using the same amount of material.

Keywords: Energy Trapping Systems, Beams, Elastic Deformation, Multistable Structures, Finite Element Method

ÖZ

BİRDEN FAZLA KARARLI HALE SAHİP ELASTİK BİR KİRİŞİN ENERJİ TUZAKLAMA MİKTARINI ETKİLEYEN PARAMETRELERİN BELİRLENMESİ

ZEMBİLÖREN, Ahmet
Yüksek Lisans, Havacılık ve Uzay Mühendisliği Bölümü
Tez Yöneticisi : Doç. Dr. Ercan Gürses

Şubat 2018 , 94 sayfa

Enerji emici sistemler kişisel korumada, özel ürünlerin ambalajlanmasında, uçak ve kara araçlarında ve diğer birçok endüstride darbe emici olarak yaygın şekilde kullanılmaktadır. Geleneksel enerji emici sistemler kalıcı şekil değiştirmeye maruz kalarak darbe enerjisini emer ve bu nedenle tekrar kullanılamazlar. Birden fazla kararlı hale sahip, eğimli pozisyonda bulunan elastik bir kiriş, darbeye maruz kaldığında gerinim enerjisini hapsedebilir (tuzaklayabilir) ve boşaltma işlemi sırasında tuzaklanan enerjinin hepsini geri verebilir. Bu tamamen çevrilebilir döngü, sistemin sürekli olarak birçok kez kullanılmasını sağlar. Bu çalışmada, eğimli pozisyonda bulunan elastik bir kirişin enerji tuzaklama miktarını etkileyen faktörler sonlu elemanlar yöntemi kullanılarak belirlenmiştir. İki boyutlu düzlemsel bir kiriş ticari sonlu elemanlar analiz programı ABAQUS ile modellenmiştir. Modeli tanımlayan geometrik ve topolojik değişkenler çalışılmış ve kirişin hacmini sabit tutarak enerji tuzaklama miktarını belirlemek için birçok sonlu elemanlar analizleri yapılmıştır. Yapılan sonlu elemanlar analizleri sonucunda kirişin en uygun boyutları, eğim açısı ve geometrisi bulunmuştur. Bu çalışmanın amacı, kullanılan malzeme miktarı sabit tutulduğunda eğimli kirişin maksimum enerji tuzaklamasını sağlayan değişkenleri belirlemektir.

Anahtar Kelimeler: Enerji Tuzaklayan Sistemler, Kirişler, Elastik Şekil Değiştirme, Birden Fazla Kararlı Hale Sahip Yapılar, Sonlu Elemanlar Yöntemi

To My Father, Mother and Sister...

ACKNOWLEDGMENTS

I express my deepest gratitude to my supervisor, Assoc. Prof. Dr. Ercan GÜRSES for his guidance and invaluable feedback in any time and any circumstances during my thesis research. This thesis would not have been possible without helps of him. I also thank to Prof. Dr. Yavuz YAMAN and my bachelor degree supervisor Prof. Dr. Aydın DOĞAN for their help and guidance.

I would like to thank to my dear friend Erdem ÜNAL for his motivation during my thesis. I thank to Mehran GHASABEH for his help at the beginning of the finite element analyses. I thank to our neighbour Bülent DERELİ for his guidance. I also thank to my all friends who contributed the completion of my thesis.

I want to give special thanks to my dearest Elif Ecem COŞKUN for her support and love.

Above all, I would like to thank my family members for their endless love, encouragements and support for my whole life.

TABLE OF CONTENTS

ABSTRACT v

ÖZ vi

ACKNOWLEDGMENTS ix

TABLE OF CONTENTS x

LIST OF TABLES xiv

LIST OF FIGURES xv

LIST OF ABBREVIATIONS xx

CHAPTERS

1 INTRODUCTION 1

1.1 Motivation of the Thesis 1

1.2 Objective of the Thesis 2

1.3 Literature Review 3

1.3.1 Energy Absorbing Structures 3

1.3.2 Energy Trapping Structures 3

1.4 Organization of the Thesis 8

2 FINITE ELEMENT MODELING OF INCLINED STRAIGHT ENERGY TRAPPING BEAMS 11

2.1 Problem Definition 12

2.1.1 Geometry 12

2.1.2 Material Properties 13

2.1.3 Finite Element Model 14

2.1.4 Boundary Conditions 15

2.1.5 Effects of *Element Type*, *Procedure Type*, *Mesh Size* and *Initial Increment Size* on Mechanical Response of the Reference Beam 17

2.1.6 Energy Calculation Method 20
2.2 Tilt Angle Study 23
2.3 Straight Beam Aspect Ratio Study 27
2.4 Energy Trapping Capacity of Two Reference Beams 30
3 FINITE ELEMENT MODELING OF INCLINED CURVED ENERGY TRAPPING BEAMS 33
3.1 Problem Definition 33
3.1.1 Geometry 34
3.1.2 Material Properties 35
3.1.3 Finite Element Model 35
3.1.4 Boundary Conditions 36
3.2 Morphological Study 36
3.3 Tilt Angle Study 40
3.4 Curved Beam Aspect Ratio Study 44
4 CONCLUSION 49
REFERENCES 53
APPENDICES
A DEFORMED AND UNDEFORMED SHAPES OF STRAIGHT BEAMS RELATED TO ANGLE STUDY 55
A.1 Images Taken from Analysis of the Straight Beam Having Tilt Angle 30° 55
A.2 Images Taken from Analysis of the Straight Beam Having Tilt Angle 35° 56
A.3 Images Taken from Analysis of the Straight Beam Having Tilt Angle 40° (The Reference Beam) 57
A.4 Images Taken from Analysis of the Straight Beam Having Tilt Angle 45° 58
A.5 Images Taken from Analysis of the Straight Beam Having Tilt Angle 50° 59
A.6 Images Taken from Analysis of the Straight Beam Having Tilt Angle 55° (Crashed) 60

B DEFORMED AND UNDEFORMED SHAPES OF STRAIGHT BEAMS RELATED TO ASPECT RATIO STUDY 61

B.1 Images Taken from Analysis of the Straight Beam with L5%↑, t5%↓ 61

B.2 Images Taken from Analysis of the Straight Beam with L10%↑, t9%↓ 62

B.3 Images Taken from Analysis of the Straight Beam with L15%↑, t13%↓ 63

B.4 Images Taken from Analysis of the Straight Beam with L20%↑, t17%↓ 64

B.5 Images Taken from Analysis of the Straight Beam with L25%↑, t20%↓ 65

B.6 Images Taken from Analysis of the Straight Beam with L5%↓, t5%↑ 66

B.7 Images Taken from Analysis of the Straight Beam with L10%↓, t11%↑ 67

B.8 Images Taken from Analysis of the Straight Beam with L15%↓, t18%↑ (Crashed) 68

C DEFORMED AND UNDEFORMED SHAPES OF BEAMS RELATED TO MORPHOLOGICAL STUDY 69

C.1 Images Taken from the Curved Beam Analysis Named *Reversed S-Shape* 69

C.2 Images Taken from the Curved Beam Analysis Named *3S-Shape* 70

C.3 Images Taken from the Curved Beam Analysis Named *Convex* 71

C.4 Images Taken from the Curved Beam Analysis Named *Concave* 72

C.5 Images Taken from Analysis of the Straight Beam (The Reference Beam) 73

C.6 Images Taken from the Curved Beam Analysis Named *2S-Shape* 74

C.7 Images Taken from the Curved Beam Analysis Named *S-Shape-R20* 75

C.8 Images Taken from the Curved Beam Analysis Named *S-Shape-R6* 76

C.9 Images Taken from the Curved Beam Analysis Named *S-Shape-R5* . . . 77

C.10 Images Taken from the Curved Beam Analysis Named *S-Shape-R4* (Crashed) . . . 78

D DEFORMED AND UNDEFORMED SHAPES OF THE CURVED BEAM NAMED S-SHAPE-R5 AT DIFFERENT TILT ANGLES . . 79

D.1 Images Taken from Analysis of *S-Shape-r5* for 30° Tilt Angle 79

D.2 Images Taken from Analysis of *S-Shape-r5* for 35° Tilt Angle 80

D.3 Images Taken from Analysis of *S-Shape-r5* for 40° Tilt Angle 81

D.4 Images Taken from Analysis of *S-Shape-r5* for 45° Tilt Angle 82

D.5 Images Taken from Analysis of *S-Shape-r5* for 45° Tilt Angle (Showing Self Contact Occurred During the Analysis) . . 83

D.6 Images Taken from Analysis of *S-Shape-r5* for 50° Tilt Angle 84

D.7 Images Taken from Analysis of *S-Shape-r5* for 50° Tilt Angle (Showing Two Self Contacts Occurred During the Analysis) . . . 85

E DEFORMED AND UNDEFORMED SHAPES RELATED TO ASPECT RATIO STUDY OF THE CURVED BEAM S-SHAPE-R5 . . . 87

E.1 Images Taken from Analysis of the Curved Beam S-Shape-r5 with L5 % ↑, t5 % ↓ . . . 88

E.2 Images Taken from Analysis of the Curved Beam S-Shape-r5 with L10 % ↑, t9 % ↓ . . . 89

E.3 Images Taken from Analysis of the Curved Beam S-Shape-r5 with L5 % ↓, t5 % ↑ . . . 90

E.4 Images Taken from Analysis of the Curved Beam S-Shape-r5 with L10 % ↓, t11 % ↑ . . . 91

E.5 Images Taken from Analysis of the Curved Beam S-Shape-r5 with L10%↓, t11%↑ (Showing Self Contact Occurred During the Analysis) . . . 92

F DEFORMED AND UNDEFORMED SHAPES OF A STRAIGHT MODEL CONSISTING OF TWO BEAMS . . . 93

F.1 Undeformed Shape Images Taken from Analysis of the Constructed Model Consisting of Two Reference Beams . . . 93

F.2 Deformed Shape Images Taken from Analysis of the Constructed Model Consisting of Two Reference Beams . . . 94

LIST OF TABLES

Table 2.1 Material properties 13

Table 2.2 Details of the finite element model of the reference beam 15

Table 2.3 Effects of *element type*, *procedure type* and *initial increment size* on the F_R-U curve of the reference beam 20

Table 2.4 Energy trapping results of tilt angles 30°, 35°, 40°, 45°, 50° 25

Table 2.5 Comparison of $E_{in} - E_{out}$ values for analyzed straight beam tilt angles derived from strain energy output data given by ABAQUS and calculated according to the method explained in Section 2.1.6 26

Table 2.6 Energy trapping results of the straight beams at different aspect ratios 29

Table 2.7 Energy trapping results of the modeled system consisting of two reference beams and the reference beam itself 32

Table 3.1 Geometrical parameters of the investigated curved beams 37

Table 3.2 Energy trapping results of the beams having different geometries . . 40

Table 3.3 Energy trapping results of the beams *s-shape-r5* with tilt angles 30°, 35°, 40°, 45° and 50° 42

Table 3.4 Energy trapping results related to aspect ratio study of the curved beam s-shape-r5 46

LIST OF FIGURES

Figure 1.1 A sample elastic energy absorbing structure (left), and its minimal unit (right) [1] 2

Figure 1.2 a) Axially compressed elastic beam (no energy trapping) b) Two stable configurations of elastic tilted beam when one end of it is vertically moved (energy trapping) [1] 4

Figure 1.3 A) Stress-strain graph of a recoverable structure made of ceramic hollow nano tubes. B(I), C(II), D(III) and E(IV) are visuals of the recoverable ceramic nano structure showing its deformed and undeformed states. F) Stress-strain graph of a non-recoverable structure made of ceramic hollow nano tubes. G(I), H(II), I(III) and J(IV) are visuals of the non-recoverable ceramic nano structure showing its deformed and undeformed states [2] 5

Figure 1.4 Design examples of energy trapping systems. a) Figure is taken from [3] b) Figure is taken from [4] c) Figure is taken from [5] d) Figure is taken from [1] 7

Figure 1.5 Bistability check graph and energy comparison graph for different types of materials [6] 8

Figure 2.1 a) Beam geometry b) Boundary conditions for the finite element model 13

Figure 2.2 2D finite element beam model with global mesh size 0.05 mm . . . 14

Figure 2.3 Bistability Check. a) Undeformed beam and boundary conditions b) Beam is deformed by applying displacement at the top. After the removal of the prescribed displacement c) the non-bistable beam returns to its original undeformed position, while d) the bistable beam preserves the deformed shape 16

Figure 2.4 Screenshots of a bistable and a non-bistable beam taken from a video of the existing study [1]. a) Initial position of a bistable beam, b) deformed position of a bistable beam when a vertical load is applied by hand, c) final position of a bistable beam after removal of applied load. d) Initial position of a non-bistable beam, e) deformed position of a non-bistable beam when a vertical load is applied by hand, f) final position of a non-bistable beam after removal of applied load. 17

Figure 2.5 F_R-U curves of the digitized reference beam and computed results for 0.05 mm, 0.075 mm and 0.1 mm mesh sizes 18

Figure 2.6 A typical load-displacement curve of a bi-stable beam. Stored energy-spent energy regions in a F_R-U graph 21

Figure 2.7 Screenshots showing deformed shapes of a straight beam when a prescribed displacement is applied in vertical direction. At point A) the beam is at its first stable state, no displacement is applied yet. At point B) a certain displacement is applied and the beam is at the point where the reaction force is maximum. At point C) the beam is unstable and transformation of the beam from one stable state to another takes place (snap-through phenomenon). At point D) the beam is at its second stable state. 22

Figure 2.8 A typical F_R-U curve of a non-bistable beam 23

Figure 2.9 F_R-U curves of the beams for 40°, 45°, 50° tilt angles 24

Figure 2.10 F_R-U curves of the beams for 30°, 35°, 40° tilt angles 24

Figure 2.11 Percent change in trapped energy with tilt angle of straight beams . 27

Figure 2.12 F_R-U curves of the beams that are more slender than the reference beam 28

Figure 2.13 F_R-U curves of the beams that are less slender than the reference beam 29

Figure 2.14 Percent change in the trapped energy for different length-width pairs of straight beams 30

Figure 2.15 F_R-U curves of the reference beam and modeled system consisting of two reference beams 31

Figure 3.1 Curved beam geometry 34

Figure 3.2 2D finite element model of a curved beam with global mesh size 0.05 mm 36

Figure 3.3 F_R-U curves of the beams performing worse than the reference beam in terms of energy trapping capacity 38

Figure 3.4 F_R-U curves of the beams performing better than the reference beam in terms of energy trapping capacity 39

Figure 3.5 F_R-U curves of the reference beam and the beams *s-shape-r5* with tilt angles 30° and 35° 41

Figure 3.6 F_R-U curves of the reference beam and the beam *s-shape-r5* having tilt angles 40°, 45° and 50° 42

Figure 3.7 Percent change in trapped energy with tilt angle of the curved beam *s-shape-r5* 43

Figure 3.8 F_R-U curves of the curved beam *s-shape-r5* for aspect ratios that perform worse than the reference beam and the beam *s-shape-r5* with original dimensions in terms of energy trapping capacity 45

Figure 3.9 F_R-U curves of the curved beam *s-shape-r5* for aspect ratios that perform better than the reference beam and the beam *s-shape-r5* with original dimensions in terms of energy trapping capacity 46

Figure 3.10 Percent change in trapped energy for different length-width pairs of the curved beam *s-shape-r5* 47

Figure A.1 Undeformed-deformed shape of the beam for 30° tilt angle 55

Figure A.2 Undeformed-deformed shape of the beam for 35° tilt angle 56

Figure A.3 Undeformed-deformed shape of the beam for 40° tilt angle (the reference beam) 57

Figure A.4 Undeformed-deformed shape of the beam for 45° tilt angle 58

Figure A.5 Undeformed-deformed shape of the beam for 50° tilt angle 59

Figure A.6 Undeformed-deformed shape of the beam which crashed when its tilt angle is increased to 55° 60

Figure B.1 Undeformed-deformed shape of the beam for 5% increase in length, 5% decrease in width 61

Figure B.2 Undeformed-deformed shape of the beam for 10% increase in length, 9% decrease in width 62

Figure B.3 Undeformed-deformed shape of the beam for 15% increase in length, 13% decrease in width 63

Figure B.4 Undeformed-deformed shape of the beam for 20% increase in length, 17% decrease in width 64

Figure B.5 Undeformed-deformed shape of the beam for 25% increase in length, 20% decrease in width 65

Figure B.6 Undeformed-deformed shape of the beam for 5% decrease in length, 5% increase in width 66

Figure B.7 Undeformed-deformed shape of the beam for 10% decrease in length, 11% increase in width 67

Figure B.8 Undeformed-deformed shape of the beam for 15% decrease in length, 18% increase in width 68

Figure C.1 Undeformed-deformed shape of the beam for *reversed s-shape* . . . 69

Figure C.2 Undeformed-deformed shape of the beam for *3s-shape* 70

Figure C.3 Undeformed-deformed shape of the beam for *convex* 71

Figure C.4 Undeformed-deformed shape of the beam for *concave* 72

Figure C.5 Undeformed-deformed shape of the reference beam 73

Figure C.6 Undeformed-deformed shape of the beam for *2s-shape* 74

Figure C.7 Undeformed-deformed shape of the beam for *s-shape-r20* 75

Figure C.8 Undeformed-deformed shape of the beam for *s-shape-r6* 76

Figure C.9 Undeformed-deformed shape of the beam for *s-shape-r5* 77

Figure C.10 Undeformed-deformed shape of the beam *s-shape-r4* which crashed when radius of its both concave and convex arcs is reduced from 5 mm to 4 mm 78

Figure D.1 Undeformed-deformed shape of the beam *s-shape-r5* for 30° tilt angle 79

Figure D.2 Undeformed-deformed shape of the beam *s-shape-r5* for 35° tilt angle 80

Figure D.3 Undeformed-deformed shape of the beam *s-shape-r5* for 40° tilt angle 81

Figure D.4 Undeformed-deformed shape of the beam *s-shape-r5* for 45° tilt angle 82

Figure D.5 Deformed shape of the beam *s-shape-r5* with self contact occurred at about 3 mm vertical displacement of its upper end for 45° tilt angle . . . 83

Figure D.6 Undeformed-deformed shape of the beam *s-shape-r5* for 50° tilt angle 84

Figure D.7 Deformed shape of the beam *s-shape-r5* with self contact occurred at about 2 mm vertical displacement of its upper end for 50° tilt angle . . . 85

Figure D.8 Deformed shape of the beam *s-shape-r5* with self contact occurred at about 3.5 mm vertical displacement of its upper end for 50° tilt angle . . 85

Figure E.1 Undeformed-deformed shape of the curved beam s-shape-r5 for 5% increase in length, 5% decrease in width 88

Figure E.2 Undeformed-deformed shape of the curved beam s-shape-r5 for 10% increase in length, 9% decrease in width 89

Figure E.3 Undeformed-deformed shape of the curved beam s-shape-r5 for 5% decrease in length, 5% increase in width 90

Figure E.4 Undeformed-deformed shape of the curved beam s-shape-r5 for 10% decrease in length, 11% increase in width 91

Figure E.5 Deformed shape of the curved beam s-shape-r5 with 10% decrease in length showing self contact occurred at about 1,8 mm vertical displacement of its upper end 92

Figure F.1 Undeformed shapes of the constructed model consisting of two reference beams 93

Figure F.2 Deformed shapes of the constructed model consisting of two reference beams 94

LIST OF ABBREVIATIONS

L	Length of the Beam
t	Width of the Beam
θ	Tilt Angle of the Beam
d	Out of plane thickness of the Beam
F_R	Reaction Force
U	Displacement
μ	Shear Modulus
κ	Bulk Modulus
E_{in}	Amount of Energy Stored Inside the Beam
E_{out}	Amount of Energy Spent by the Beam
$\overline{I}_1$	First deviatoric strain invariant
J^{el}	Elastic volume ratio
Ψ	Strain energy per unit volume

CHAPTER 1

INTRODUCTION

1.1 Motivation of the Thesis

Energy trapping systems are being widely used in personnel protection, aircraft and land vehicles, packaging of special products and in many other industries as impact absorbers. Impact absorbers can absorb energy mainly in two ways; the first way is by undergoing plastic deformation, and the second way is by undergoing elastic deformation. Conventional energy trapping systems absorb impact energy usually by plastic deformation which does not provide re-usability [4]. Architected materials [7] and metamaterials [8] have attracted great interest in developing tunable systems and for the future reusable energy trapping and impact protection systems. Current trend in energy absorbing system designs is to use elastic materials instead of plastic ones to enable re-usability of the system. A sample structure taken from [1] is given in Figure 1.1.

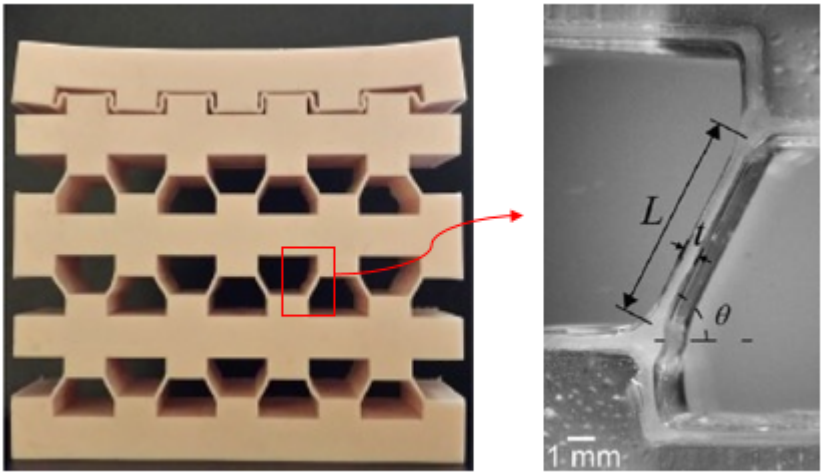

Figure 1.1: A sample elastic energy absorbing structure (left), and its minimal unit (right) [1]

In this thesis work, a tilted multistable elastic beam proposed in [1] as shown in Figure 1.1 is considered. The multistable energy absorbers could provide cost advantage over conventional energy absorbing systems due to their re-usability. Although the amount of energy absorbed by elastic energy absorbers are low compared to plastic energy absorbers, ongoing studies may help to find new ways of absorbing larger amounts of energy by undergoing elastic deformations only.

1.2 Objective of the Thesis

In the context of development of energy absorbers, numerical simulations play an increasing role to substitute more and more the time- and cost-expensive experimental testing efforts by more efficient virtual numerical testing [9]. The computational tools offer tremendous benefits in analyzing new candidate materials and conducting extensive parametric studies [10]. In [1], energy absorbing capacity of a structure is both numerically and experimentally tested. In this thesis, the energy absorbing structure proposed in [1] which consists of inclined beams is further studied numerically. Geometrical and topological changes are made in the inclined beam structure to increase the energy absorption capacity of the modeled beam.

The objective of this thesis work is to determine the parameters of the tilted beam

yielding to maximum energy trapping while using the same amount of material. Factors effecting energy-trapping capacity of the elastic tilted beam are determined by using finite element method (FEM). A 2D planar beam is modeled with the commercial FE program ABAQUS. Geometrical and topological parameters defining the model are varied and many FE runs are conducted to determine the energy trapping capacity of the beam while keeping the volume of the beam constant. The optimum beam dimensions, tilt angle and geometry are found.

1.3 Literature Review

1.3.1 Energy Absorbing Structures

The primary objective of energy absorbers is to keep the reactive force below a threshold which will cause damage or injury [11]. In each specific case, factors leading to need of an energy absorber should be well defined and an appropriate energy absorber should be chosen to prevent failure. Ideal energy absorber material would exhibit high energy absorption capacity/weight ratio and should allow multiple use [12]. Strategies including plastic deformation in metals, fragmentation in ceramics, and rate dependent viscous processes have been investigated for energy absorption. However, these systems present challanges associated with either reusability or rate dependency [13]. Many energy-absorbing structures for impact, crash or blast loads are based on cellular structures due to advantage of low weight [9]. There are also many examples of energy absorbing structures in nature such as presence of the cellular structure in a human femur, the cellular structure of woods, honeycombs, cellular graded structure in a banana peel [11], cross-bridges in muscles [14], etc.

1.3.2 Energy Trapping Structures

Reusable energy absorbers trap some portion of the impact energy inside the system and fully recovers it when the system returns to its initial position. The rest of the energy gets dissipated by the damping of the base material and/or by the interaction of the system with the medium [5]. Energy trapping characteristics of such systems arise

due to a phenomenon known as snap-through between stable equilibrium configurations of structure's bi-stable constituents [14]. Snap-through phenomenon is sudden transformation of a structure from one stable state to another under proper circumstances. Bi-stable constituents are the structure's one of two stable states on which the structure preserves its position when no external force is applied. The energy trapping mechanism of an energy absorber exists only if there is reversible change in state of structural geometries of the structure [1].

Figure 1.2 shows deformation scheme of a bi-stable and a non-bistable elastic tilted beam. In the upper side of Figure 1.2, there is a non-bistable beam which comes to its original position when an applied load is removed. Therefore, no energy is being trapped in the beam. On the other hand, in lower side of Figure 1.2 there is a bistable beam which preserves its deformed position after removal of the applied load. As can also be seen from Force-Displacement graph located in lower side of Figure 1.2 a certain amount of energy is trapped inside the bistable beam.

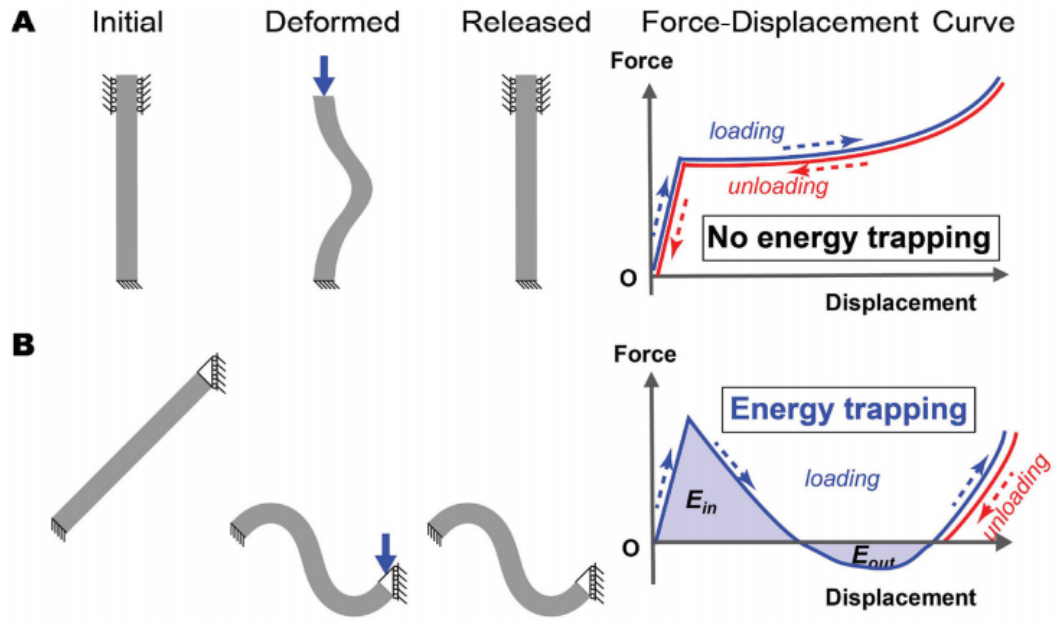

Figure 1.2: a) Axially compressed elastic beam (no energy trapping) b) Two stable configurations of elastic tilted beam when one end of it is vertically moved (energy trapping) [1]

In order to allow reversible change of a structural transformation in a system, a proper choice of an elastic base material and proper topological and geometrical designs of

the unit cell must be attained [5]. In literature, apart from using polymeric materials for energy absorbing purposes, even a ceramic material at nano scale is used for recoverable energy absorption [2]. In the existing study, a nano-structure is constructed from alumina hollow tubes at nano-scale. A uni-directional compressive load is applied to the structure and for particular parameters, recovery up to 98% of their original height after compression to 50% strain is achieved. However, the structure was not bi-stable. Figure 1.3 shows deformed and undeformed states of the structure along with its stress-strain curve.

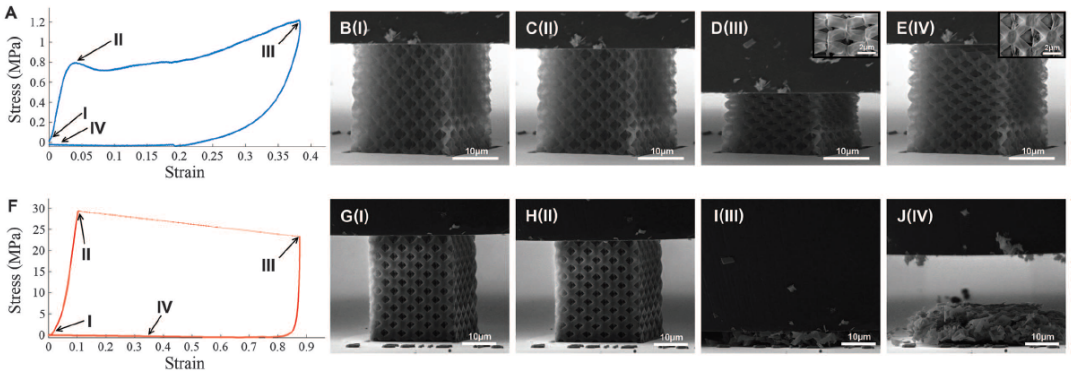

Figure 1.3: A) Stress-strain graph of a recoverable structure made of ceramic hollow nano tubes. B(I), C(II), D(III) and E(IV) are visuals of the recoverable ceramic nano structure showing its deformed and undeformed states. F) Stress-strain graph of a non-recoverable structure made of ceramic hollow nano tubes. G(I), H(II), I(III) and J(IV) are visuals of the non-recoverable ceramic nano structure showing its deformed and undeformed states [2]

Energy trapping systems gain their unusual, sometimes extraordinary, mechanical properties from their underlying architecture, rather than the composition of their constituents [15]. There are different models of energy trapping systems in literature. The bi-stable unit actuator in [3], the negative stiffness beams in [4], the phase transforming cellular material in [5], the multistable architected beams in [1] are all examples of energy trapping systems which are, at the same time, reusable energy absorbers. Visuals of the constructed models that are given as example are shown in Figure 1.4. In [3], designs are varied between flat and curved configurations and length of bi-stable material changed. It is concluded that required bi-stability triggering force can be tuned at some range depending on the geometry of deployable struc-

ture. In [4] energy absorption results of negative stiffness honeycombs (NSH) are compared with results of conventional honeycombs. Conventional honeycombs performed better than NSHs in terms of energy absorption. This can be partly explained by the permanent deformation and lack of energy recovery of the conventional honeycombs. Also, NSHs have not yet been optimized to maximize energy absorption. In [5], theoretical energy absorbed per unit mass of a phase transforming cellular structure is compared with the corresponding values of honeycombs made out of metals and polymers respectively. It is concluded that to obtain reversible phase transformation usage of bi-stable structures is required. Also, geometry of the unit cell must be chosen such that the stress at any point in the cell does not exceed the yield stress of the base material during structural transformation. Moreover, the unit cell must counteract the Poisson's effect to provide the balance in strain energy required to obtain bi-stable behavior of the structure. In [1], effects of tilt angle, beam slenderness (t/L where t: thickness, L=length) and strain rate on energy trapping capacity of the beams are investigated. The study reveals that the energy absorption is unaffected by the loading rate or history and the energy that the system traps increases as a function of both the tilt angle and t/L. There are also studies about using energy trapping bi-stable elastic beams as micro-actuators since no energy is required to keep them in either undeformed or deformed states [16, 17].

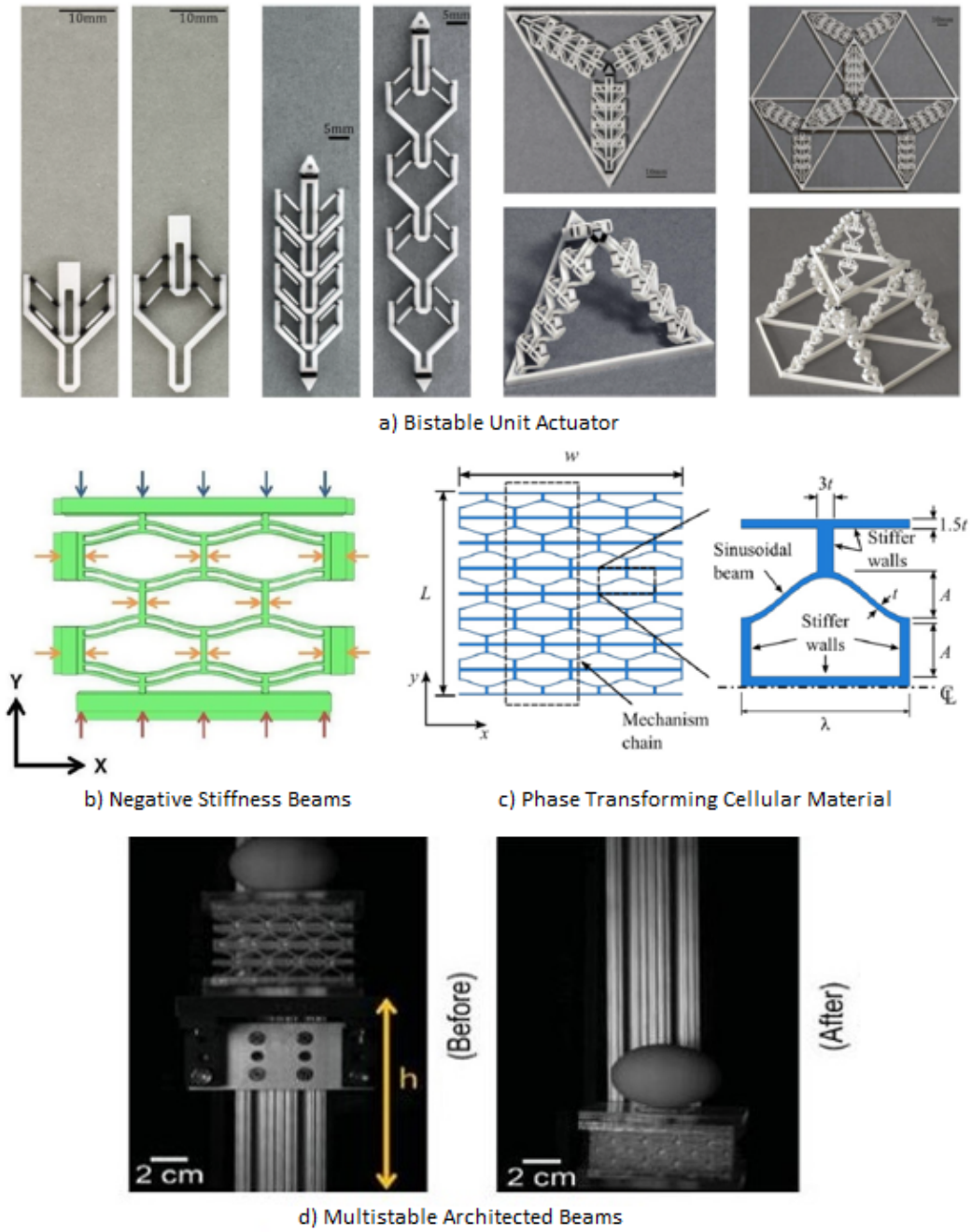

Figure 1.4: Design examples of energy trapping systems. a) Figure is taken from [3] b) Figure is taken from [4] c) Figure is taken from [5] d) Figure is taken from [1]

As mentioned previously, energy trapping structures snap-through between their bi-stable constituents. Therefore, there is also risk of snap-back behavior which is sructure's return to its first stable state after removal of an applied load. Geometrical and morphological changes may effect the structure's ability of snap-through and snap-back [14]. Moreover, energy may be undesirably returned to the system via snap-back events [18]. In [6], a phase stability parameter is defined as S_2/S_1 where S_1 and S_2 represents the maximum and minimum force values between the first and third equilibrium points, respectively, in force-displacement curve. The phase stability parameter is defined to decide whether the design is bi-stable or not. Figure 1.5 shows regions of stability behavior and absorbed energy per unit volume versus compressive strength graph for different types of materials. Risk of snap back behavior increases as phase stability parameter (S_2/S_1) increases.

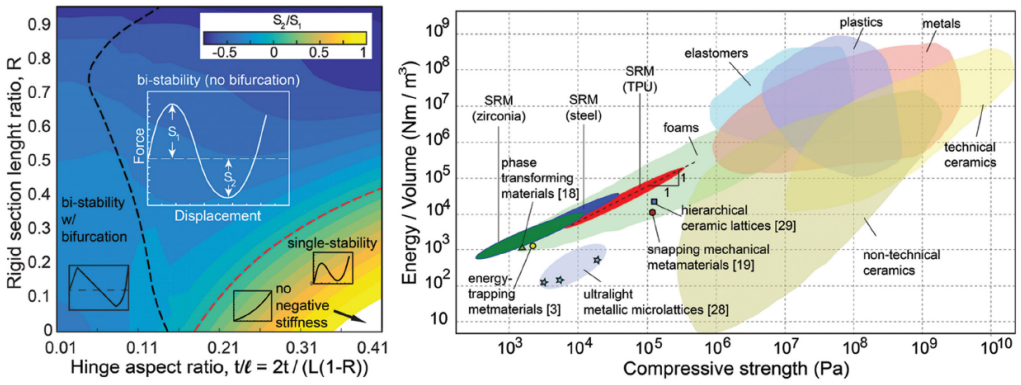

a) Phase Stability Parameter S_2/S_1 for a Specific Structure

b) Absorbed Energy per Unit Volume Versus Compressive Strength Graph for Different Types of Materials

Figure 1.5: Bistability check graph and energy comparison graph for different types of materials [6]

1.4 Organization of the Thesis

In Chapter 2, the reference beam parameters are defined. Finite element model of the inclined beam is explained. Energy trapping results of tilt angle and width/length ratio studies for a straight beam are presented. A comparison of all gathered results with the reference beam results is also presented. A finite element model consisting of two reference beams is constructed to compare the system's energy trapping capacity with the energy trapping capacity of a single reference beam.

In Chapter 3, geometrical variations of a tilted beam apart from straight shape are shown. Energy trapping results of these variations and their comparison with the reference beam results are presented. A particular curved beam having the best energy trapping capacity among geometrical trials is chosen. Effect of tilt angle on the chosen beam's energy trapping capacity is investigated. Energy trapping results for each analysis with different tilt angles are compared with the results of the reference beam. Moreover, effect of aspect ratio on the chosen beam's energy trapping capacity is also investigated. Energy trapping results for each analysis with different aspect ratios are compared with the results of the reference beam.

In Chapter 4, conclusions and discussions are presented.

CHAPTER 2

FINITE ELEMENT MODELING OF INCLINED STRAIGHT ENERGY TRAPPING BEAMS

In this chapter finite element models of inclined straight energy trapping beams are explained. To this end, finite element analysis parameters of straight inclined beams are defined. Effects of the tilt angle and the width/length ratio on energy trapping capacity are investigated. Energy trapping capacity of each beam is directly derived from the total strain energy data gathered from ABAQUS. Besides, a mathematical method used to calculate energy trapping capacity of each beam for the purpose of comparison is explained. In all analyses, a 2D planar beam is modeled in ABAQUS 6.12-3. In case of a modular system, energy trapping results of this single beam enables estimation of energy trapping performance of the whole system that consists of many beams.

Energy can be trapped in an inclined beam system only if the system is bi-stable. Bi-stable systems have more than one stable configuration. An advantage of bi-stable systems is that no power is needed to keep the system at either of its two stable states [17]. Therefore, reversibility of the structural transformation is not automatic for the bi-stable systems, subsequent external actuation is needed in reverse direction for recovery [7]. These systems are often used as switches and also in microrobotic applications [19]. For an inclined straight beam, the beam undergoes so-called snap through behaviour which is basically transformation of the beam from one stable configuration to another when a vertical force is applied. Snap through behaviour and bi-stability are two important phenomena for understanding energy trapping systems. According to the minimal energy principle, the beam will find the path with the

least energy such as the first and second buckling modes in the snap through process [20]. Interestingly, buckling has long been considered as an unwanted mechanical instability. Therefore, recently, it is exploited for obtaining mechanical bi-stability, multi-stability or programmable behavior [12].

In Section 2.1 the problem geometry, material properties, the finite element model, boundary conditions and the method of trapped energy calculation are discussed. In Section 2.2 energy trapping results regarding tilt angle study of the straight beam are presented. Similarly, energy trapping results regarding width/length ratio study of the straight beam are presented in Section 2.3. In Section 2.4 a finite element model consisting of two reference beams is constructed to compare the system's energy trapping capacity with the energy trapping capacity of a single reference beam.

2.1 Problem Definition

A 2D planar beam standing in tilted position is modeled in ABAQUS as shown in Figure 2.1a. A displacement boundary condition is applied to one end of the beam in vertical direction while the other end is constrained in vertical and horizontal directions as shown in Figure 2.1b. Reaction force-displacement graphs are obtained for each analysis. Details of the geometry, material parameters, parameters of the finite element model and boundary conditions are provided in the following sections.

2.1.1 Geometry

A multistable elastic beam geometry as proposed in [1] is chosen as a reference beam geometry for finite element analyses. Dimensions of the reference beam geometry are shown in Figure 2.1a. In figure L is the length, t is the width and θ is the tilt angle of the reference beam and they are taken as 5.06 mm, 0.61 mm and 40° respectively. Out of plane thickness (d) of the reference beam is taken as 14.8 mm. It is set high as proposed in [1] to prevent out of plane buckling.

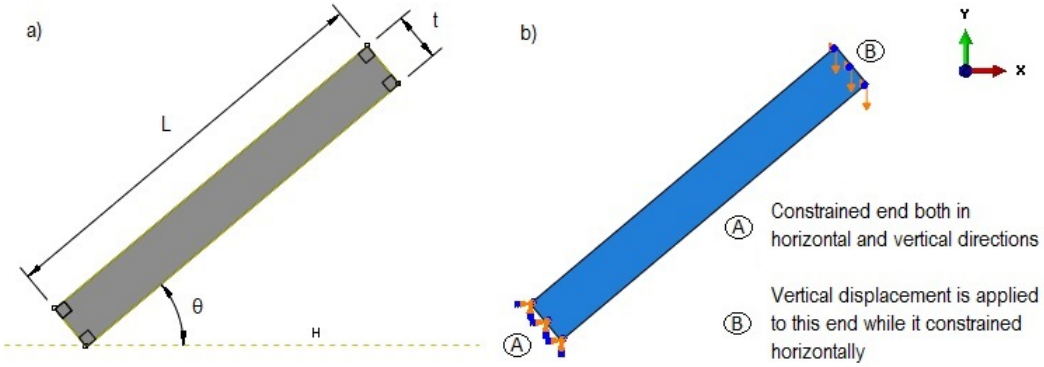

Figure 2.1: a) Beam geometry b) Boundary conditions for the finite element model

The length, the width and the tilt angle of the straight beam are the parameters that are changed while the out of plane thickness of the beam is kept constant. Energy trapping results for each analysis are compared with results of the reference beam.

2.1.2 Material Properties

Material properties of the beam are provided in Table 2.1. The same material parameters are used in all analyses throughout the study. Material behavior is defined as hyper-elastic Neo-Hookean to model moderate to large deformations. C_{10} and D_1 coefficients required for Neo-Hookean model are provided in [1] from the tension test experiments of the material "polydimethylsiloxane (PDMS)" which is commonly known as silicone rubber.

Table 2.1: Material properties

Bulk Modulus (κ) [MPa]	Shear Modulus (μ) [MPa]
800	0.32

The relation of C_{10} and D_1 coefficients with the Neo-Hookean strain energy potential is given in Equation(2.1) [21]. In the equation, Ψ is the strain energy per unit volume, $\overline{I}_1$ is the first deviatoric strain invariant, J^{el} is the elastic volume ratio, C_{10} is $\frac{\mu}{2}$ and D_1 is $\frac{2}{\kappa}$. Note that μ and κ correspond to the shear modulus and bulk modulus, respectively.

$$\Psi = C_{10}(\overline{I}_1 - 3) + \frac{1}{D_1}(J^{el} - 1)^2 \tag{2.1}$$

2.1.3 Finite Element Model

Figure 2.2 shows the finite element model of the straight beam with 0.05 mm element size. In all analyses, six node CPE6MH elements are used. CPE6MH is a modified, hybrid element with linear pressure. It has also hourglass control.

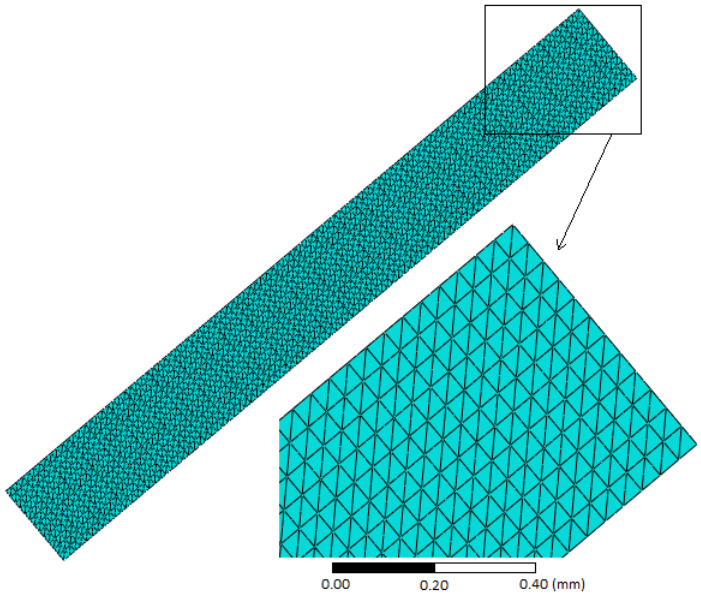

Figure 2.2: 2D finite element beam model with global mesh size 0.05 mm

Table 2.2 gives details of the finite element model of the reference beam. Effects of *element type*, *procedure type* and *initial increment size* on F_R-U curve of the reference beam are studied and results are presented in Table 2.3. Mesh size is determined through a mesh refinement study. Figure 2.5 shows F_R-U curves of the reference beam having different global mesh sizes. In "step" module, "nlgeom" option is switched on to enable large deformations. Plane strain conditions are assumed and implicit runs are carried out.

Table 2.2: Details of the finite element model of the reference beam

element type	CPE6MH
number of elements	2424
number of nodes	5075
global element size [mm]	0.05

2.1.4 Boundary Conditions

Boundary conditions of the constructed beam model are shown in Figure 2.1b. All nodes at the beam end named A in Figure 2.1b are constrained both in x and y directions. A prescribed displacement is applied in y direction to the all nodes at the beam end named B in Figure 2.1b, while all nodes at this end are constrained in x direction. The magnitude of the applied displacement is ranged between 5-7 mm depending on the angle and aspect ratio of the analyzed beam. The complete load-displacement response of the beam can be determined when a prescribed displacement is applied. For this reason, a prescribed displacement is defined instead of prescribed load [22].

Analyses are carried out in two steps as shown in Figure 2.3. At the first step, lower end of the beam is constrained in horizontal and vertical directions and a prescribed displacement is applied to the upper end of the beam in vertical direction. At the second step, applied vertical displacement is removed to check whether the beam is bi-stable or not. If the beam returns to its initial position, it is not a bistable beam. If the beam preserves its deformed position, it is called as a bistable beam. Bi-stability of the beam is required to trap the strain energy stored in the system; otherwise stored energy will be released upon removal of the displacement boundary condition.

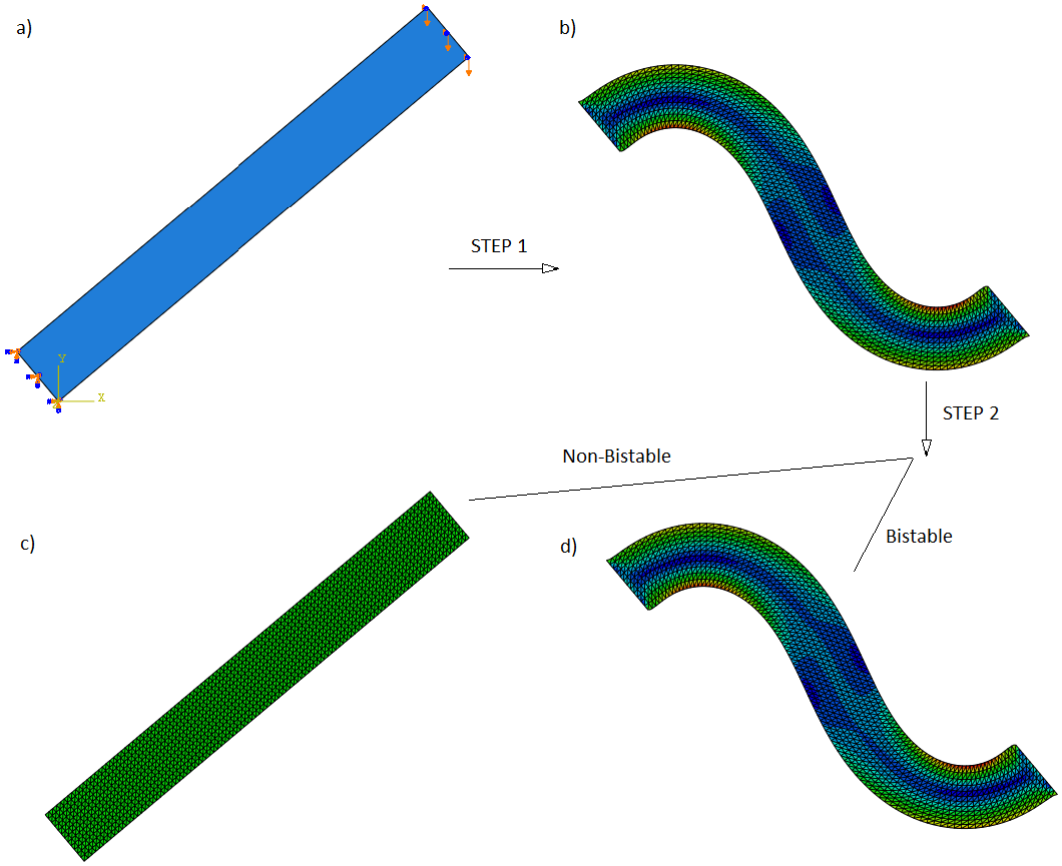

Figure 2.3: Bistability Check. a) Undeformed beam and boundary conditions b) Beam is deformed by applying displacement at the top. After the removal of the prescribed displacement c) the non-bistable beam returns to its original undeformed position, while d) the bistable beam preserves the deformed shape

Figure 2.4 shows screenshots taken from the supplementary material of the [1]. Figure 2.4a-c show initial, deformed and final positions of a bistable beam when a load is applied in vertical direction by hand and removed afterwards. Figure 2.4d-f show initial, deformed and final positions of a non-bistable beam when a load is applied in vertical direction by hand and removed afterwards. The only difference that makes these two beams either bistable or non-bistable is their aspect ratio. As can be seen on lower side of each screenshot in Figure 2.4, the bistable beam has an aspect ratio of t/L=0.12 while the non-bistable beam has an aspect ratio of t/L=0.15.

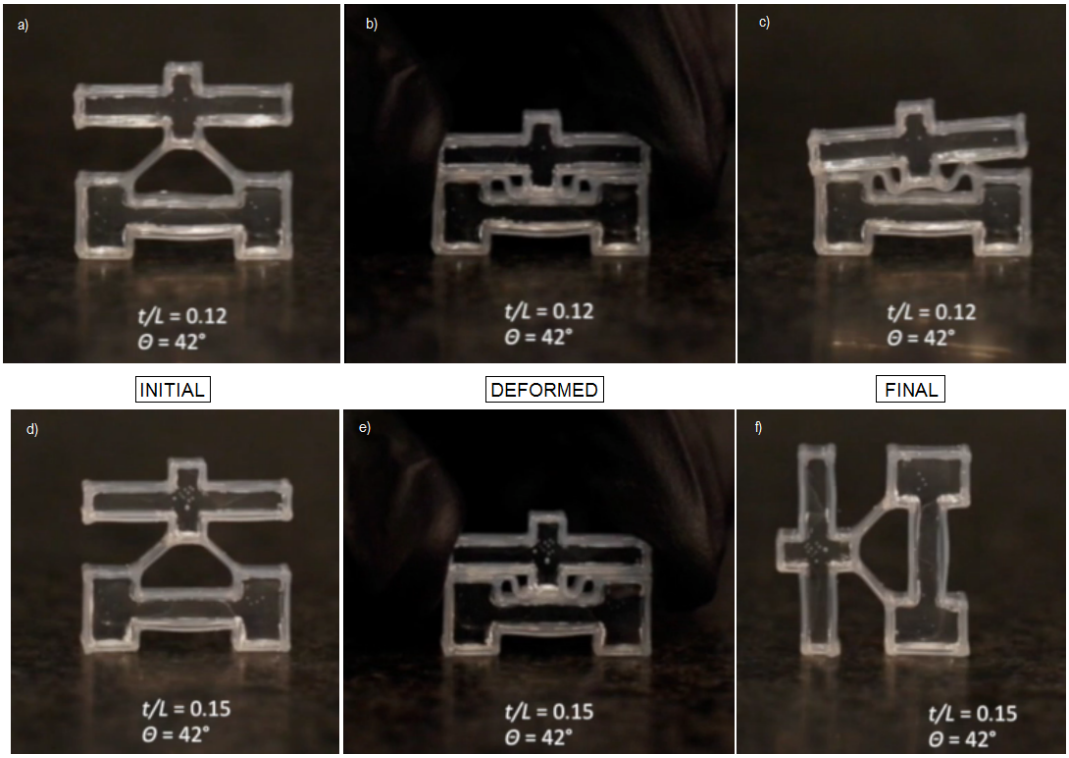

Figure 2.4: Screenshots of a bistable and a non-bistable beam taken from a video of the existing study [1]. a) Initial position of a bistable beam, b) deformed position of a bistable beam when a vertical load is applied by hand, c) final position of a bistable beam after removal of applied load. d) Initial position of a non-bistable beam, e) deformed position of a non-bistable beam when a vertical load is applied by hand, f) final position of a non-bistable beam after removal of applied load.

2.1.5 Effects of *Element Type*, *Procedure Type*, *Mesh Size* and *Initial Increment Size* on Mechanical Response of the Reference Beam

A multistable elastic beam geometry as proposed in [1] is chosen as a reference beam geometry for finite element analyses. The load-displacement (F_R-U) curve of the reference beam shown in [1] is digitized with the help of a software. The curve provided in [1] is obtained through numerical studies. The results of this theses are compared with the numerical results of the existing study [1]. For digitization of the existing curve, maximum and minimum points of the F_R-U curve are provided to the software as input data and random points on the curve are clicked as many as possible to digitize it more precisely. Then the software gives F_R-U data set corresponding

to each clicked point as output. The obtained F_R-U data set is used to re-draw the F_R-U curve of the reference beam for the purpose of comparison with the results of this thesis. Finite element parameters given in [1] are used in the same manner to get more reliable comparison of the digitized curve with the computed curve. As can be seen from Figure 2.5, digitized F_R-U curve of the existing study [1] does not precisely coincide with the computed curve obtained through a numerical analysis carried out during this thesis. The reason might be a discrepancy written in [1] about element type of the finite element beam models. In [1], it is claimed that ABAQUS/-Explicit is used and 2D finite element beam models are constructed using CPE6MH element type. Therefore, CPE6MH elements are only available in the element library of ABAQUS/Standard but not in ABAQUS/Explicit.

Figure 2.5 shows F_R-U curve of the digitized reference beam and the reference beam trials for 0.05 mm, 0.075 mm and 0.1 mm mesh sizes. As can be seen from the Figure 2.5 F_R-U curves of the different mesh sizes 0.05 mm, 0.075 mm and 0.1 mm overlap. Moreover, the solution times of three meshes are very close to each other. For these reasons, a mesh size of 0.05 mm is chosen for all analyses of this study to get more reliable results.

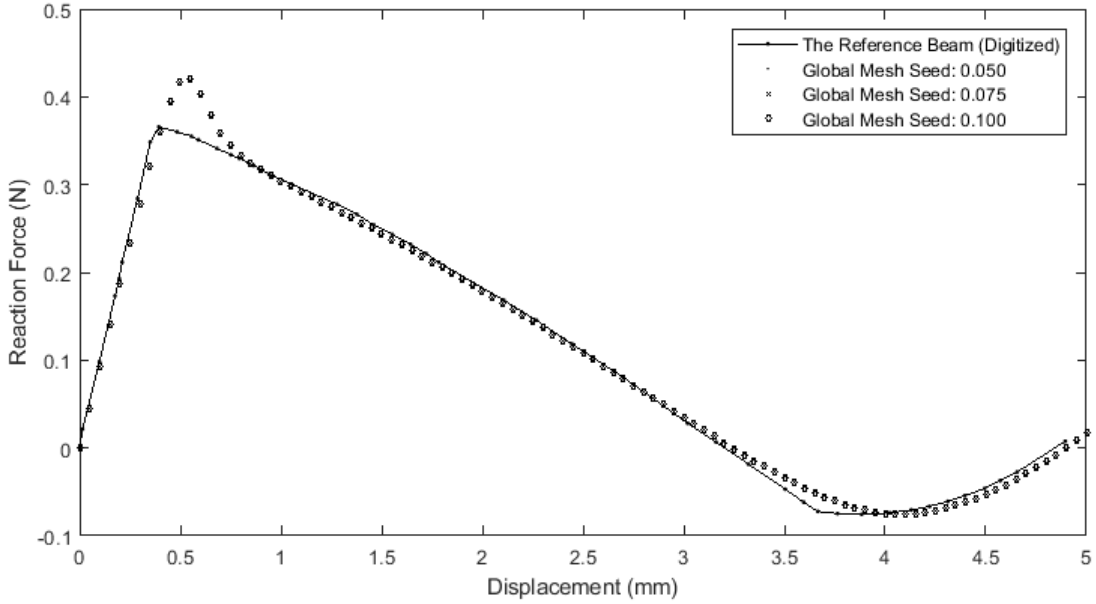

Figure 2.5: F_R-U curves of the digitized reference beam and computed results for 0.05 mm, 0.075 mm and 0.1 mm mesh sizes

ABAQUS/Explicit solves dynamic response problems using an explicit direct-integration procedure while *ABAQUS/Standard* offers complete flexibility in making the distinction between static and dynamic responses. In *ABAQUS/Standard*, the same analysis can contain several static and dynamic phases. Thus, a static pre-load might be applied, and then the linear or nonlinear dynamic response can be computed (see ABAQUS Documentation 6.9 [23]).

Effects of *element type*, *procedure type* and *initial increment size* on the F_R-U curve of the reference beam are studied. Table 2.3 shows a comparison of all results. If the obtained F_R-U curve for the reference beam having particular *element type*, *procedure type* and *initial increment size* almost overlaps with the digitized F_R-U curve, then the comparison named *good*. If the F_R-U curves do not overlap, then the comparison named either *average* or *bad* depending on the amount of deviation. According to results presented in Table 2.3 *CPE6MH* element type, *static* procedure type and *0.01* initial increment size are found to yield the best result compared to the digitized one from [1]. For this reason, element type of *CPE6MH*, procedure type of *static* and initial increment size of *0.01* are used in all analyses of this study.

Table 2.3: Effects of *element type*, *procedure type* and *initial increment size* on the F_R-U curve of the reference beam

No	Element Type (Standard/Explicit)	Procedure Type (Visco/Static)	Initial Increment Size	Agreement with the Digitized Curve (Good/Average/Bad)
1	Standard (CPE6MH)	Visco	0.1	Average
2	Standard (CPE6MH)	Visco	0.01	Good
3	Standard (CPE6MH)	Visco	0.001	Bad
4	Standard (CPE6MH)	Static	0.1	Average
5	Standard (CPE6MH)	Static	0.01	Good
6	Standard (CPE6MH)	Static	0.001	Average
7	Explicit (CPE6M)	Visco	0.1	Average
8	Explicit (CPE6M)	Visco	0.01	Average
9	Explicit (CPE6M)	Visco	0.001	Average
10	Explicit (CPE6M)	Static	0.1	Average
11	Explicit (CPE6M)	Static	0.01	Average
12	Explicit (CPE6M)	Static	0.001	Average

2.1.6 Energy Calculation Method

Trapped energy value for each beam model is computed by the total strain energy data gathered from ABAQUS. Besides, a mathematical method is used to calculate the trapped energy values of randomly chosen beams for comparison. To this end, deformation history of the beam is recorded while the prescribed displacement is applied. Recorded deformation history contains the following data: (i) the reaction force values of the nodes at the lower end of the beam which is named A in Figure 2.1b and (ii) the displacement values of the nodes at the upper end of the beam which is named B in Figure 2.1b. The reaction force (F_R)-displacement (U) graphs are drawn for each analysis with the help of this data. The energy trapping capacity of the beams

are computed from the area under F_R-U curve. For the computations, the whole F_R-U curve is divided into small rectangles. Short edge of the rectangle is determined by subtracting two consecutive displacement values while the long edge is determined by taking the half of the sum of two consecutive reaction force values. The area of all small rectangles are integrated to compute loaded, dissipated and trapped energy values for each analysis.

Figure 2.6 is a typical F_R-U curve of a bi-stable elastic beam under loading. Areas under the positive part of F_R-U curve and the negative part of F_R-U curve are pointed out and named 1 and 2, respectively. These two areas gives corresponding strain energy values. Some portion of the loaded energy is being trapped and the rest is being structurally dissipated by the system itself and/or dissipated by the interaction of the system with the medium [1]. The value calculated for the area 1 is the strain energy stored in the beam after the boundary condition is applied. The value calculated for the area 2 is the energy spent by the beam itself after the boundary condition is applied. Difference between the stored and the spent energy values is equal to the value of trapped energy in the bi-stable beam.

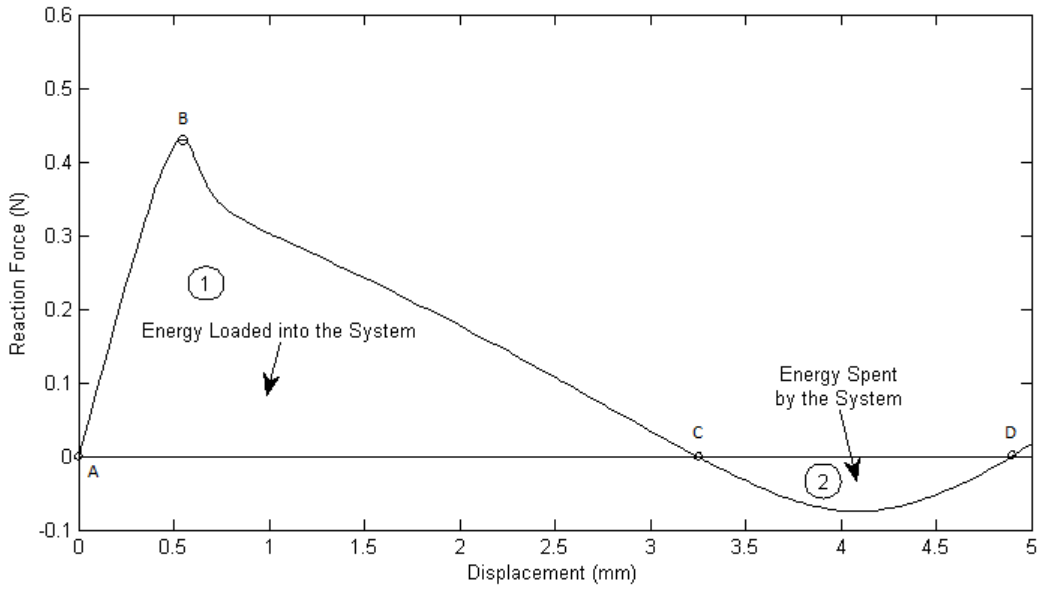

Figure 2.6: A typical load-displacement curve of a bi-stable beam. Stored energy-spent energy regions in a F_R-U graph

In Figure 2.6, the beam is first in a stable state at the point A where the displace-

ment is zero and the reaction force is zero. The beam tip goes downward direction under applied displacement boundary condition and the system reaches to the point B where the reaction force is maximum. As the beam tip keeps going downward direction, the system comes to point C where the beam is unstable and the snap-through phenomenon takes place. At this point, the system makes a large displacement until the second stable state D [16]. In Figure 2.7, the deformed shapes of the beam at points A, B, C and D are shown.

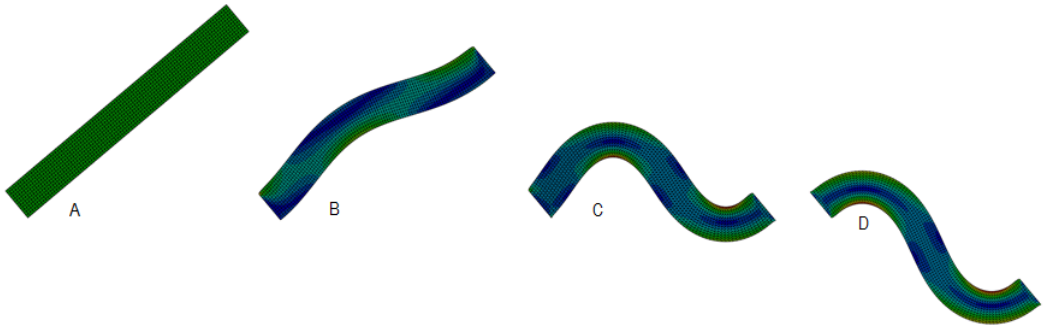

Figure 2.7: Screenshots showing deformed shapes of a straight beam when a prescribed displacement is applied in vertical direction. At point A) the beam is at its first stable state, no displacement is applied yet. At point B) a certain displacement is applied and the beam is at the point where the reaction force is maximum. At point C) the beam is unstable and transformation of the beam from one stable state to another takes place (snap-through phenomenon). At point D) the beam is at its second stable state.

Figure 2.8 is a typical F_R-U curve of a non-bistable elastic beam under loading and unloading. As seen in the figure, reaction force values of the loading and unloading curves are all positive. There is no certain displacement value at which the reaction force of the beam becomes zero. For this reason, the beam returns to its initial position when the prescribed displacement is removed. Therefore, no energy is trapped in the system.

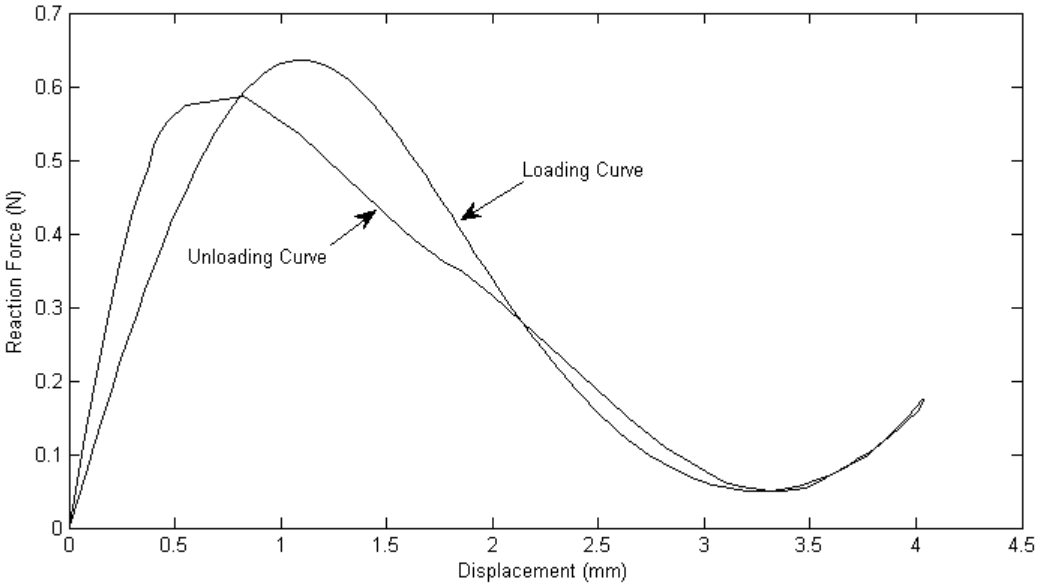

Figure 2.8: A typical F_R-U curve of a non-bistable beam

2.2 Tilt Angle Study

Effect of the tilt angle of the beam on its energy trapping capacity is investigated in this section. Bi-stability is required for the beam to be able to trap the energy as mentioned previously. Therefore, there may be some tilt angles for which the beam is not bi-stable and cannot trap the energy. The reason for being non-bistable is the snap-back behaviour of the beam instead the snap-through mechanism. Note that, there are also numerical problems for some finite element models such as self contact and penetration.

The reference tilt angle of the beam is 40 degrees. Beams having tilt angles higher and lower than 40 degrees are analyzed and results are presented in this section.

Figure 2.9 shows F_R-U curves of three different beams having tilt angles 40°, 45° and 50°. Deformed and undeformed shapes of beams having 40°, 45° and 50° tilt angle are given in Appendix A.

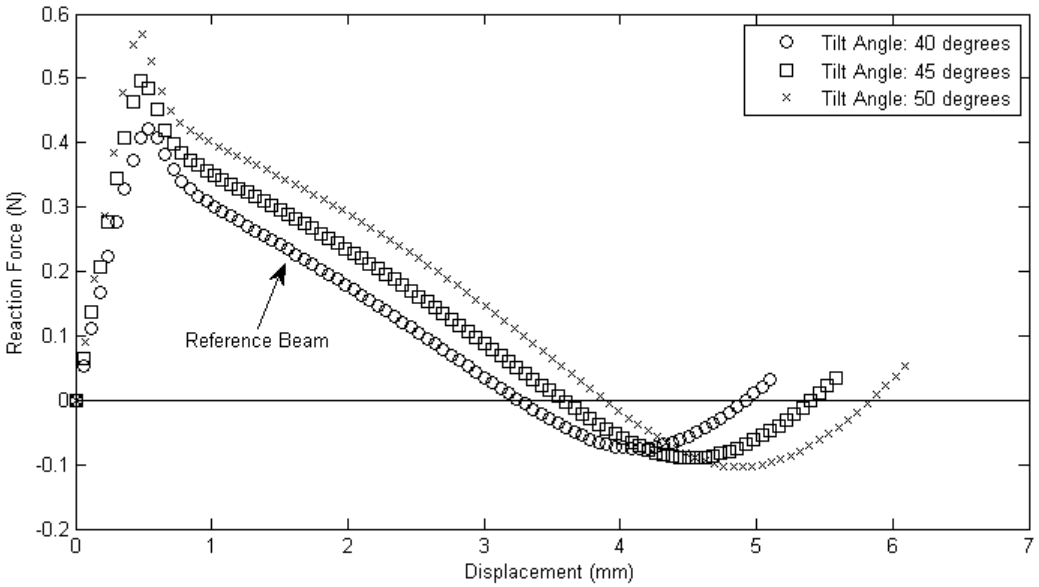

Figure 2.9: F_R-U curves of the beams for 40°, 45°, 50° tilt angles

Figure 2.10 shows F_R-U curves of three different beams having tilt angles 30°, 35° and 40°. Deformed and undeformed shapes of beams having 30°, 35° and 40° tilt angle are given in Appendix A.

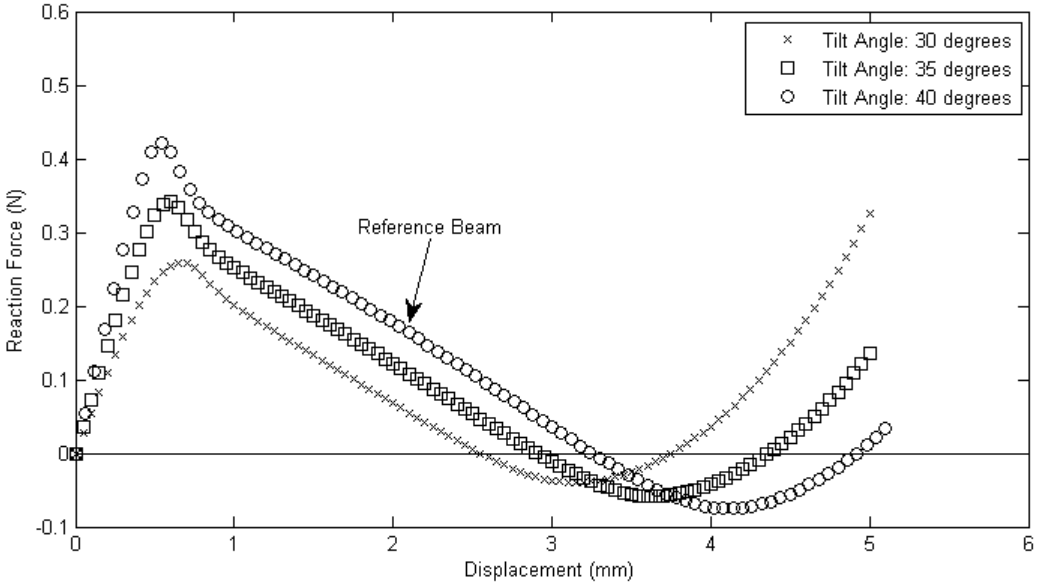

Figure 2.10: F_R-U curves of the beams for 30°, 35°, 40° tilt angles

Trapped energies for five different tilt angles are calculated and results are presented in Table 2.4. In the table, E_{in} is the amount of energy that is stored inside the beam. E_{out} is the amount of energy that is structurally dissipated by the beam itself and/or dissipated by the interaction of the beam with the medium. $E_{in} - E_{out}$ is the amount of energy that is trapped in the beam. Energy trapping values obtained from ABAQUS for each tilt angle are compared with respect to the reference beam and results are presented in the "change in trapped energy" column. The bi-stability check is also made for each trial as visualized in Figure 2.3 and results are presented in "bi-stability check" column.

Table 2.4: Energy trapping results of tilt angles 30°, 35°, 40°, 45°, 50°

Tilt Angle [°]	E_{in} [N mm]	E_{out} [N mm]	$E_{in} - E_{out}$ [N mm]	Change in Trapped Energy [%]	Bistability Check
30	0.3322	0.0273	0.3049	-44.66	Bistable
35	0.4716	0.0513	0.4203	-23.72	Bistable
40	0.6284	0.0774	0.5510	0.00	Bistable
45	0.8019	0.1043	0.6976	26.61	Bistable
50	0.9902	0.1314	0.8588	55.86	Bistable

Energy values written in Table 2.4 are calculated by ABAQUS itself. Output data given by ABAQUS at the end of each analysis enables to discover total strain energy of the modeled beam at specific displacements. Similarly, strain energy value of the beam at a point where the beam is at its second stable configuration (the point "D" in Figure 2.6) can be determined from this output data. Displacement value corresponding to the point "D" in Figure 2.6 can be specified from data compiling F_R-U curve. Total strain energy for the beam at point "D" in Figure 2.6 corresponds to the amount of strain energy that is trapped inside the beam. Trapped energy obtained directly from ABAQUS strain energy output data and calculated according to the method explained in Section 2.1.6 are compared for analyzed tilt angles and results are presented in Table 2.5.

Table 2.5: Comparison of $E_{in} - E_{out}$ values for analyzed straight beam tilt angles derived from strain energy output data given by ABAQUS and calculated according to the method explained in Section 2.1.6

Tilt Angle [°]	$E_{in} - E_{out}$ According to the Method Explained in Section 2.1.6 [N mm]	$E_{in} - E_{out}$ According to ABAQUS Output Data [N mm]	Deviation [%]
30	0.3029	0.3049	-0.66
35	0.4248	0.4203	1.07
40 (The Reference Beam)	0.5644	0.5510	2.43
45	0.7200	0.6976	3.21
50	0.8910	0.8588	3.75

It is observed from the energy results presented in Table 2.4 that the amount of trapped energy increases as tilt angle increases. Figure 2.11 shows how the trapped energy changes with tilt angle. The beam is bi-stable for the defined range of tilt angles, i.e., 30° to 50°. Tilt angles higher than 50° crash the finite element analyses. Numerical problems such as self contact and penetration arise when the tilt angle of the beam is above 50°. As an example of this, deformed and undeformed shapes of the beam with 55° tilt angle are shown in Figure A.6. Table 2.5 shows that the trapped energy values calculated by using the calculation method explained in Section 2.1.6 deviate up to 3.75% from the values obtained directly from ABAQUS strain energy output data. The reason behind this deviation might be that the method explained in Section 2.1.6 does not take into account the exact displacement values where the reaction force is zero (the points C and D in Figure 2.6). Instead, it takes into account the closest displacement point to the points C and D in Figure 2.6.

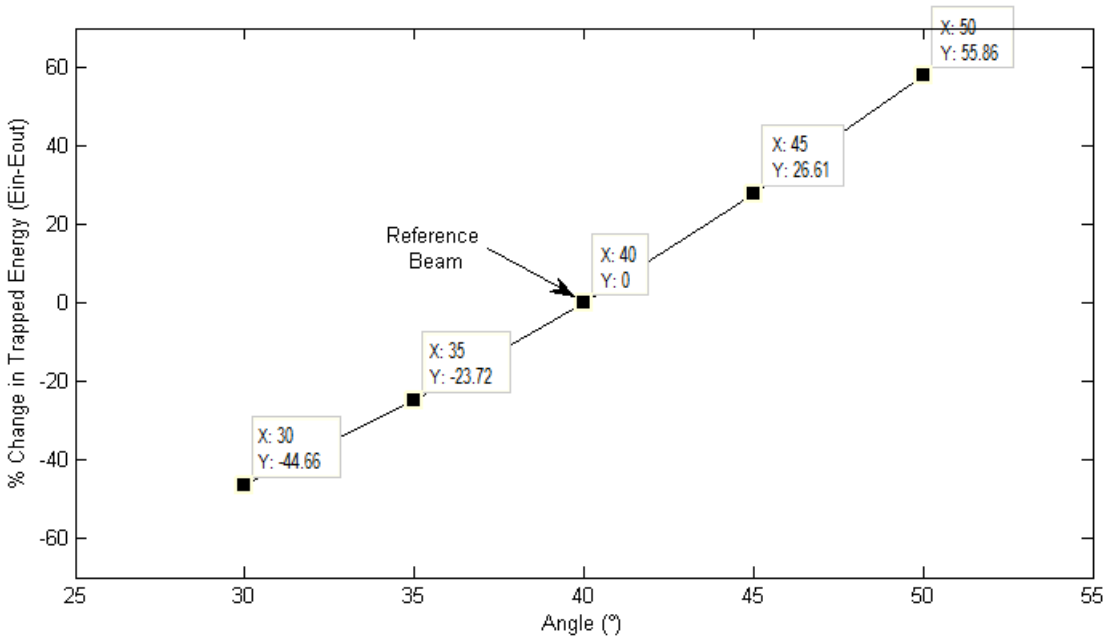

Figure 2.11: Percent change in trapped energy with tilt angle of straight beams

2.3 Straight Beam Aspect Ratio Study

The width and the length of the reference beam are 0.61 mm and 5.06 mm, respectively. Beams having more and less slender geometry than the reference beam are analyzed and energy trapping results are presented in this section. The tilt angle of the reference beam is 40° and it is kept constant in this section. Except the beam aspect ratio all other parameters of the finite element model is the same as explained in Sections 2.1.2, 2.1.3 and 2.1.4.

In analyses of this subsection, aspect ratio of the reference beam is changed. First the effects of 5 %, 10 %, 15 %, 20 % and 25 % increase of the length of the beam are analyzed. In order to keep the volume constant the width of the beam is decreased by 5%, 9%, 13%, 17% and 20% respectively. Therefore, dimensional changes are adjusted such that the volume of the beam does not change and remain the same as the reference beam. The reaction force (F_R)- displacement (U) curves of analyses are shown in Figure 2.12. Deformed and undeformed shapes of beams having 5 %, 10 %, 15 %, 20 % and 25 % increase in length are given in Appendix B.

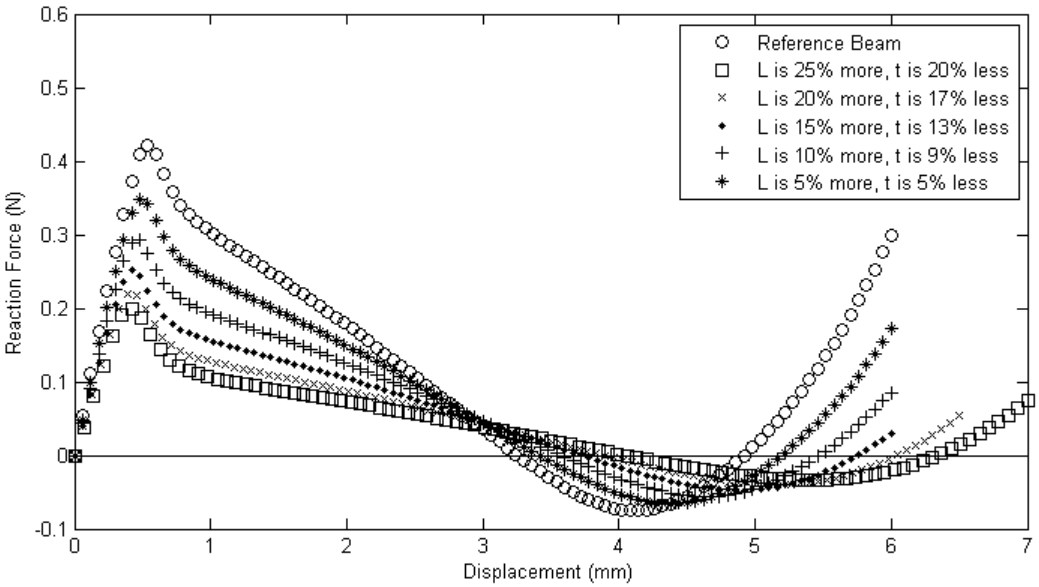

Figure 2.12: F_R-U curves of the beams that are more slender than the reference beam

Next the effects of 5 $\%$, 10 $\%$ and 15 $\%$ decrease of length of the beam are studied. In order to keep the volume constant the widths of the beams are increased by 5$\%$, 11$\%$ and 18$\%$ respectively. Calculated energy trapping results are presented in Table 2.6. The reaction force (F_R)- displacement (U) curves of each analysis are shown in Figure 2.13. Deformed and undeformed shapes of beams having 5 $\%$, 10 $\%$ and 15 $\%$ decrease in length are given in Appendix B.

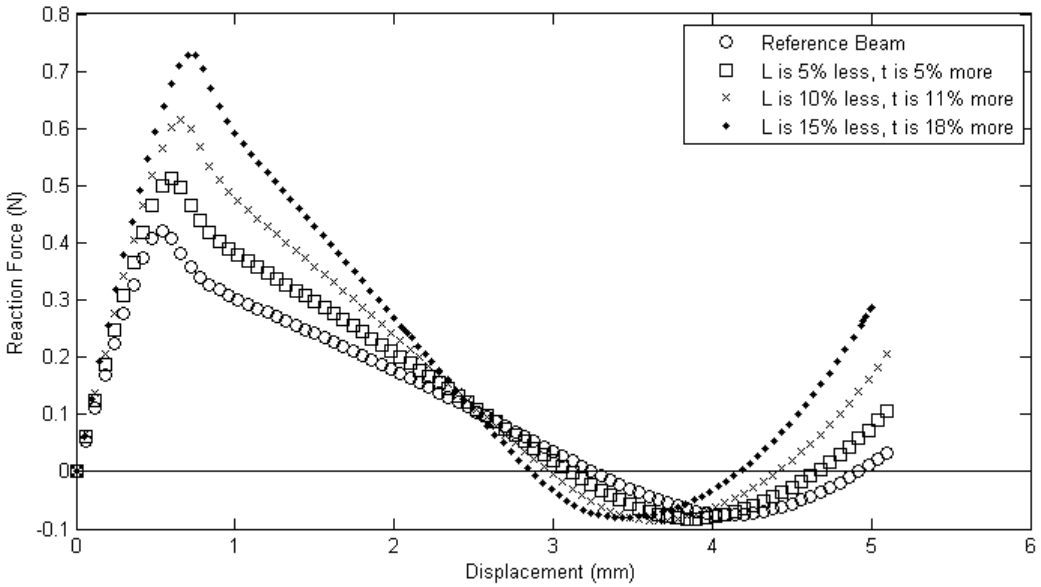

Figure 2.13: F_R-U curves of the beams that are less slender than the reference beam

Trapped energies for nine different aspect ratios are calculated and results are presented in Table 2.6. Energy trapping capacity of each analysis is compared with the reference beam and results are presented in the "change in trapped energy" column. Bi-stability check is also made for each analysis as visualized in Figure 2.3 and results are presented in "bi-stability check" column.

Table 2.6: Energy trapping results of the straight beams at different aspect ratios

Change in Width of the Beam [%]	Change in Length of the Beam [%]	E_{in} [N mm]	E_{out} [N mm]	$E_{in}-E_{out}$ [N mm]	Change in Trapped Energy [%]	Bistability Check
-20	25	0.2794	0.0447	0.2347	-57.40	Bistable
-17	20	0.3224	0.0507	0.2717	-50.69	Bistable
-13	15	0.3782	0.0586	0.3196	-42.00	Bistable
-9	10	0.4464	0.0564	0.3810	-30.85	Bistable
-5	5	0.5236	0.0719	0.4517	-18.02	Bistable
0	0	0.6284	0.0774	0.5510	0.00	Bistable
5	-5	0.7479	0.0793	0.6686	21.34	Bistable
11	-10	0.8997	0.0749	0.8248	49.69	Bistable
18	-15	0.9413	0.0932	0.8481	53.92	Bistable

It is observed that further decrease of length of the beam causes numerical problems

such as self contact and penetration which crash the computations. Self contact and penetration are also observed when the length of the reference beam is decreased by 15 % as seen in Figure B.8 but this analysis, unlike analyses with more than 15 % length decrease, completes successfully. Energy results presented in Table 2.6 show that the amount of trapped energy increases as the beam gets less slender. On the contrary, the amount of trapped energy decreases as the beam gets more slender. Figure 2.14 shows how trapped energy value of the beams changes for different length-width pairs. The beam is bi-stable for length increase up to 25% and length decrease up to 15%.

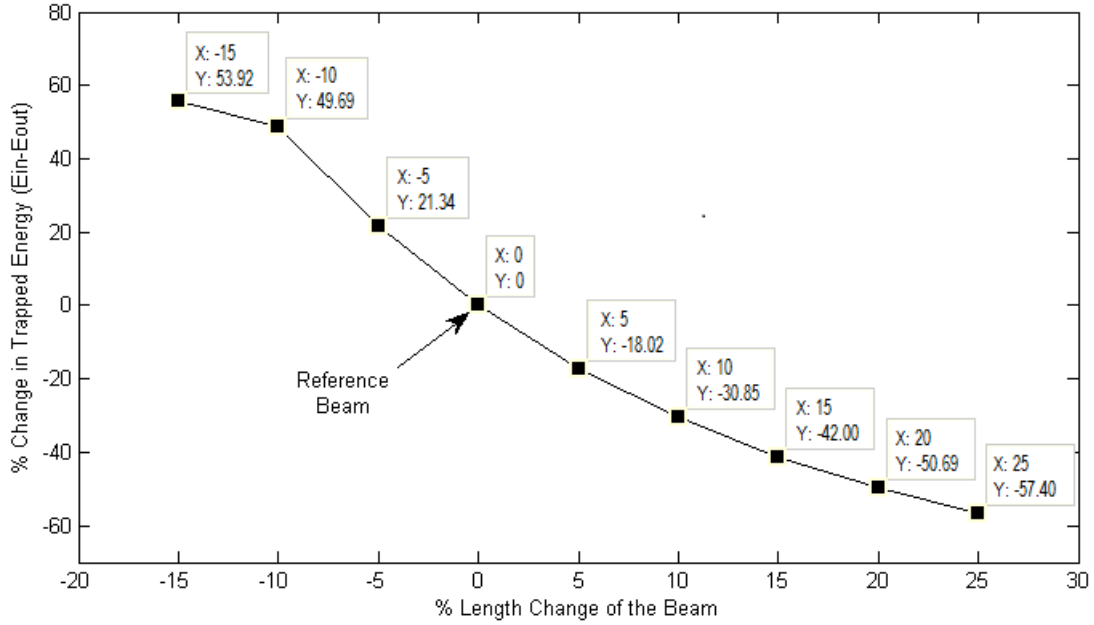

Figure 2.14: Percent change in the trapped energy for different length-width pairs of straight beams

2.4 Energy Trapping Capacity of Two Reference Beams

In case of a modular system, energy trapping capacity of a single beam enables estimation of energy trapping performance of the whole system that consists of many beams. To verify this assumption, a finite element model similar to the one in [1] is drawn. The model consists of two beams standing in tilted position and drawn according to the reference beam parameters. Very stiff material blocks are placed to the

upper and lower ends of the beams so that they do not deform during the application of the boundary condition.

Figure 2.15 shows F_R-U curve of the modeled system consisting of two reference beams along with the F_R-U curve of a single reference beam. Deformed and undeformed shapes of the constructed model consisting of two reference beams are shown in Appendix F. Table 2.7 shows trapped energy results of a single reference beam and the constructed model consisting of two reference beams. Trapped energy value of the constructed model with two reference beams is compared with value of a single reference beam and results are presented in the *Change in Trapped Energy* column.

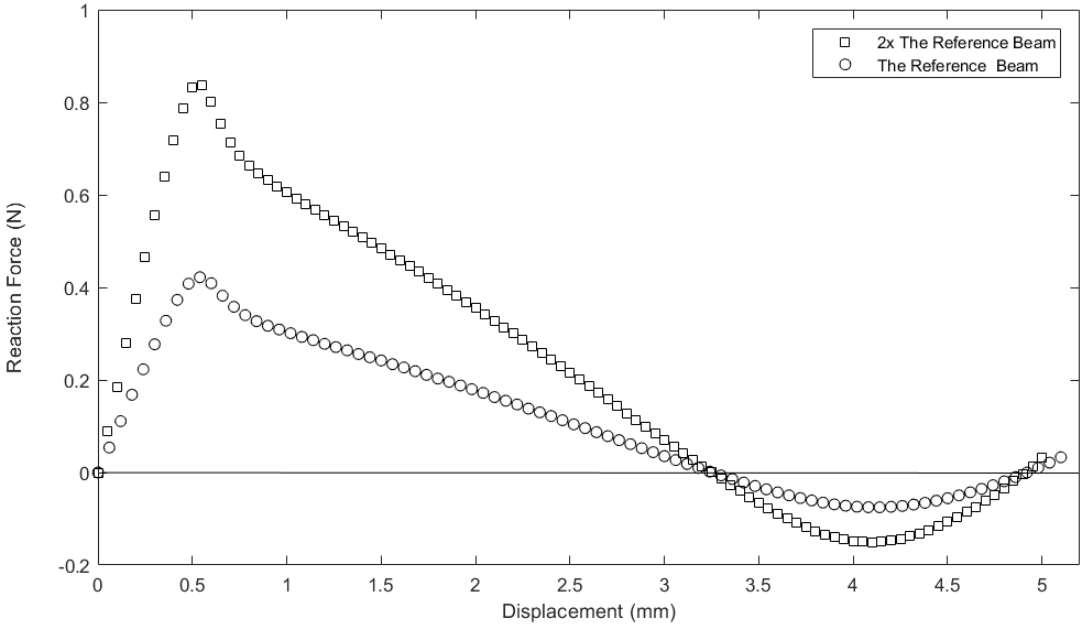

Figure 2.15: F_R-U curves of the reference beam and modeled system consisting of two reference beams

Table 2.7: Energy trapping results of the modeled system consisting of two reference beams and the reference beam itself

Name of the Analysis	E_{in} [N mm]	E_{out} [N mm]	$E_{in}-E_{out}$ [N mm]	Change in Trapped Energy [$\%$]	Bistability Check
The Reference Beam	0.6284	0.0774	0.5510	0.00	Bistable
2x The Reference Beam	1.2567	0.1549	1.1018	99.96	Bistable

It is observed that the constructed model consists of two reference beams can trap 99.96$\%$ more energy than a single reference beam. This verifies that the energy trapping capacity of a single beam can be used to compute the of energy trapping performance of the whole system.

CHAPTER 3

FINITE ELEMENT MODELING OF INCLINED CURVED ENERGY TRAPPING BEAMS

In this chapter finite element models of inclined curved energy trapping beams are explained and their analyses parameters are defined. Effects of morphological changes of the beam on its energy trapping capacity are investigated. The tilt angle and the aspect ratio studies are carried out for the curved beam that gives the best energy trapping performance. In all analyses a 2D planar beam is modeled in ABAQUS 6.12-3. Energy trapping results of each analysis are compared with the reference beam parameters that are provided in Section 2.1.1. The energy trapping values given in this section are obtained from total strain energy output data of ABAQUS.

In Section 3.1 the problem geometry, material properties, the finite element model and boundary conditions are discussed. In Section 3.2 energy trapping results regarding morphological study of the beam are presented. In Section 3.3, energy trapping results regarding tilt angle study of the curved beam which yields the best energy trapping performance among morphological trials are presented. In Section 3.4, energy trapping results regarding aspect ratio study of the curved beam which yields the best energy trapping performance among morphological trials are presented.

3.1 Problem Definition

In this chapter 2D planar beams having different geometry than the straight shaped beams investigated in Chapter 2 are considered. A displacement boundary condition is applied to one end of the beam in vertical direction while the other end is con-

strained in vertical and horizontal directions as previously explained in Section 2.1.4. Reaction force-displacement graphs are obtained for all analyses. The bi-stability check is also made for each trial as visualized previously in Figure 2.3. Details of the geometry, material parameters, parameters of the finite element model and boundary conditions are provided in the following sections.

3.1.1 Geometry

The reference beam has a straight geometry parameters of which are explained previously in Section 2.1.1. In this section, multistable elastic beams having curved geometries similar to the one shown in Figure 3.1 are analyzed. In Figure 3.1 L is the length, t is the width, θ is the tilt angle of the beam. The beam is defined with four arcs two of which are convex (arc 1 and arc 3) and the other two are concave (arc 2 and arc 4). Total number of nine geometrical variations are considered by changing number of arcs and/or radius values of arcs of the geometry shown in Figure 3.1.

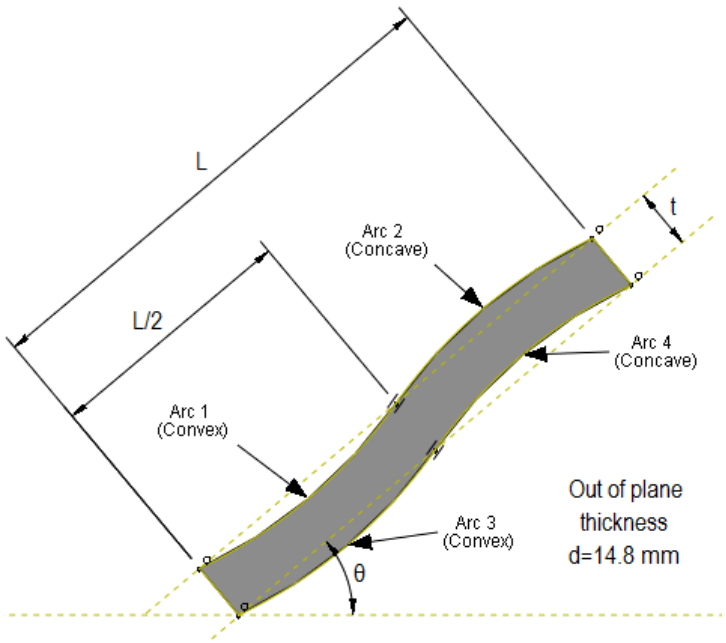

Figure 3.1: Curved beam geometry

Out of plane thickness (d) of all beams analyzed in Section 3 is taken as 14.8 mm similar to the reference beam. In all analyses of Section 3.2 L is taken as 5.06 mm, t is taken as 0.61 mm and θ is taken as 40° similar to the reference beam. Only

number of arcs and/or radius values of arcs are changed for analyses. A particular curved beam yielding the best energy trapping performance is chosen according to results of Section 3.2. In Section 3.3 the effect of the tilt angle and in Section 3.4 the effect of the aspect ratio on the chosen curved beam's energy trapping capacity are investigated. Energy trapping results for each analysis are compared with results of the reference beam and related tables are presented in Section 3.2, Section 3.3 and Section 3.4.

3.1.2 Material Properties

The material properties given in Table 2.1 are also used in all analyses of this chapter. Material behavior is again defined as hyper-elastic Neo-Hookean to model moderate to large deformations.

3.1.3 Finite Element Model

Figure 3.2 shows the finite element model of the curved beam with 0.05 mm element size. In all analyses of this section, six node CPE6MH elements are used as in Section 2. Mesh size is determined through a mesh refinement study. In "step" module, "nlgeom" option is switched on to enable large deformations. Plane strain conditions are assumed and implicit runs are carried out similar to Section 2.

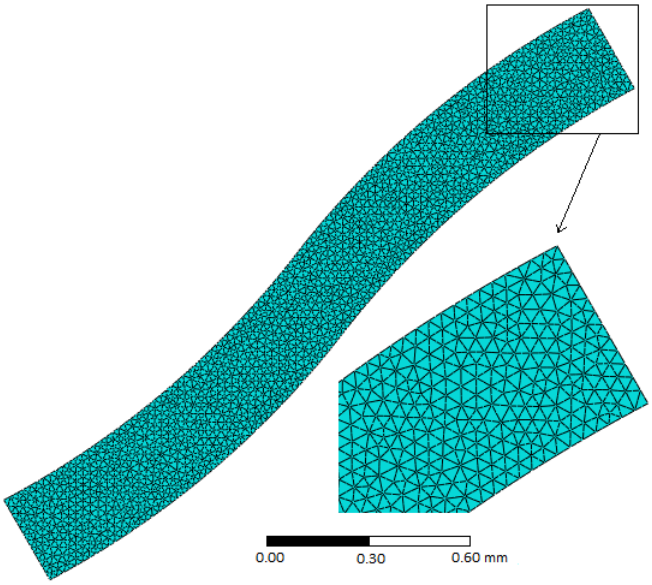

Figure 3.2: 2D finite element model of a curved beam with global mesh size 0.05 mm

3.1.4 Boundary Conditions

Boundary conditions as visualized in Figure 2.1b are applied for all curved beam models constructed in this section. The straight beam geometry shown in Figure 2.1a is replaced with a curved beam geometry for analyses of this section. The beam ends named A and B in figure remain the same. All nodes at A in Figure 2.1b are constrained both in x and y directions. A prescribed displacement is applied in y direction to all nodes at B, while they are constrained in x direction. Analyses are carried out in two steps similar to Section 2. Visualization of these two steps are previously shown in Figure 2.3.

3.2 Morphological Study

The reference beam has a straight geometry which is standing in a tilted position. The beams analyzed in this section are not restricted to have straight edges. To this end, concave, convex and s-shaped beams are studied and the energy trapping results are presented. The tilt angle of the reference beam is 40° and it is kept constant in all

analyses. Except the beam geometry all other parameters of the finite element model are the same as explained in Sections 3.1.2, 3.1.3 and 3.1.4.

A name is given to analyses. These names are given in Table 3.1 along with the corresponding geometrical parameters. Total number of nine beams including the reference beam are analyzed. The reaction force (F_R)- displacement (U) curves of each analysis are shown in Figure 3.3 and Figure 3.4.

Table 3.1: Geometrical parameters of the investigated curved beams

Name of the Analysis	Number of Arcs	Radius of the Arcs[mm]	Position of the Arcs
Reversed S-Shape	4	5	2 convex, 2 concave
3S-Shape	12	1	6 convex, 6 concave
Convex	2	15	2 convex
Concave	2	15	2 concave
The Reference Beam	0	0	Straight Shape
2S-Shape	8	5	4 convex, 4 concave
S-Shape-r20	4	20	2 convex, 2 concave
S-Shape-r6	4	6	2 convex, 2 concave
S-Shape-r5	4	5	2 convex, 2 concave

Figure 3.3 shows F_R-U curves of five different beams named *reversed s-shape*, *3s-shape*, *convex*, *concave* and the reference beam. The beams named *reversed s-shape*, *3s-shape*, *convex*, *concave* perform worse than the reference beam in terms of energy trapping capacity. Deformed and undeformed shapes of the beams named *reversed s-shape*, *3s-shape*, *convex*, *concave* and the reference beam are given in Appendix C.

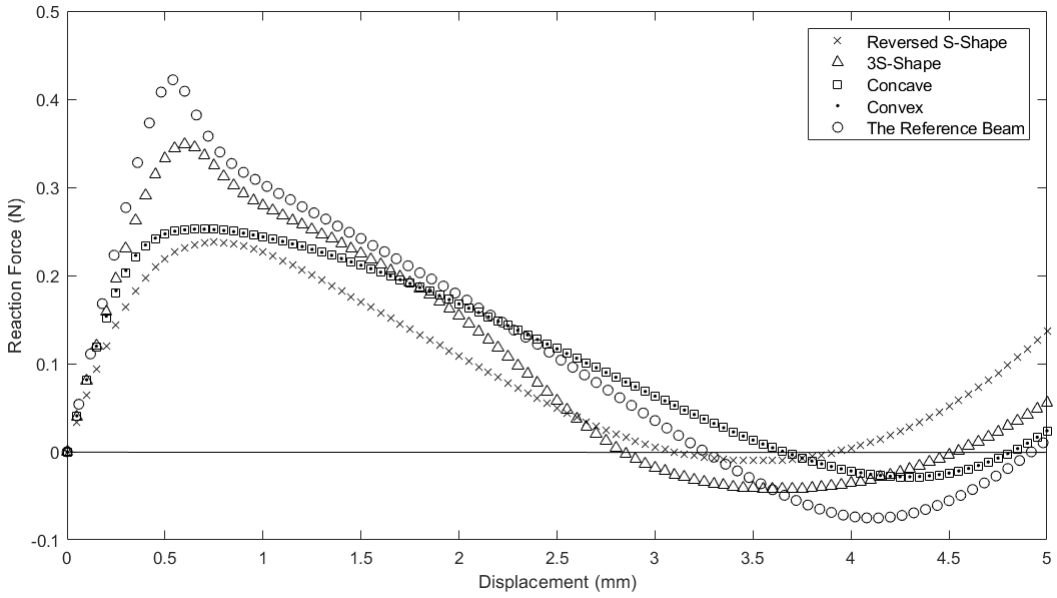

Figure 3.3: F_R-U curves of the beams performing worse than the reference beam in terms of energy trapping capacity

Figure 3.4 shows F_R-U curves of five different beams named *2s-shape*, *s-shape-r20*, *s-shape-r6*, *s-shape-r5* and the reference beam. The beams named *2s-shape*, *s-shape-r20*, *s-shape-r6*, *s-shape-r5* perform better than the reference beam in terms of energy trapping capacity. Another s-shape beam named *s-shape-r4* is modeled by further reducing the radius of concave and convex arcs but this analysis crashed due to numerical problems such as self contact and penetration. Deformed and undeformed shapes of the beams named *2s-shape*, *s-shape-r20*, *s-shape-r6*, *s-shape-r5*, the reference beam and also crashed analysis *s-shape-r4* are given in Appendix C.

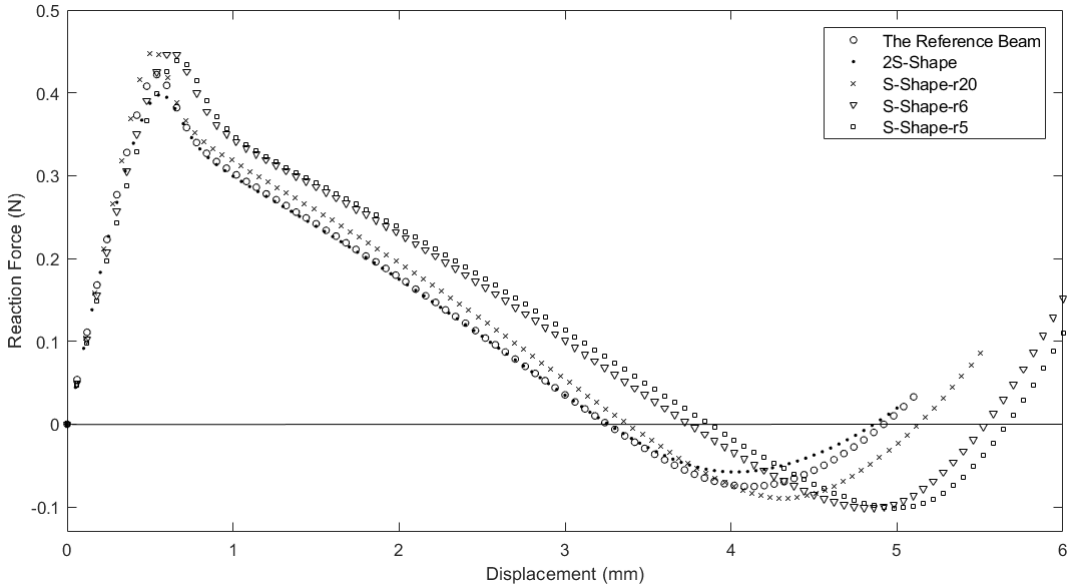

Figure 3.4: F_R-U curves of the beams performing better than the reference beam in terms of energy trapping capacity

Trapped energies for nine different curved beams including the reference beam are calculated and results are presented in Table 3.2. In the table, E_{in} is the amount of energy that is stored inside the beam. E_{out} is the amount of energy that is structurally dissipated by the beam itself and/or dissipated by the interaction of the beam with the medium. $E_{in} - E_{out}$ is the amount of energy that is trapped in the beam. Energy trapping values obtained from ABAQUS for each curved beam are compared with respect to the reference beam and results are presented in the "change in trapped energy" column. The bi-stability check is also made for each trial as visualized in Figure 2.3 and results are presented in "bi-stability check" column.

Table 3.2: Energy trapping results of the beams having different geometries

Name of the Analysis	E_{in} [N mm]	E_{out} [N mm]	$E_{in}-E_{out}$ [N mm]	Change in Trapped Energy [%]	Bistability Check
Reversed S-Shape	0.4077	0.0002	0.4075	-26.04	Bistable
3S-Shape	0.5187	0.0417	0.4770	-13.43	Bistable
Concave	0.5507	0.0198	0.5309	-3.65	Bistable
Convex	0.5512	0.0197	0.5315	-3.54	Bistable
The Reference Beam	0.6284	0.0774	0.5510	0.00	Bistable
2S-Shape	0.6184	0.0569	0.5615	1.91	Bistable
S-Shape-r20	0.6797	0.0980	0.5817	5.57	Bistable
S-Shape-r6	0.7788	0.1170	0.6618	20.11	Bistable
S-Shape-r5	0.7999	0.1192	0.6807	23.54	Bistable

As can be seen from the energy results presented in Table 3.2 a particular *s* shape of the beam can increase the energy trapping capacity up to 23.54%. *Concave* and *convex* shapes of the beam decrease its energy trapping capacity. The beam named *s-shape-r5* has the highest energy trapping capacity among other morphological trials and it has four arcs two of which are drawn concave and the other two are drawn convex. Increasing the number of arcs in an *s-shape* beam geometry does not provide extra energy trapping capacity to the beam. The arc radius of the *s-shape* beam effects the beam's energy trapping capacity. For *s-shape* beams, as the radius of the arcs decreases the energy trapping capacity of the beam increases. However, finite element analyses start to crash for lower values of arc radius. Numerical problems such as self contact and penetration arise when the radius of arcs is set very low. All beams analyzed in this section are found to be bi-stable.

3.3 Tilt Angle Study

Morphological study carried out in Section 3.2 showed that the beam named *s-shape-r5* has the highest energy trapping capacity among the other geometrical trials. Effects of tilt angle of the beam *s-shape-r5* on its energy trapping capacity are further studied in this section. To this end, except the tilt angle all other parameters of the finite element model of the beam *s-shape-r5* are kept constant. In Section 3.2, the tilt angle of the beam *s-shape-r5* is taken the same as the reference tilt angle, 40°. Beam *s-*

shape-r5 having 30°, 35°, 40°, 45° and 50° tilt angle are analyzed and energy trapping results are presented in this section.

Figure 3.5 shows F_R-U curves of the reference beam and the beams *s-shape-r5* having tilt angles 30° and 35°. Beams *s-shape-r5* having tilt angles 30° and 35° perform worse than the reference beam in terms of energy trapping capacity. On the contrary, Figure 3.6 shows F_R-U curves of the reference beam and the beams *s-shape-r5* having tilt angles 40°, 45° and 50°. Beams *s-shape-r5* with tilt angles 40°, 45° and 50° perform better than the reference beam in terms of energy trapping capacity. Deformed and undeformed shapes of the beams *s-shape-r5* with various tilt angles are given in Appendix D.

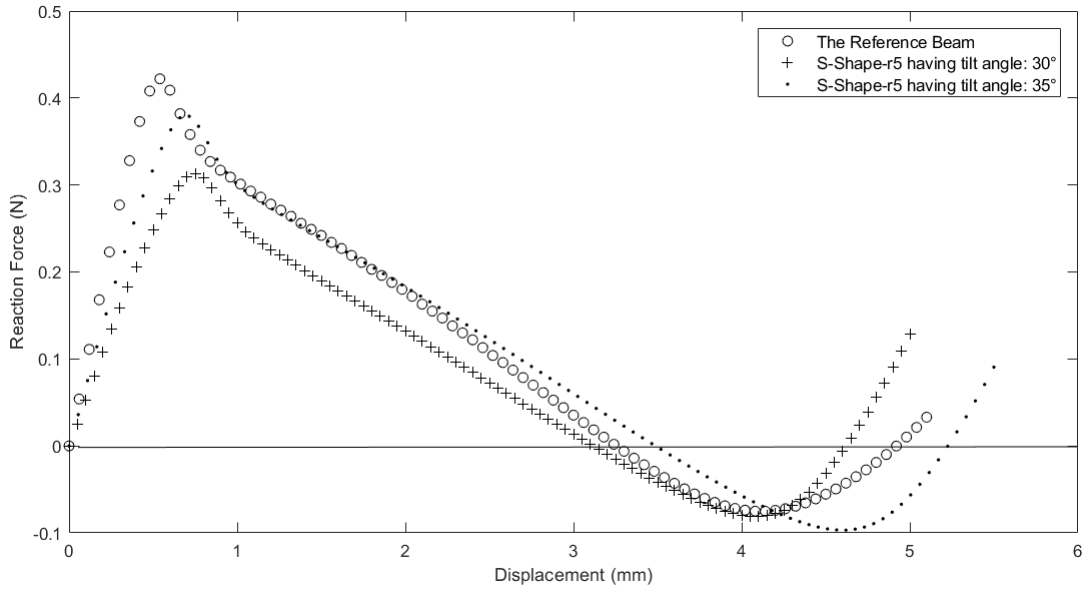

Figure 3.5: F_R-U curves of the reference beam and the beams *s-shape-r5* with tilt angles 30° and 35°

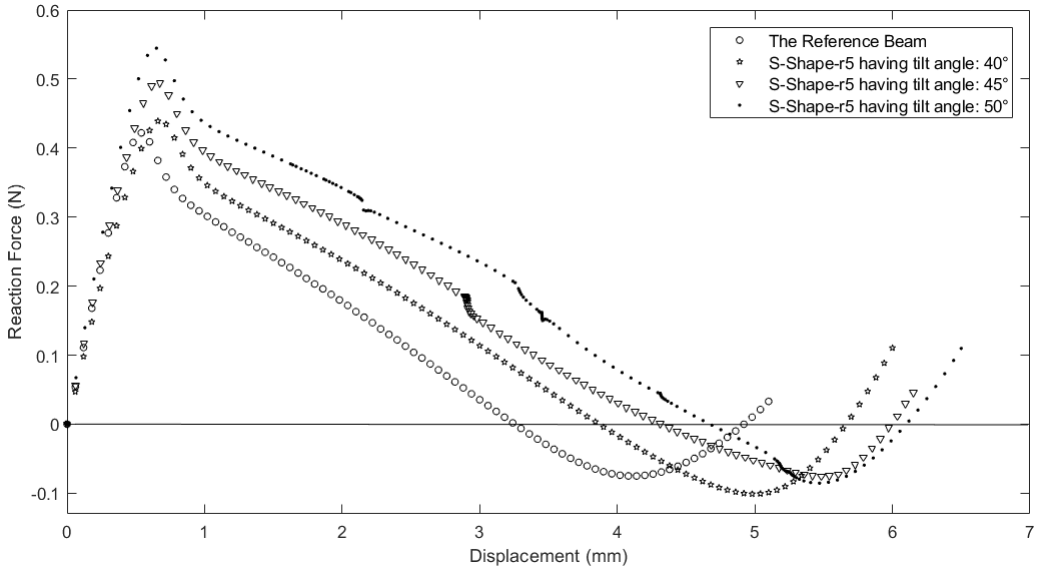

Figure 3.6: F_R-U curves of the reference beam and the beam *s-shape-r5* having tilt angles 40°, 45° and 50°

Trapped energies for five different tilt angles 30°, 35°, 40°, 45° and 50° of the beam *s-shape-r5* are calculated and results are presented in Table 3.3. Energy trapping capacity of each analysis is compared with the reference beam and results are presented in the "change in trapped energy" column. The bi-stability check is also made for each analysis as visualized in Figure 2.3 and results are presented in "bistability check" column.

Table 3.3: Energy trapping results of the beams *s-shape-r5* with tilt angles 30°, 35°, 40°, 45° and 50°

Tilt Angle [°]	E_{in} [N mm]	E_{out} [N mm]	$E_{in} - E_{out}$ [N mm]	Change in Trapped Energy [%]	Bistability Check
30	0.4673	0.0781	0.3892	-29.36	Bistable
35	0.6223	0.1082	0.5141	-6.70	Bistable
The Reference Beam	0.6284	0.0774	0.5510	0.00	Bistable
40	0.7999	0.1192	0.6807	23.54	Bistable
45	0.9649	0.0857	0.8792	59.56	Bistable
50	1.1944	0.0926	1.1018	99.96	Bistable

It is observed from the energy results presented in Table 3.3 that the amount of trapped

energy increases as the tilt angle increases. The beam is bi-stable for the defined range of tilt angles, i.e., 30° to 50°. Figure 3.7 shows how the trapped energy changes with tilt angle of the curved beam *s-shape-r5*. Finite element analyses crash for tilt angles higher than 50. Numerical problems such as self contact and penetration arise when the tilt angle of the beam *s-shape-r5* is above 50°. During the analyses of the beam *s-shape-r5* for 45° and 50° tilt angles self contact also occur at particular vertical displacements of the upper end of the beam. It occurs at about 3 mm vertical displacements of the upper end of the beam for 45° and it occurs at about 2 mm and 3.5 mm vertical displacements of the upper end of the beam for 50° tilt angle. Therefore, as the vertical displacement of the upper end of the beam increases self contacts disappear and both analyses complete successfully. The deformed shape of the beam *s-shape-r5* with mentioned self contact at 45° tilt angle is shown in Figure D.5 and deformed shapes of the beam *s-shape-r5* with mentioned self contacts at 50° tilt angle are shown in Figures D.7 and D.8.

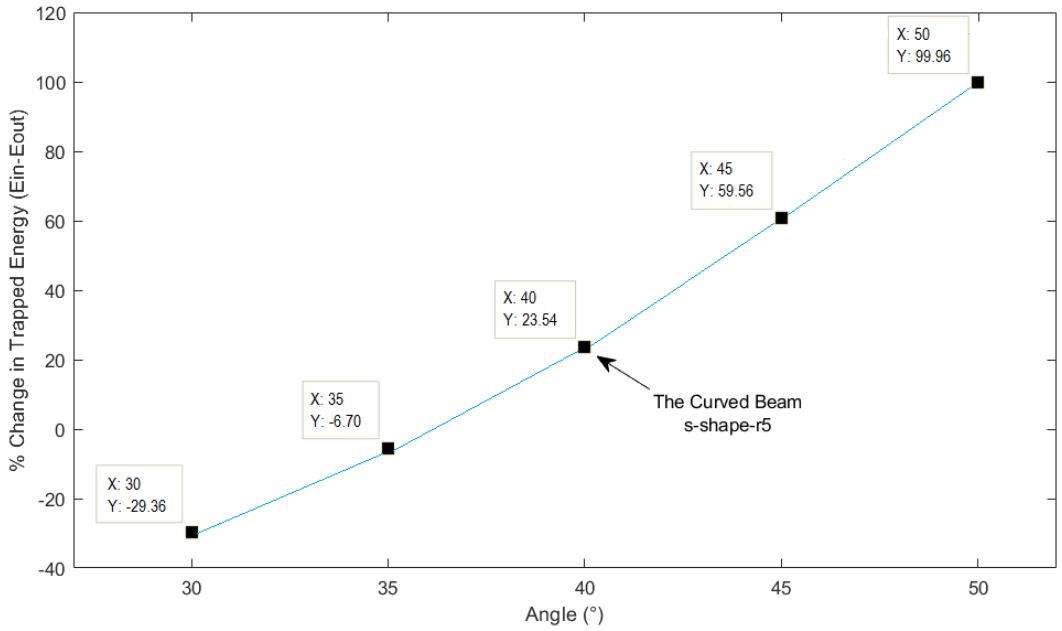

Figure 3.7: Percent change in trapped energy with tilt angle of the curved beam *s-shape-r5*

3.4 Curved Beam Aspect Ratio Study

The width and the length of the beam *s-shape-r5* are 0.61 mm and 5.06 mm, respectively. Beams having more and less slender geometry than the beam *s-shape-r5* are analyzed and energy trapping results are presented in this section. The tilt angle of the beam *s-shape-r5* is 40° and it is kept constant in this section. Except the beam aspect ratio all other parameters of the finite element model is the same as explained in Sections 3.1.2, 3.1.3 and 3.1.4.

In analyses of this subsection, aspect ratio of the curved beam *s-shape-r5* is changed. First the effects of 5 % and 10 % increase of the length of the beam are analyzed. In order to keep the volume constant the width of the beam is decreased by 5% and 9% respectively. Therefore, dimensional changes are adjusted such that the volume of the beam does not change and remain the same as the reference beam. The reaction force (F_R)- displacement (U) curves of the analyses *s-shape-r5* with 5 % and 10 % increase of the length along with curves of the reference beam and the beam *s-shape-r5* with original dimensions are shown in Figure 3.8. Deformed and undeformed shapes of beams having 5 % and 10 % increase in length are given in Appendix E.

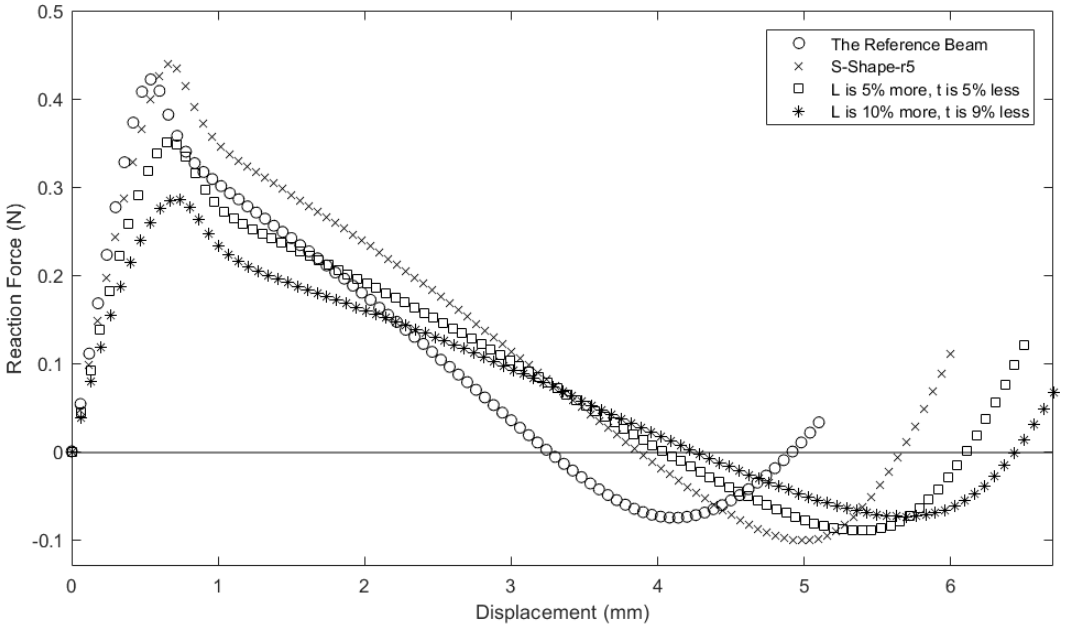

Figure 3.8: F_R-U curves of the curved beam *s-shape-r5* for aspect ratios that perform worse than the reference beam and the beam *s-shape-r5* with original dimensions in terms of energy trapping capacity

Next the effects of 5 $\%$ and 10 $\%$ decrease of length of the beam are studied. In order to keep the volume constant the widths of the beams are increased by 5$\%$ and 11$\%$ respectively. Calculated energy trapping results are presented in Table 3.4. The reaction force (F_R)- displacement (U) curves of the analyses *s-shape-r5* with 5 $\%$ and 10 $\%$ decrease of the length along with curves of the reference beam and the beam *s-shape-r5* with original dimensions are shown in Figure 3.9. Deformed and undeformed shapes of beams having 5 $\%$ and 10 $\%$ decrease in length are given in Appendix E.

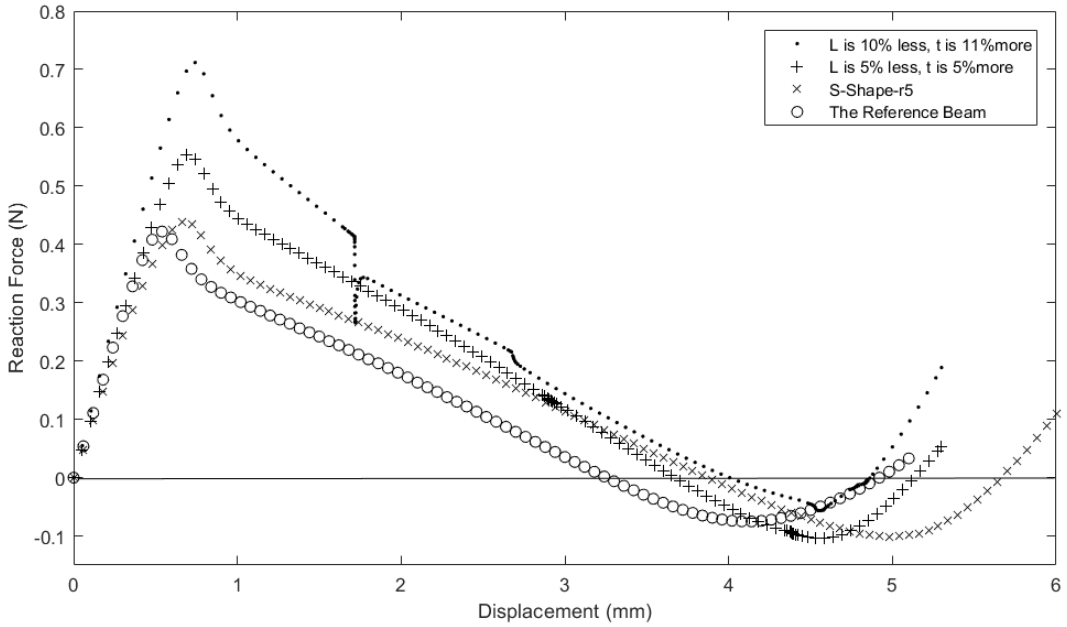

Figure 3.9: F_R-U curves of the curved beam *s-shape-r5* for aspect ratios that perform better than the reference beam and the beam *s-shape-r5* with original dimensions in terms of energy trapping capacity

Trapped energies for four different aspect ratios are calculated and results are presented in Table 3.4 along with the results of the curved beam *s-shape-r5* with original dimensions and the reference beam. Energy trapping capacity of each analysis is compared with the reference beam and results are presented in the "change in trapped energy" column. Bi-stability check is also made for each analysis as visualized in Figure 2.3 and results are presented in "bi-stability check" column.

Table 3.4: Energy trapping results related to aspect ratio study of the curved beam s-shape-r5

Change in Width of the Beam [%]	Change in Length of the Beam [%]	E_{in} [N mm]	E_{out} [N mm]	$E_{in}-E_{out}$ [N mm]	Change in Trapped Energy [%]	Bistability Check
-9	10	0.5629	0.1074	0.4555	-17.33	Bistable
-5	5	0.6606	0.1230	0.5376	-2.43	Bistable
The Reference Beam		0.6284	0.0774	0.5510	0.00	Bistable
0	0	0.7999	0.1192	0.6807	23.54	Bistable
5	-5	0.9591	0.1011	0.8580	55.72	Bistable
11	-10	1.1186	0.0343	1.0843	96.79	Bistable

It is observed that further decrease on length of the beam *s-shape-r5* causes numerical problems such as self contact and penetration which crash the computations. Self contact and penetration are also observed when the length of the beam *s-shape-r5* is decreased by 10 % as seen in Figure E.4 but this analysis, unlike analyses with more than 10 % length decrease, completes successfully. The deformed shape of the beam *s-shape-r5* with 10 % decrease of length is shown in Figure E.5 with mentioned self contact occurred at about 1.8 mm displacement. Energy results presented in Table 3.4 shows that the amount of trapped energy increases as the beam *s-shape-r5* gets less slender. The beam is bi-stable for length increase up to 10% and length decrease up to 10%. Figure 3.10 shows how trapped energy value of the curved beam *s-shape-r5* changes for different length-width pairs.

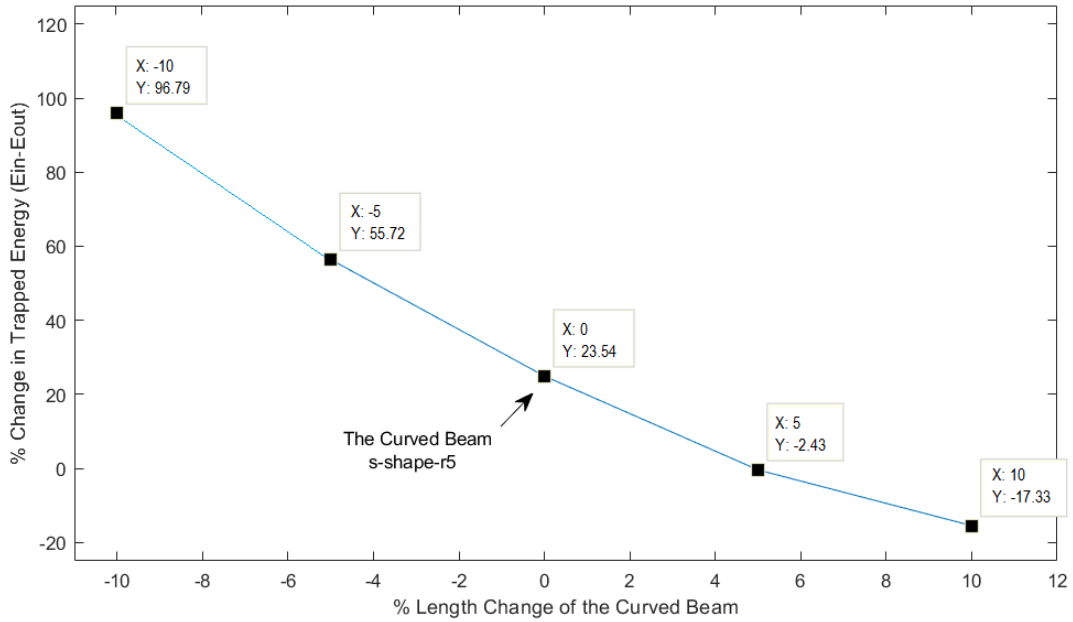

Figure 3.10: Percent change in trapped energy for different length-width pairs of the curved beam *s-shape-r5*

CHAPTER 4

CONCLUSION

In the first part of the thesis, Chapter 2, 2D planar beams having straight shapes are modeled. A straight beam geometry as proposed in [1] is chosen as a reference beam geometry for the finite element analyses. The tilt angle and the aspect ratio of the reference beam are changed and their effects on the beam's energy trapping capacity are investigated. The reference tilt angle of the beam is 40°. F_R-U curves of the beams for 30°, 35°, 40°, 45° and 50° tilt angles are drawn and trapped energies are calculated from the F_R-U curves. Energy trapping values calculated according to the method explained in Section 2.1.6 and obtained from ABAQUS strain energy output data are compared for randomly chosen particular analyses and results are presented. The rest of the energy trapping values are obtained from ABAQUS strain energy output data. A model consists of two reference beams is constructed to check whether its energy trapping capacity is two times the energy trapping capacity of a single reference beam. It is observed that the tilt angle of the reference beam can increase the beam's energy trapping capacity up to 55.86$\%$ and decrease it up to 44.66$\%$ for the defined range of tilt angles, i.e., 30° to 50°. It is concluded that amount of trapped energy increases as tilt angle of a straight beam increases. Bi-stability of the beam is required to trap the strain energy stored in the system. The beam is found bi-stable for investigated tilt angles 30°,35°, 40°, 45° and 50°. Tilt angles higher than 50° crash the finite element analyses. Numerical problems such as self contact and penetration arise when the tilt angle of the beam is above 50°. The width and length values of the reference beam are changed for the aspect ratio studies. Beams having more and less slender geometry than the reference beam are analyzed. To this end, 5 $\%$, 10 $\%$, 15 $\%$, 20 $\%$, 25 $\%$ increase and 5 $\%$, 10 $\%$ and 15 $\%$ decrease of the length of the beam are considered.

The width of the beam is adjusted so that the volume of the beam does not change. It is important to keep the volume of the beam constant while changing the other parameters to make a true comparison during the entire thesis. It is observed that the slenderness of the reference beam can decrease its energy trapping capacity up to 57.40% and thicker beams than the reference beam can increase it up to 53.92% for length increase up to 25% and length decrease up to 15% respectively. Decreasing the length of the reference beam more than 15 % causes numerical problems such as self contact and penetration which crash the computations. The beam is found bi-stable for length increase up to 25% and length decrease up to 15%. It is also observed that energy trapping capacity of the model consists of two reference beams is two times the energy trapping capacity of a single reference beam.

In the second part of the thesis, Chapter 3, 2D planar beams having curved shape are modeled. The beams consist of either concave or convex arcs or both unlike the straight shapes investigated in Chapter 2. Total number of nine beams are analyzed. Geometries are varied by changing number and radius of arcs. To this end, concave, convex and s-shape beams are analyzed and trapped energies are calculated. The tilt angle of the reference beam is 40° and it is kept constant for geometrical trials. It is observed among nine geometrical trials that having a curved shape can increase the reference beam's energy trapping capacity up to 23.54% and decrease it up to 26.04%. It is concluded that beams consisting of either concave or convex arcs decrease its energy trapping capacity. Therefore, the beam named *s-shape-r5* consisting of four arcs two of which are concave and the other two are convex has the highest energy trapping capacity among nine trials. Increasing the number of arcs in an *s-shape* beam geometry does not provide extra energy trapping capacity to the beam. The arc radius of the *s-shape* beams effects the beam's energy trapping capacity. For *s-shape* beams, as the radius of the arcs decreases the energy trapping capacity of the beam increases. However, finite element analyses start to crash for lower values of arc radius. All nine beams analyzed for geometrical trials are found to be bi-stable. A tilt angle study is carried out for the curved beam that gives the best energy trapping performance, namely, *s-shape-r5*. The beams *s-shape-r5* with 30°, 35°, 40°, 45° and 50° tilt angle are analyzed and trapped energies are calculated. It is observed that the tilt angle of the beam *s-shape-r5* can increase the beam's energy trapping capacity up

to 99.96% and decrease it up to 29.36% for defined range of tilt angles, i.e., 30° to 50°. It is concluded that amount of trapped energy increases as tilt angle of the beam *s-shape-r5* increases. The beams *s-shape-r5* are found bi-stable for all investigated tilt angles 30°,35°, 40°, 45° and 50°. The tilt angles higher than 50° crash the finite element analyses. Moreover, an aspect ratio study is carried out for the beam *s-shape-r5*. It is observed that the slenderness of the beam *s-shape-r5* can decrease its energy trapping capacity up to 17.33% and thicker beams than the beam *s-shape-r5* can increase it up to 96.79% for length increase up to 10% and length decrease up to 10% respectively. Decreasing the length of the beam *s-shape-r5* more than 10 % causes numerical problems such as self contact and penetration which crash the computations. The beam is found bi-stable for length increase up to 10% and length decrease up to 10%.

Numerical analyses carried out during the theses revealed that the energy trapping capacity of the beam increases either when the tilt angle of the beam increases or as the beam gets less slender. The scientific explanation of this increase can be related to bending energy and moment of inertia of the beams. All beams analyzed during the theses have the same out of plane thickness value of 14.8 mm. Therefore, the width of the beams has changed for aspect ratio studies to have more or less slender beams. Moment of inertia of the beams is directly proportional with both out of plane thickness and width of the beams. For this reason, when the beam gets less slender which means its width is increased, its moment of inertia also increases which results in more effective resistance to bending.

It is concluded from all analyses carried out during the thesis that the *s-shape* beam with length as 5.06 mm, width as 0.61 mm, radius of its all four arcs as 5 mm and the tilt angle as 50° gives the best energy trapping capacity which is 99.96% more than the reference beam. A beam *s-shape-r5* having length as 4.55 mm, width as 0.68 mm, radius of its all four arcs as 5 mm and the tilt angle as 40° gives the second highest energy trapping capacity which is 96.79% higher than the reference beam. Geometrical variations of the beam analyzed during the thesis can be extended for the future work. *S-shape* geometries are found to have two times more energy trapping capacity than the reference beam. Other geometries may give higher energy trapping results than the *s-shapes*. Effects of material type on the energy trapping capacity of

the beam can also be studied. Using especially visco-elastic materials may give good results in terms of energy trapping capacity.

One may find the trapped energy value of the beam *s-shape-r5* having the highest energy trapping capacity low to be used as an energy absorber. Therefore, dimensions of the beam is very low and hyper-elastic material properties are defined for the beam material. As a big advantage, its property of being elastic provides usage of the beam many times unlike the conventional plastically deforming energy absorbers. For instance, a bicycle helmet can be made of elastic multi-stable beams in the future. According to Canadian Standards Association, the conventional helmets are being dropped at a height of 1.6 meters and headform accelerations(g) are expected not to exceed 250 g [24]. This equals to impact energy of 80 joules [25]. The length, width and out of plane thickness of the beam *s-shape-r5* yielding the highest energy trapping capacity are 5.06 mm, 0.61 mm and 14.8 mm, respectively. An approximate mathematical calculation reveals that 72608 number of *s-shape-r5* beams are required to provide 80 joules of impact energy absorbance. This number of beams can be fit in a square prism with the dimensions of 300 x 300 x 170 mm.

REFERENCES

[1] S. Shan, S. H. Kang, J. R. Raney, P. Wang, L. Fang, F. Candido, J. A. Lewis, and K. Bertoldi, "Multistable architected materials for trapping elastic strain energy," *Advanced Materials*, vol. 27, no. 29, pp. 4296–4301, 2015.

[2] L. R. Meza, S. Das, and J. R. Greer, "Strong, lightweight, and recoverable three-dimensional ceramic nanolattices," *Science*, vol. 345, no. 6202, pp. 1322–1326, 2014.

[3] T. Chen, J. Mueller, and K. Shea, "Integrated design and simulation of tunable, multi-state structures fabricated monolithically with multi-material 3d printing," *Scientific Reports*, vol. 7, pp. 45671–45678, 2017.

[4] D. M. Correa, T. Klatt, S. Cortes, M. Haberman, D. Kovar, and C. Seepersad, "Negative stiffness honeycombs for recoverable shock isolation," *Rapid Prototyping Journal*, vol. 21, no. 2, pp. 193–200, 2015.

[5] D. Restrepo, N. D. Mankame, and P. D. Zavattieri, "Phase transforming cellular materials," *Extreme Mechanics Letters*, vol. 4, pp. 52–60, 2015.

[6] B. Haghpanah, L. Salari-Sharif, P. Pourrajab, J. Hopkins, and L. Valdevit, "Multistable shape-reconfigurable architected materials," *Advanced Materials*, vol. 28, no. 36, pp. 7915–7920, 2016.

[7] B. Haghpanah, A. Shirazi, L. Salari-Sharif, A. G. Izard, and L. Valdevit, "Elastic architected materials with extreme damping capacity," *Extreme Mechanics Letters*, vol. 17, pp. 56–61, 2017.

[8] K. Che, C. Yuan, J. Wu, H. J. Qi, and J. Meaud, "Three-dimensional-printed multistable mechanical metamaterials with a deterministic deformation sequence," *Journal of Applied Mechanics*, vol. 84, no. 1, p. 011004, 2017.

[9] S. Heimbs, "Energy absorption in aircraft structures," in *International Workshop on Hydraulic Equipment and Support Systems for Mining, Huludao, China*, pp. 17–18, 2012.

[10] M. S. Uddin, J. Quintel, and G. Zivkovic, "On the design of energy absorbing crash buffers for high speed roadways," *Open journal of safety science and technology*, vol. 6, no. 1, pp. 11–24, 2016.

[11] M. Ali, A. Qamhiyah, D. Flugrad, and M. Shakoor, "Compact energy absorbing cellular structure," *WIT Transactions on The Built Environment*, vol. 87, pp. 413–420, 2006.

[12] T. Frenzel, C. Findeisen, M. Kadic, P. Gumbsch, and M. Wegener, "Tailored buckling microlattices as reusable light-weight shock absorbers," *Advanced Materials*, vol. 28, no. 28, pp. 5865–5870, 2016.

[13] K. Bertoldi, "Harnessing instabilities to design tunable architected cellular materials," *Annual Review of Materials Research*, vol. 47, pp. 51–61, 2017.

[14] N. Kidambi, R. Harne, and K. Wang, "Strain energy trapping due to energetic asymmetry in modular structures inspired by muscle cross-bridges," in *ASME 2016 International Design Engineering Technical Conferences and Computers and Information in Engineering Conference*, pp. V008T10A052–V008T10A052, American Society of Mechanical Engineers, 2016.

[15] A. Rafsanjani, A. Akbarzadeh, and D. Pasini, "Snapping mechanical metamaterials under tension," *Advanced Materials*, vol. 27, no. 39, pp. 5931–5935, 2015.

[16] J. Casals-Terre and A. Shkel, "Dynamic analysis of a snap-action micromechanism," in *Sensors, 2004. Proceedings of IEEE*, pp. 1245–1248, IEEE, 2004.

[17] Y.-Y. Huang and Y.-J. Yang, "Study of snap-through behavior of a bistable mechanism for a mems optical switch," in *NSTI Nanotech*, vol. 3, pp. 173–176, 2007.

[18] J. Bishop, Q. Dai, Y. Song, and R. L. Harne, "Resilience to impact by extreme energy absorption in lightweight material inclusions constrained near a critical point," *Advanced Engineering Materials*, vol. 18, no. 11, pp. 1871–1876, 2016.

[19] B. Camescasse, A. Fernandes, and J. Pouget, "Bistable buckled beam: Elastica modeling and analysis of static actuation," *International Journal of Solids and Structures*, vol. 50, no. 19, pp. 2881–2893, 2013.

[20] J. Zhao, J. Jia, X. He, and H. Wang, "Post-buckling and snap-through behavior of inclined slender beams," *Journal of Applied Mechanics*, vol. 75, no. 4, p. 041020, 2008.

[21] D. Seibert and N. Schoche, "Direct comparison of some recent rubber elasticity models," *Rubber chemistry and technology*, vol. 73, no. 2, pp. 366–384, 2000.

[22] C. S. Ha, R. S. Lakes, and M. E. Plesha, "Design, fabrication, and analysis of lattice exhibiting energy absorption via snap-through behavior," *Materials & Design*, vol. 141, pp. 426–437, 2018.

[23] D. Systèmes, "Abaqus documentation," *Providence, RI, United States*, 2012.

[24] P. A. Cripton, D. M. Dressler, C. A. Stuart, C. R. Dennison, and D. Richards, "Bicycle helmets are highly effective at preventing head injury during head impact: Head-form accelerations and injury criteria for helmeted and unhelmeted impacts," *Accident Analysis & Prevention*, vol. 70, pp. 1–7, 2014.

[25] T. A. Connor, S. Meng, and D. Zouzias, *Current Standards for Sports and Automotive Helmets: A Review*, 2016. Report for HEAD PROTECTION: A EUROPEAN TRAINING NETWORK FOR ADVANCED DESIGNS IN SAFETY.

APPENDIX A

DEFORMED AND UNDEFORMED SHAPES OF STRAIGHT BEAMS RELATED TO ANGLE STUDY

A.1 Images Taken from Analysis of the Straight Beam Having Tilt Angle 30°

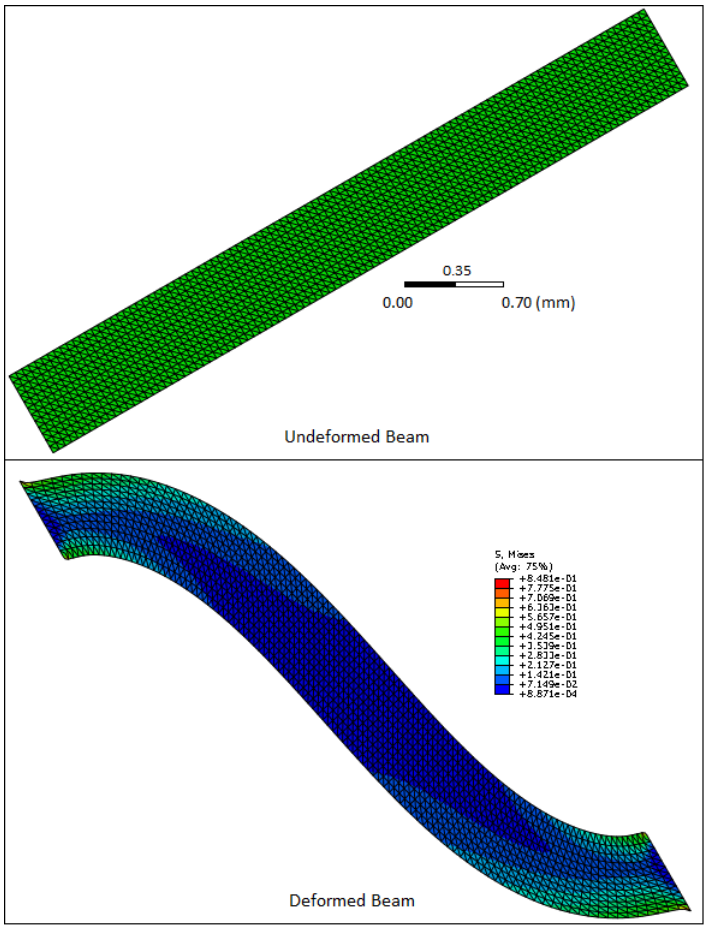

Figure A.1: Undeformed-deformed shape of the beam for 30° tilt angle

A.2 Images Taken from Analysis of the Straight Beam Having Tilt Angle 35°

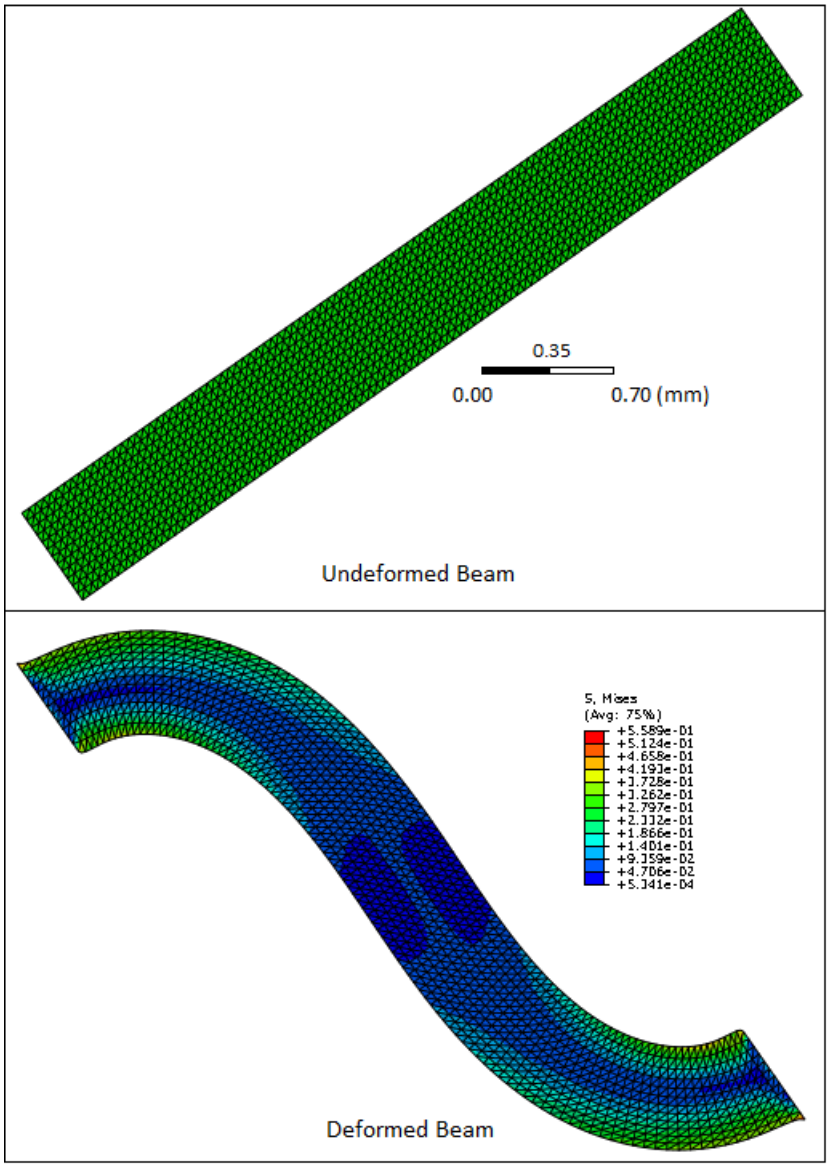

Figure A.2: Undeformed-deformed shape of the beam for 35° tilt angle

A.3 Images Taken from Analysis of the Straight Beam Having Tilt Angle 40° (The Reference Beam)

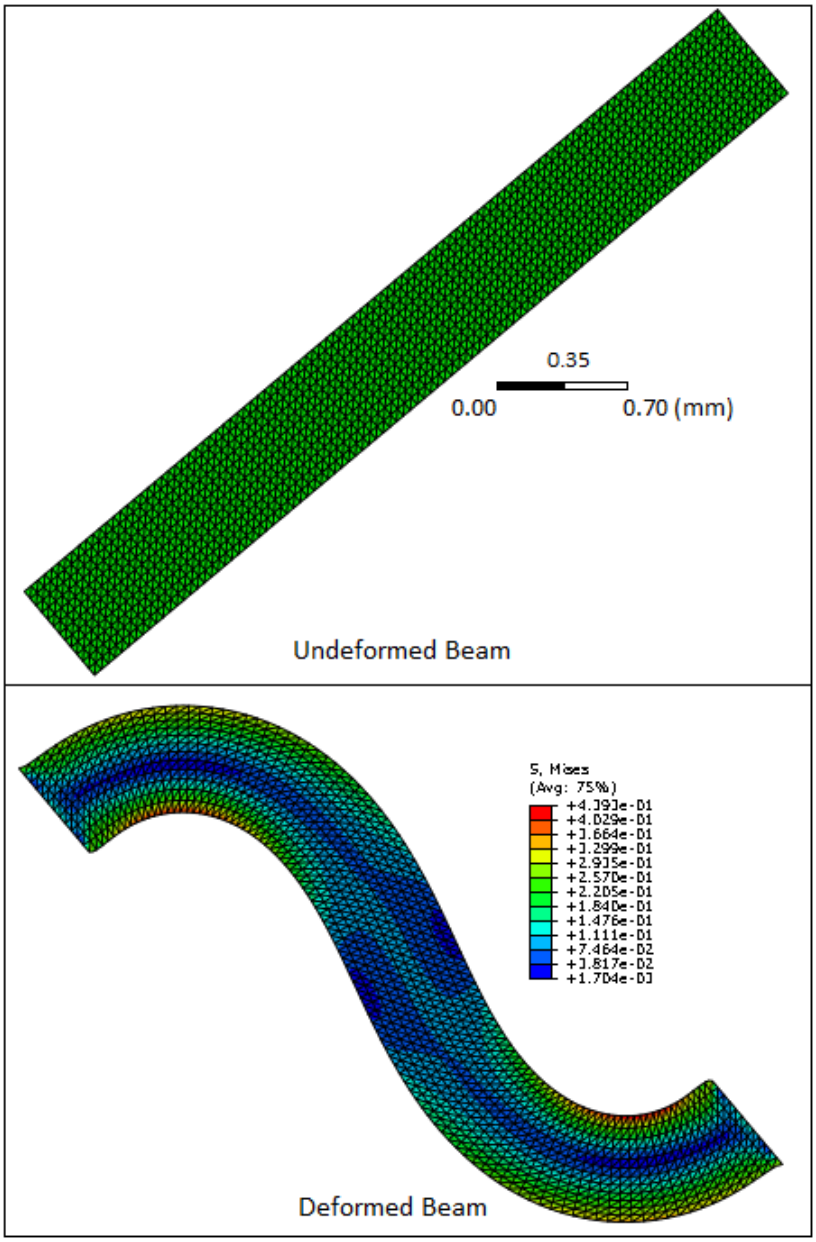

Figure A.3: Undeformed-deformed shape of the beam for 40° tilt angle (the reference beam)

A.4 Images Taken from Analysis of the Straight Beam Having Tilt Angle 45°

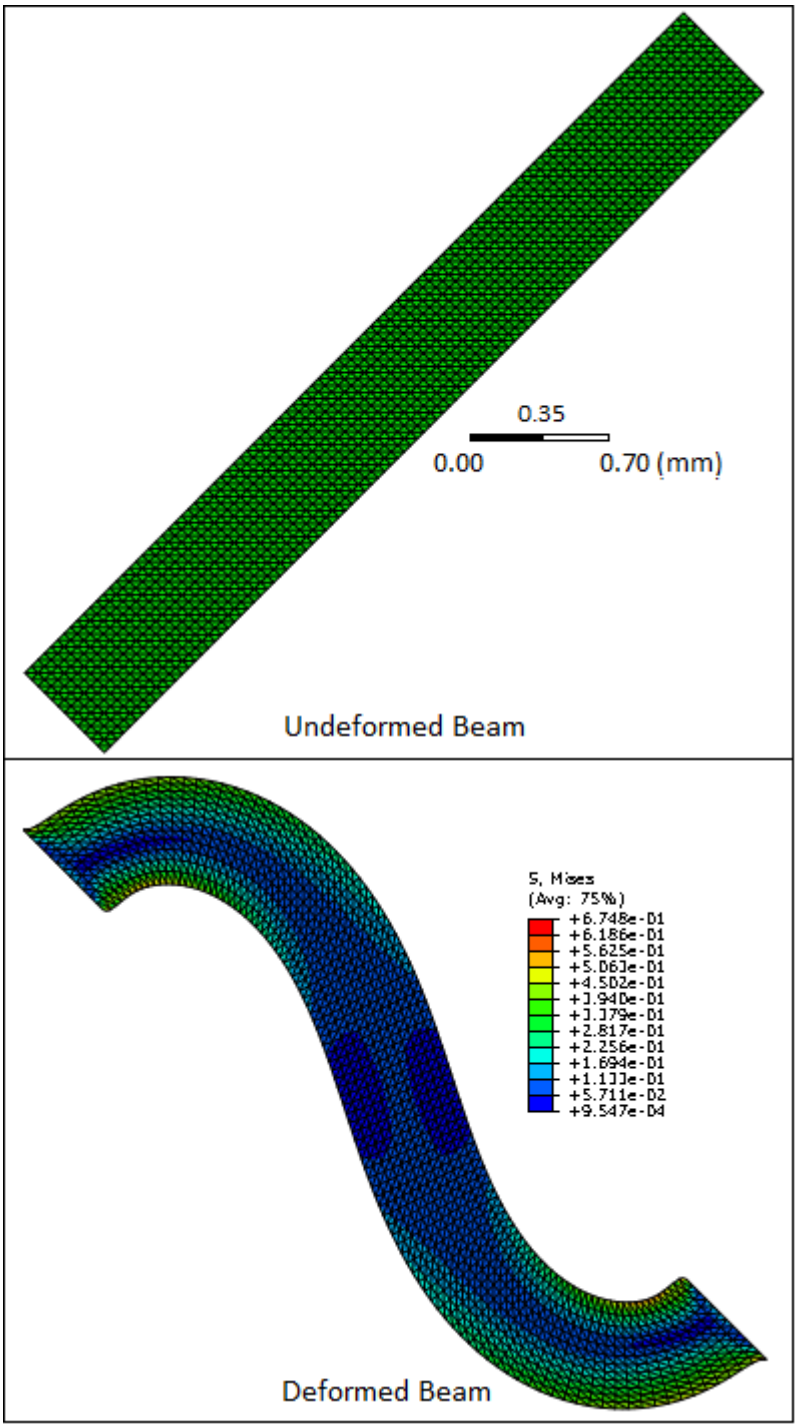

Figure A.4: Undeformed-deformed shape of the beam for 45° tilt angle

A.5 Images Taken from Analysis of the Straight Beam Having Tilt Angle 50°

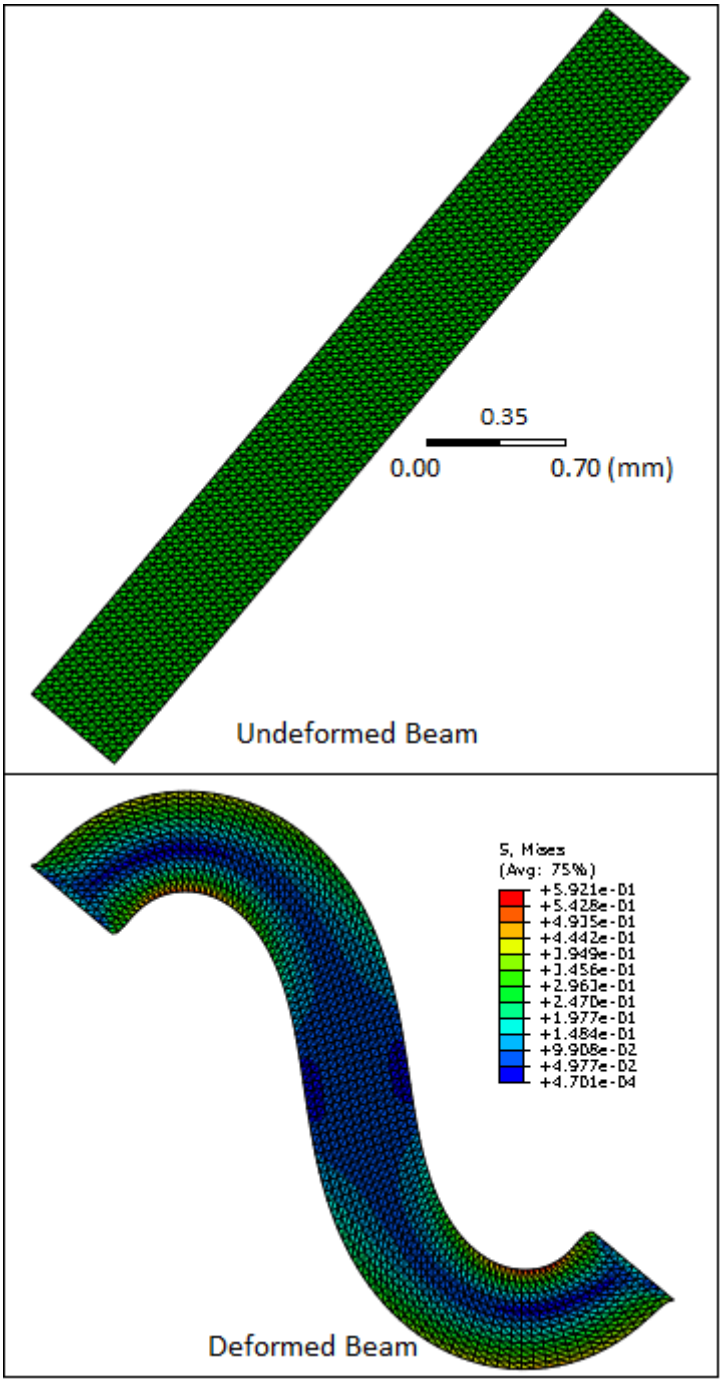

Figure A.5: Undeformed-deformed shape of the beam for 50° tilt angle

A.6 Images Taken from Analysis of the Straight Beam Having Tilt Angle 55° (Crashed)

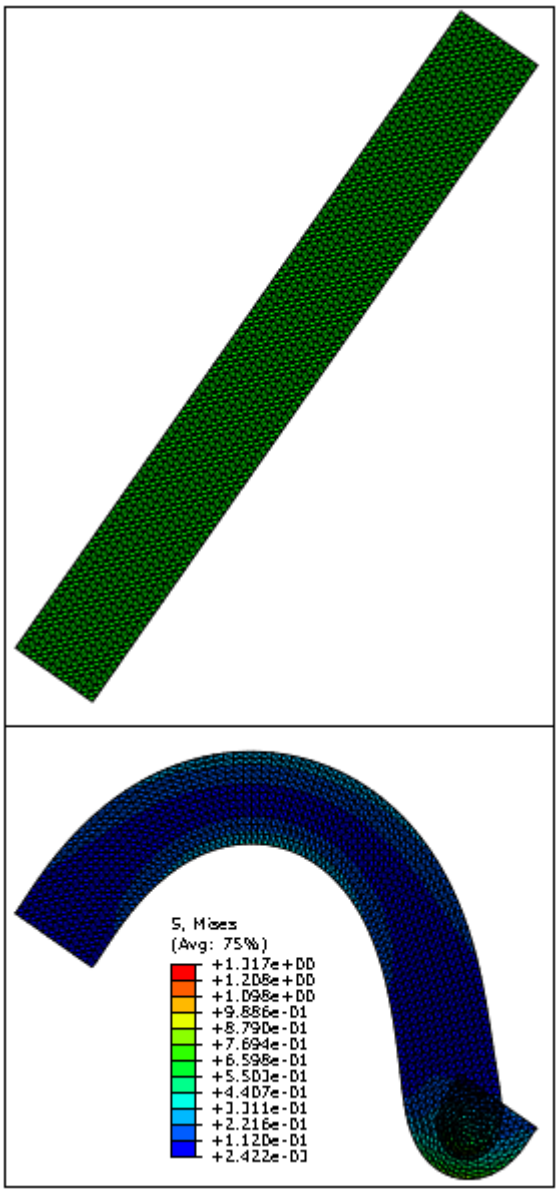

Figure A.6: Undeformed-deformed shape of the beam which crashed when its tilt angle is increased to 55°

APPENDIX B

DEFORMED AND UNDEFORMED SHAPES OF STRAIGHT BEAMS RELATED TO ASPECT RATIO STUDY

B.1 Images Taken from Analysis of the Straight Beam with L5%↑, t5%↓

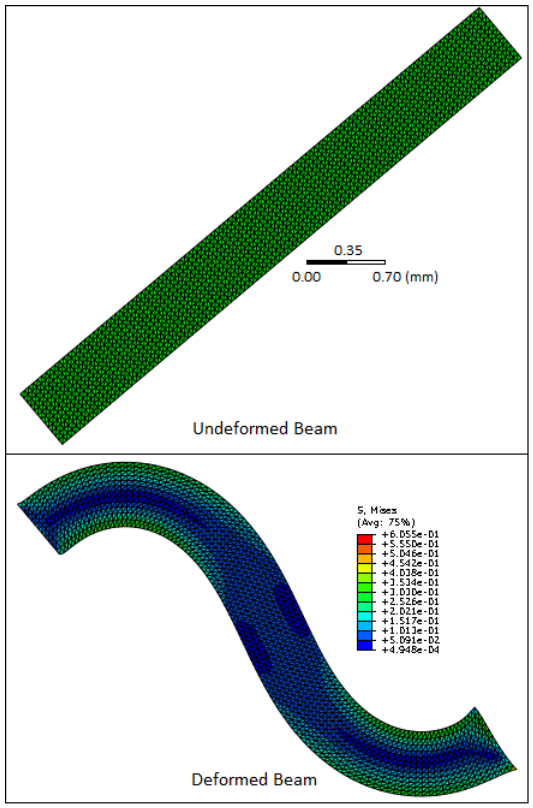

Figure B.1: Undeformed-deformed shape of the beam for 5% increase in length, 5% decrease in width

B.2 Images Taken from Analysis of the Straight Beam with L10%↑, t9%↓

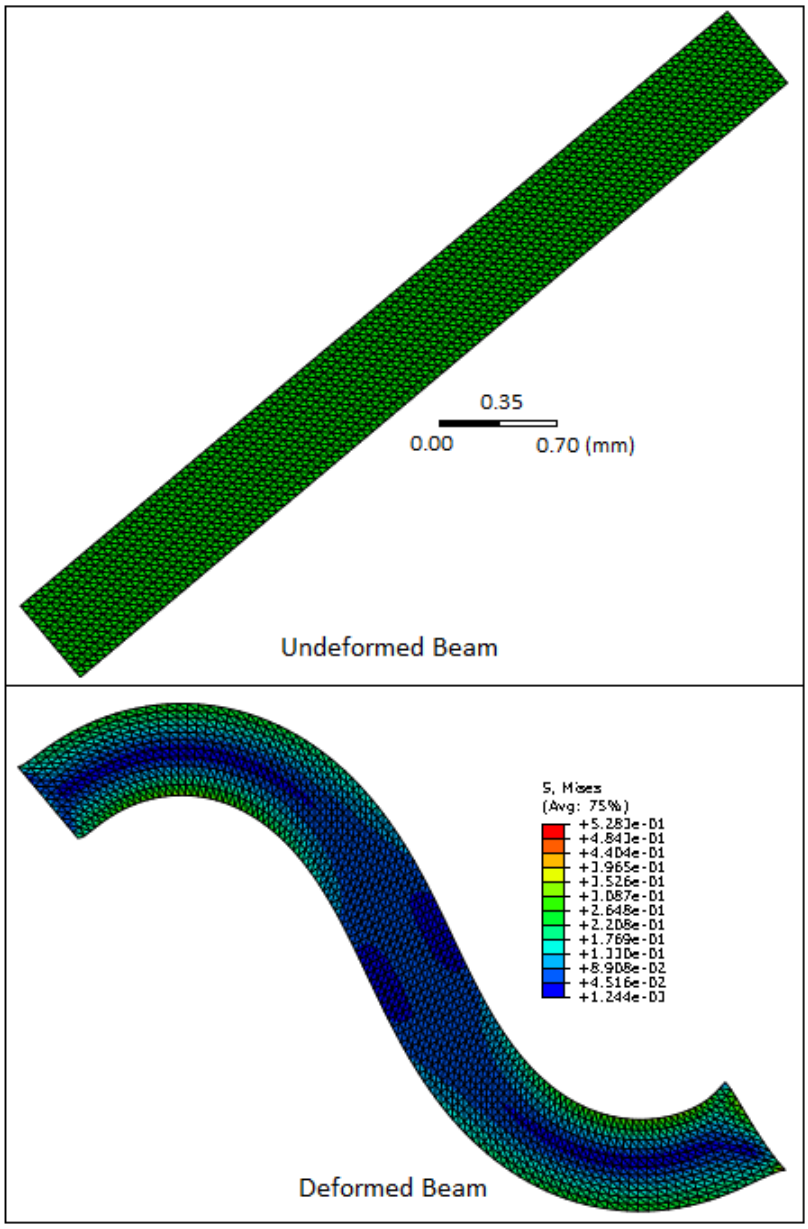

Figure B.2: Undeformed-deformed shape of the beam for 10% increase in length, 9% decrease in width

B.3 Images Taken from Analysis of the Straight Beam with L15%↑, t13%↓

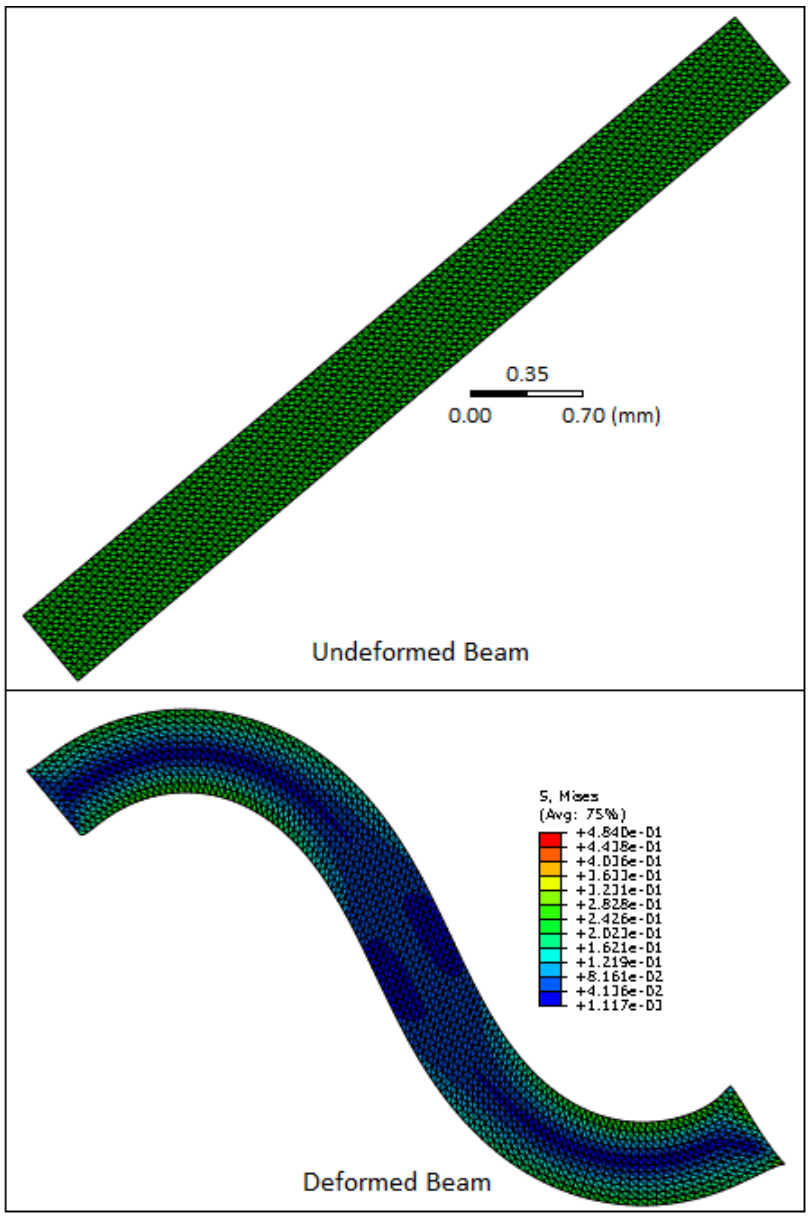

Figure B.3: Undeformed-deformed shape of the beam for 15% increase in length, 13% decrease in width

B.4 Images Taken from Analysis of the Straight Beam with L20%↑, t17%↓

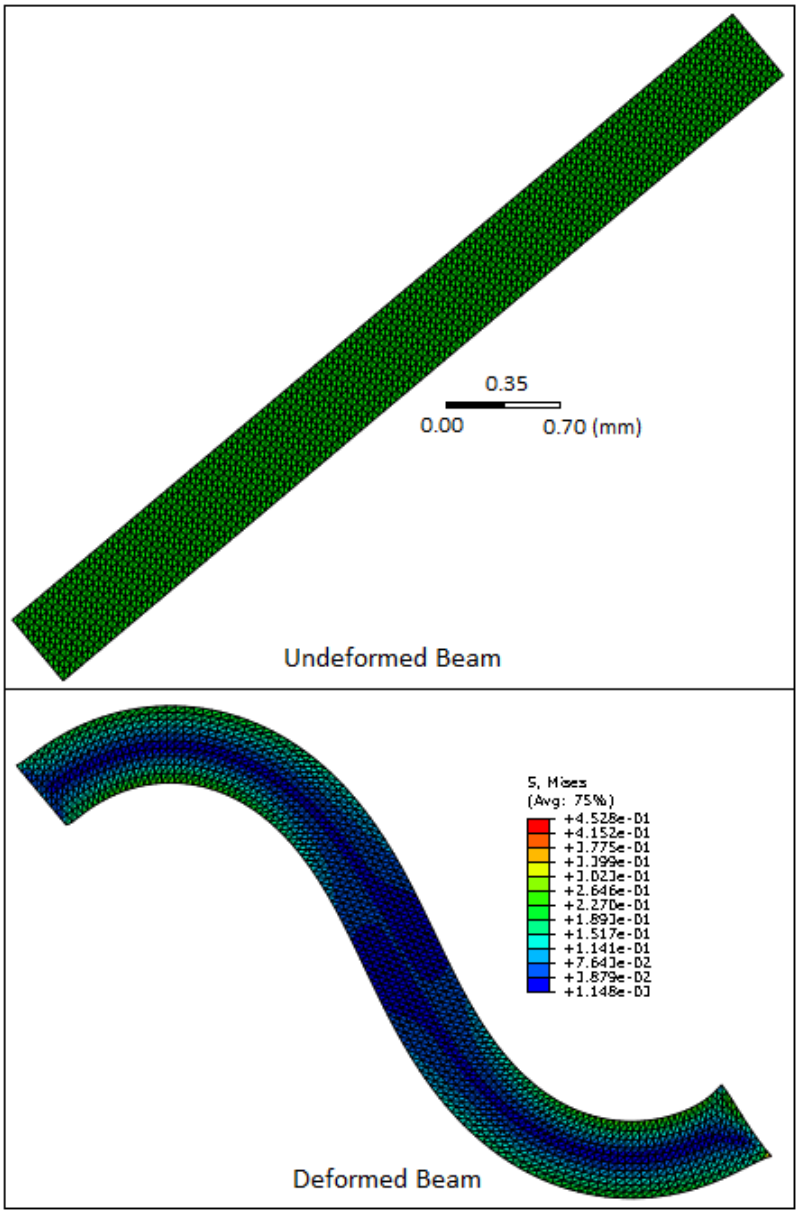

Figure B.4: Undeformed-deformed shape of the beam for 20% increase in length, 17% decrease in width

B.5 Images Taken from Analysis of the Straight Beam with L25%↑, t20%↓

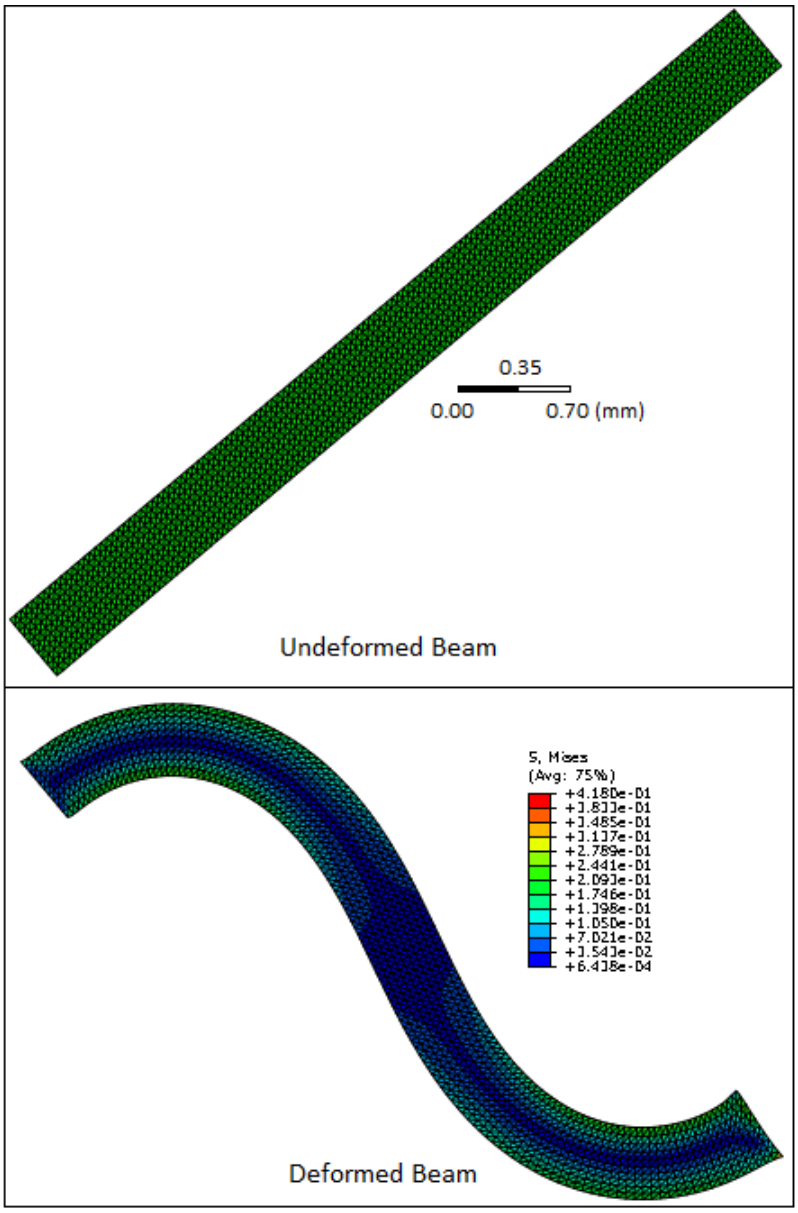

Figure B.5: Undeformed-deformed shape of the beam for 25% increase in length, 20% decrease in width

B.6 Images Taken from Analysis of the Straight Beam with L5%↓, t5%↑

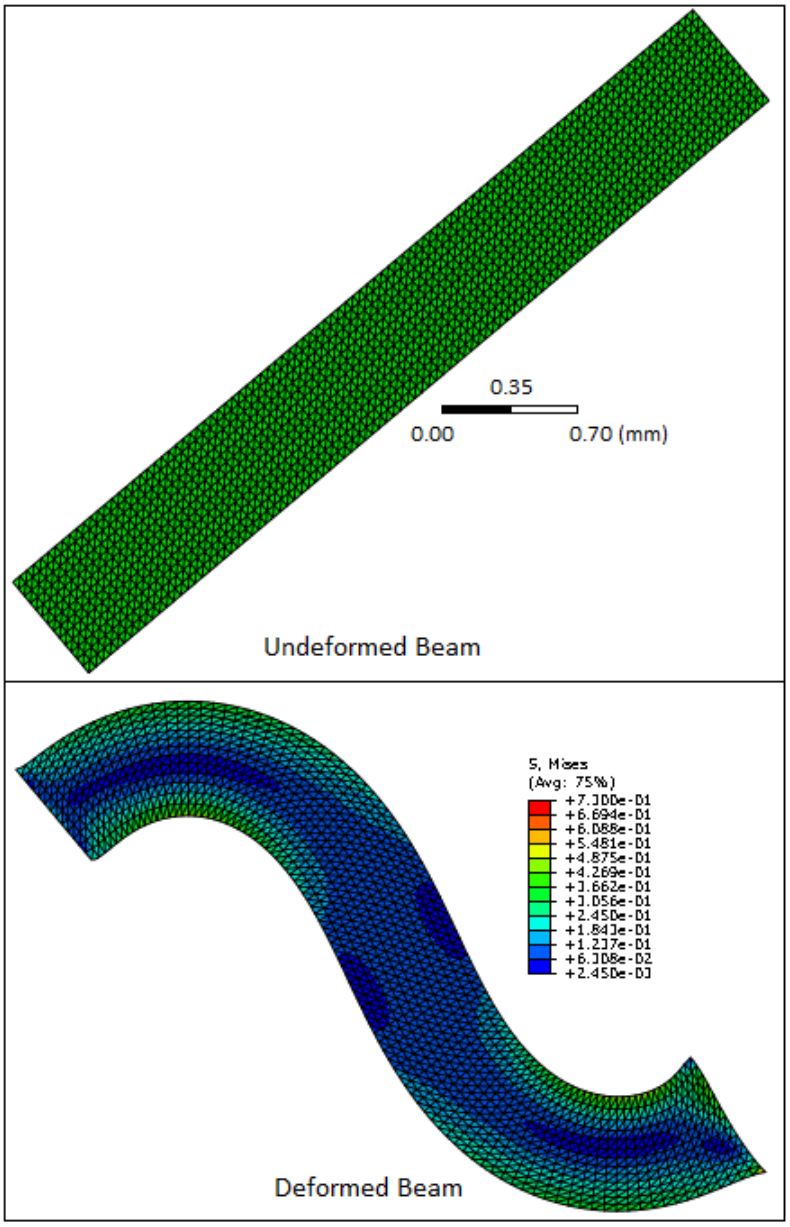

Figure B.6: Undeformed-deformed shape of the beam for 5% decrease in length, 5% increase in width

B.7 Images Taken from Analysis of the Straight Beam with L10%↓, t11%↑

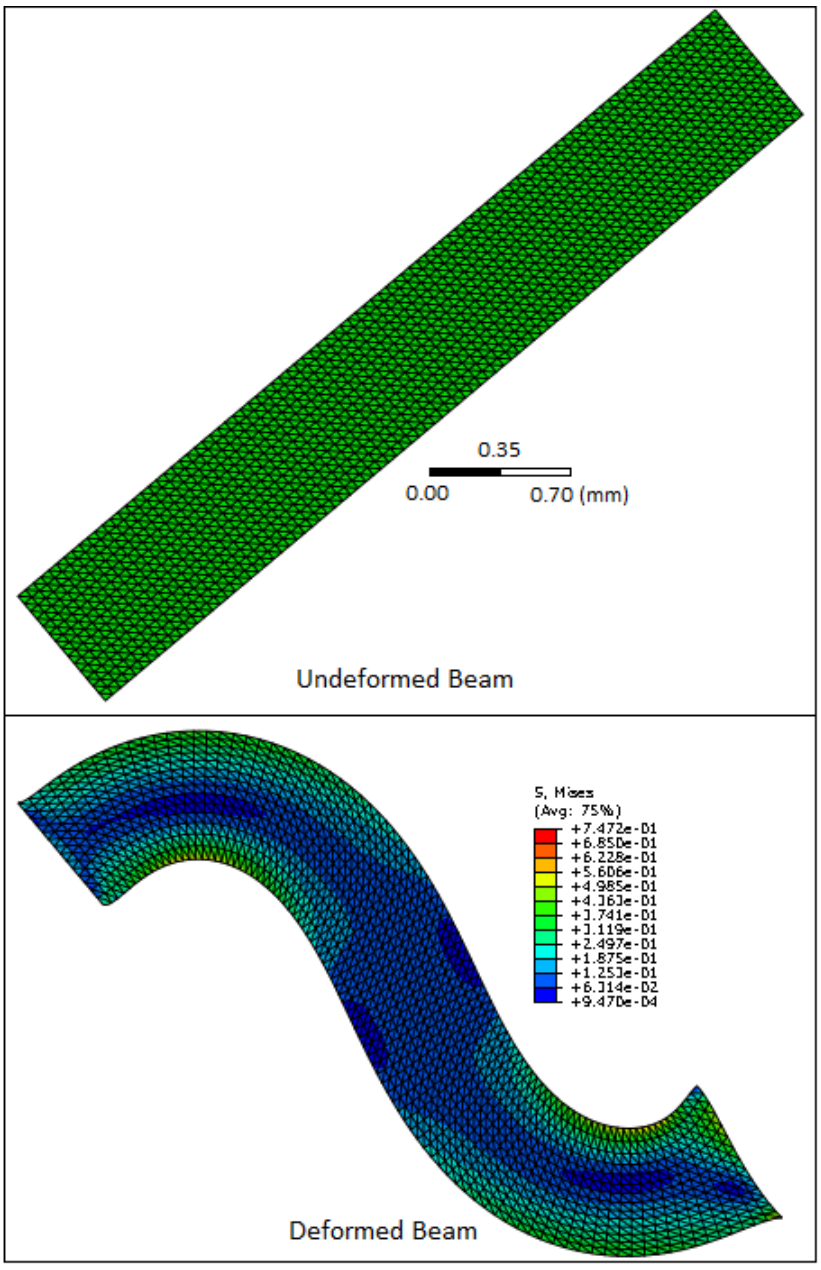

Figure B.7: Undeformed-deformed shape of the beam for 10% decrease in length, 11% increase in width

B.8 Images Taken from Analysis of the Straight Beam with L15%↓, t18%↑ (Crashed)

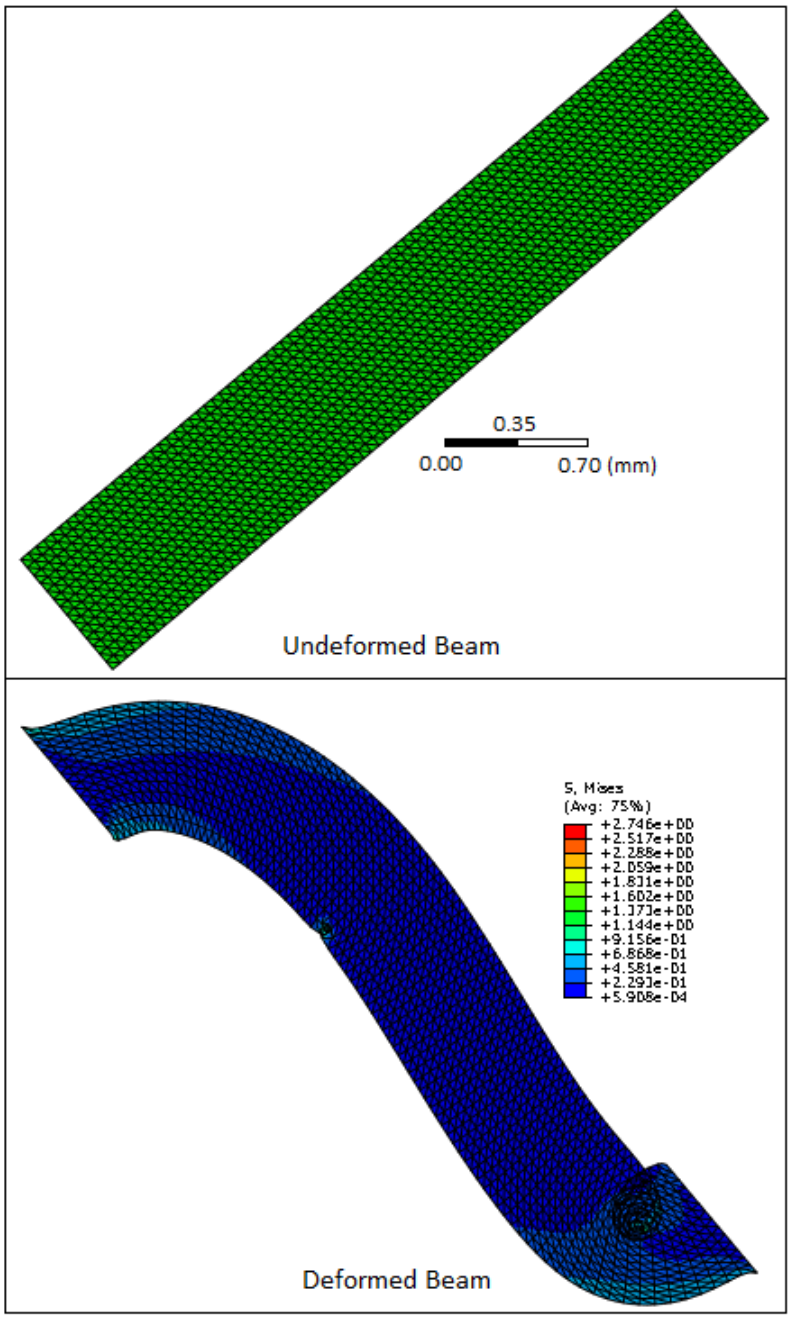

Figure B.8: Undeformed-deformed shape of the beam for 15% decrease in length, 18% increase in width

APPENDIX C

DEFORMED AND UNDEFORMED SHAPES OF BEAMS RELATED TO MORPHOLOGICAL STUDY

C.1 Images Taken from the Curved Beam Analysis Named *Reversed S-Shape*

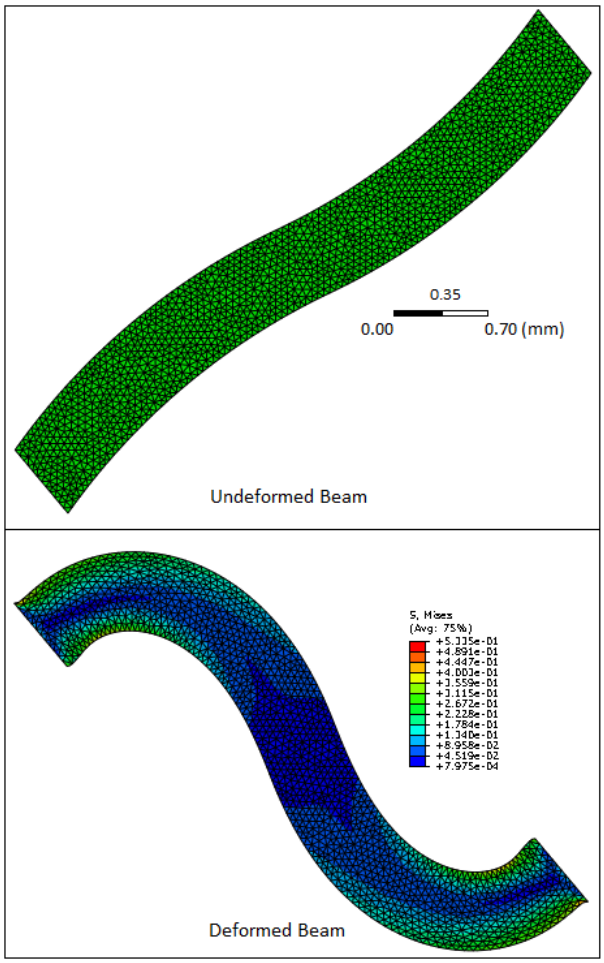

Figure C.1: Undeformed-deformed shape of the beam for *reversed s-shape*

C.2 Images Taken from the Curved Beam Analysis Named *3S-Shape*

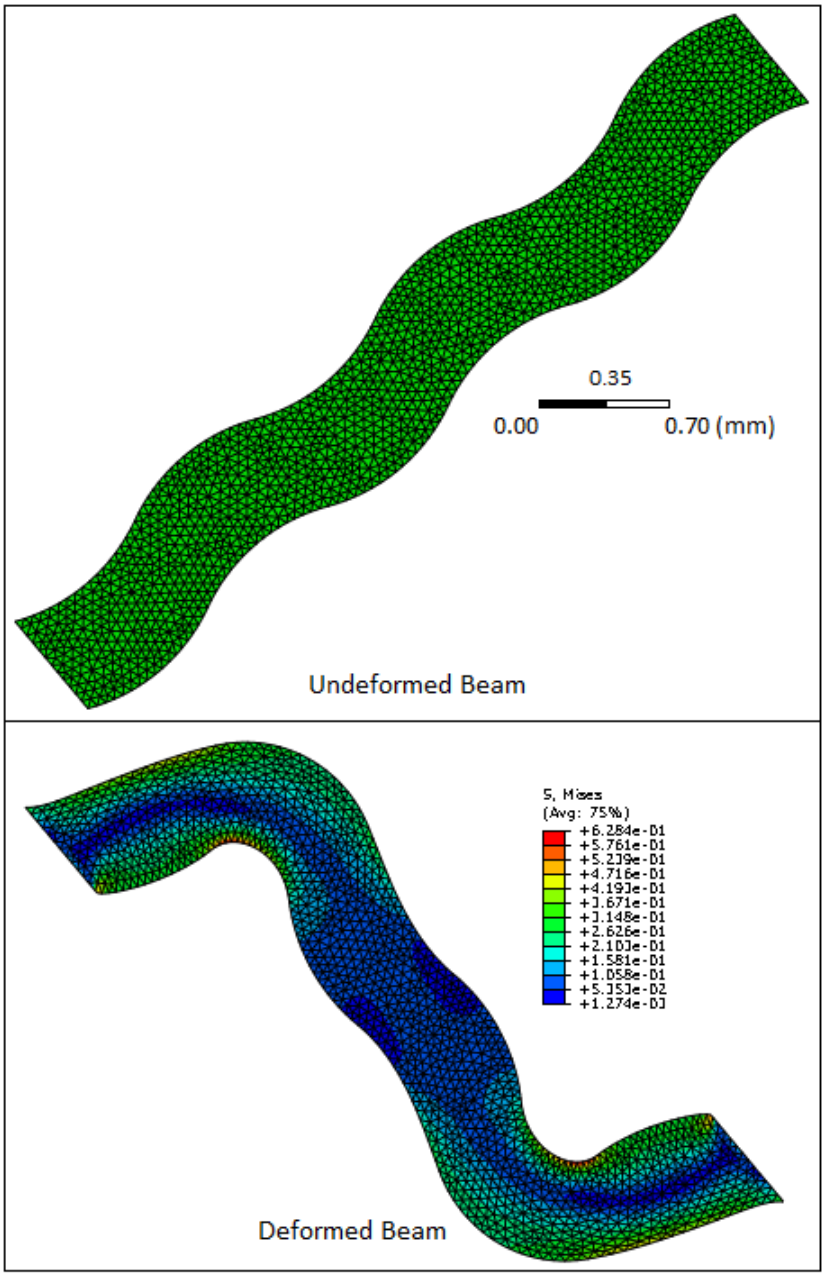

Figure C.2: Undeformed-deformed shape of the beam for *3s-shape*

C.3 Images Taken from the Curved Beam Analysis Named *Convex*

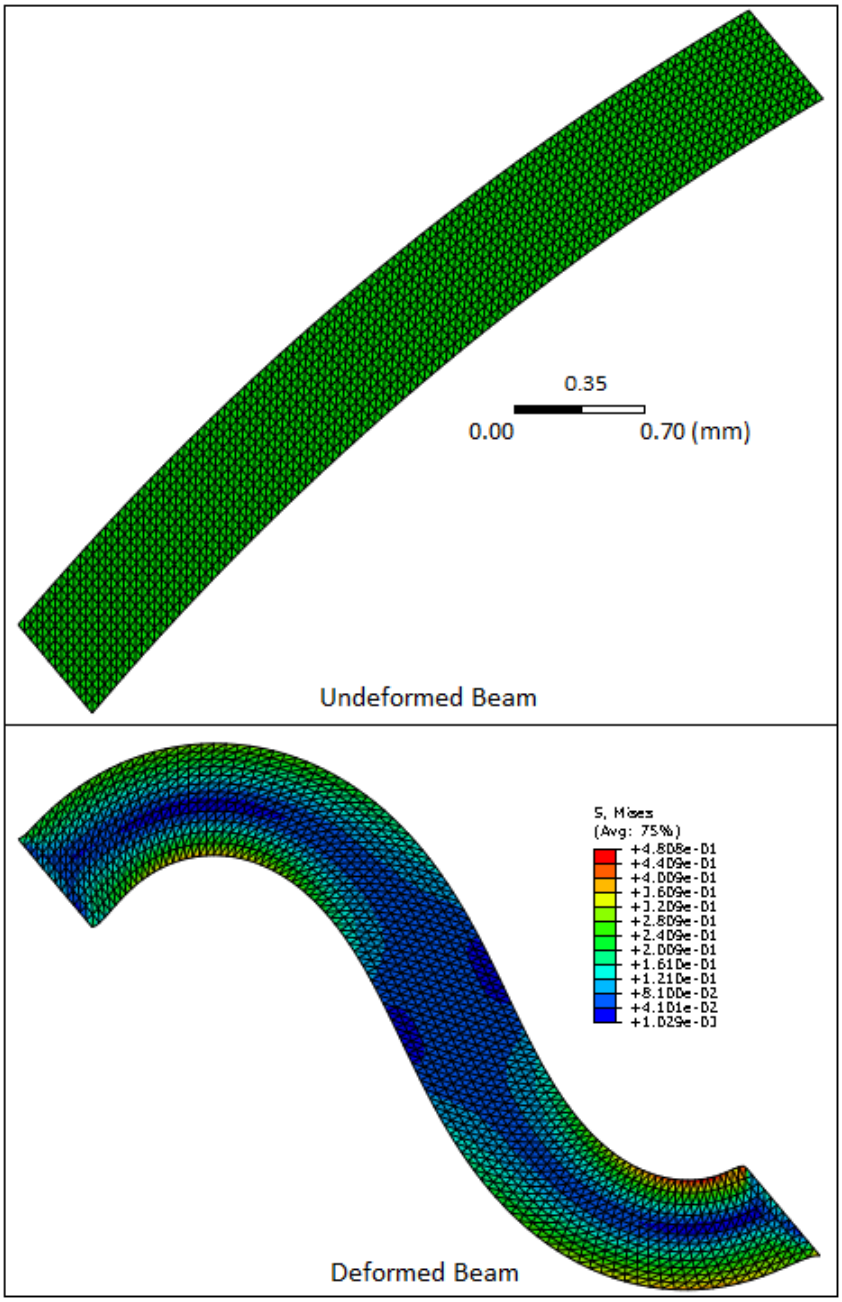

Figure C.3: Undeformed-deformed shape of the beam for *convex*

C.4 Images Taken from the Curved Beam Analysis Named *Concave*

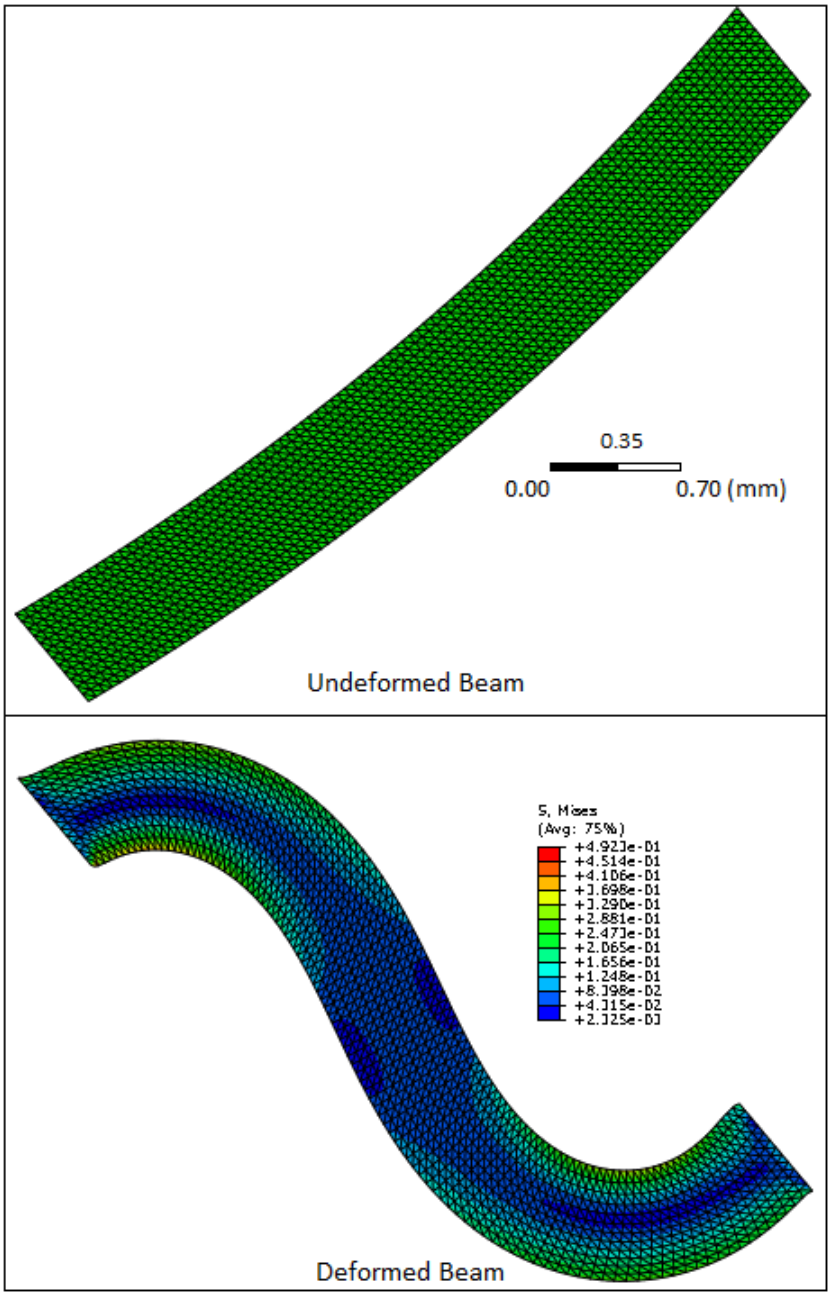

Figure C.4: Undeformed-deformed shape of the beam for *concave*

C.5 Images Taken from Analysis of the Straight Beam (The Reference Beam)

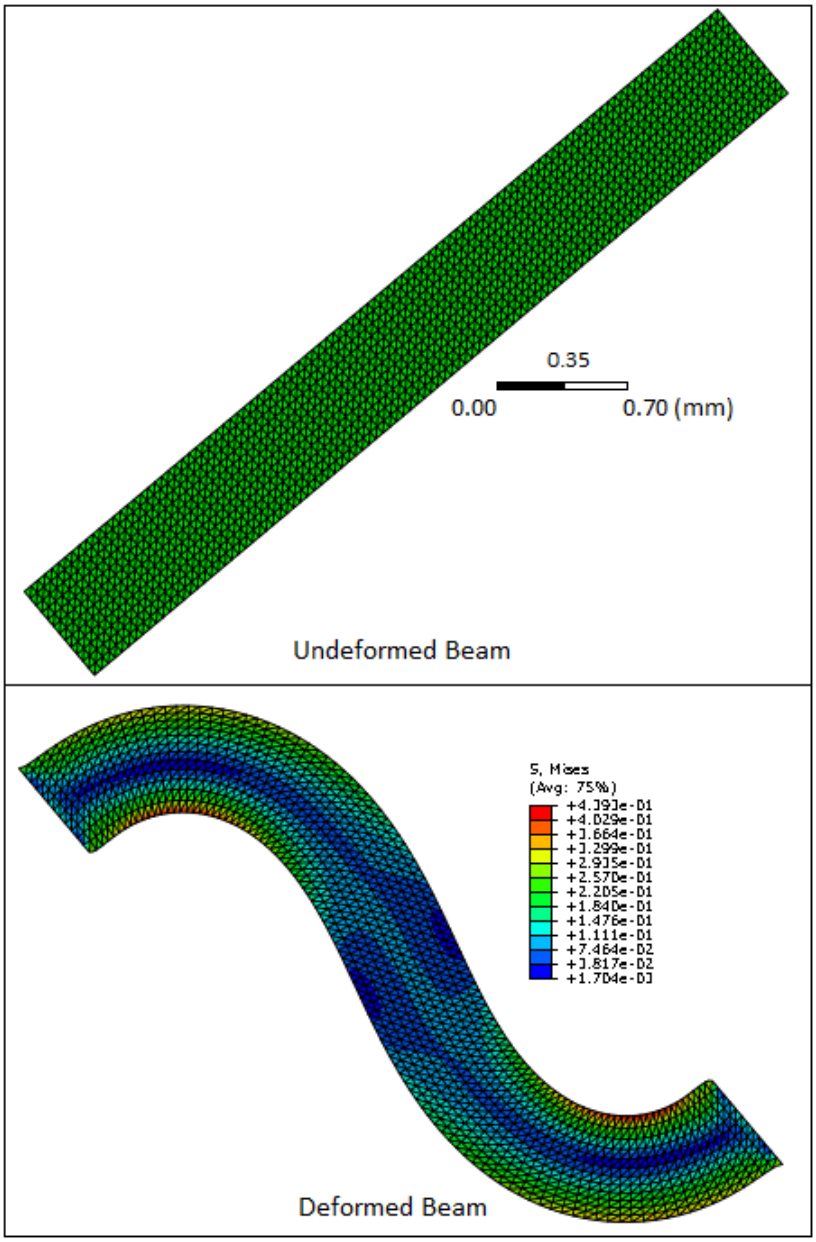

Figure C.5: Undeformed-deformed shape of the reference beam

C.6 Images Taken from the Curved Beam Analysis Named *2S-Shape*

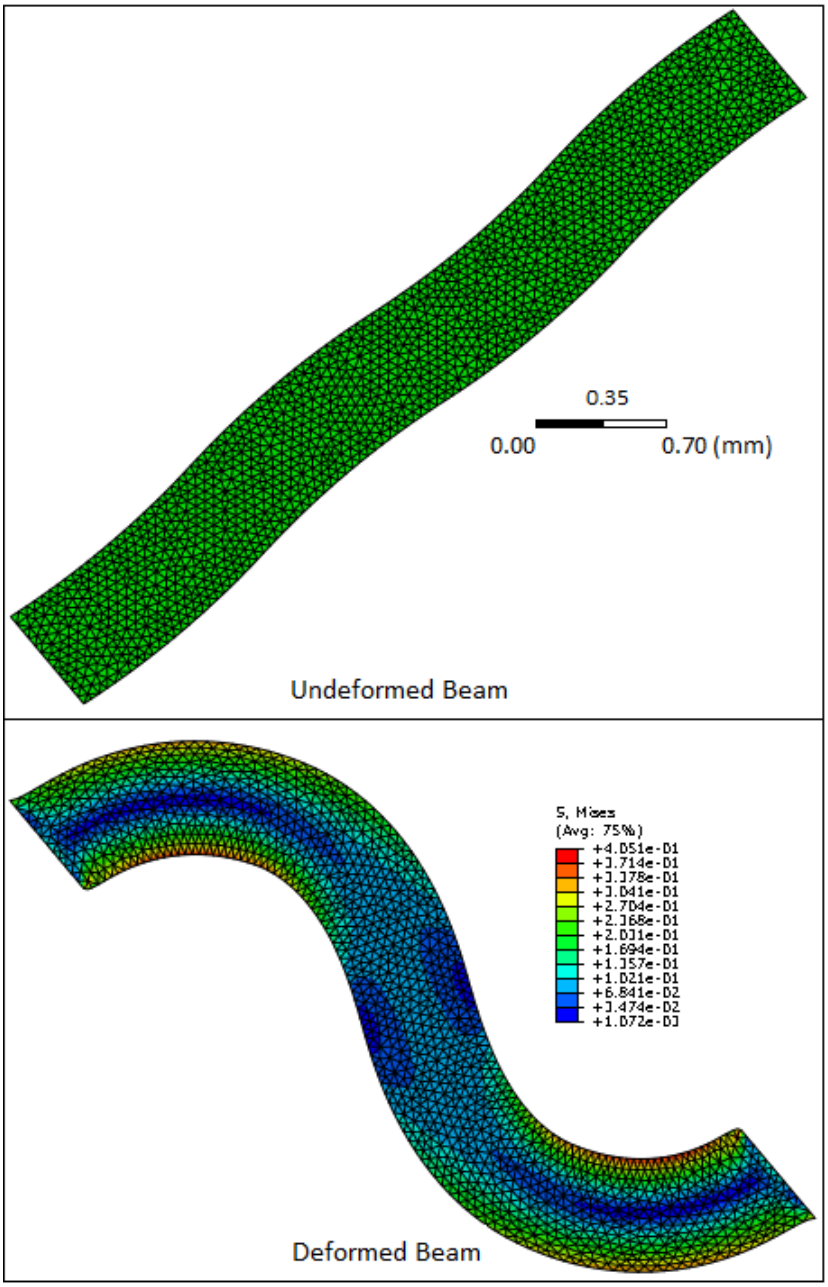

Figure C.6: Undeformed-deformed shape of the beam for *2s-shape*

C.7 Images Taken from the Curved Beam Analysis Named *S-Shape-R20*

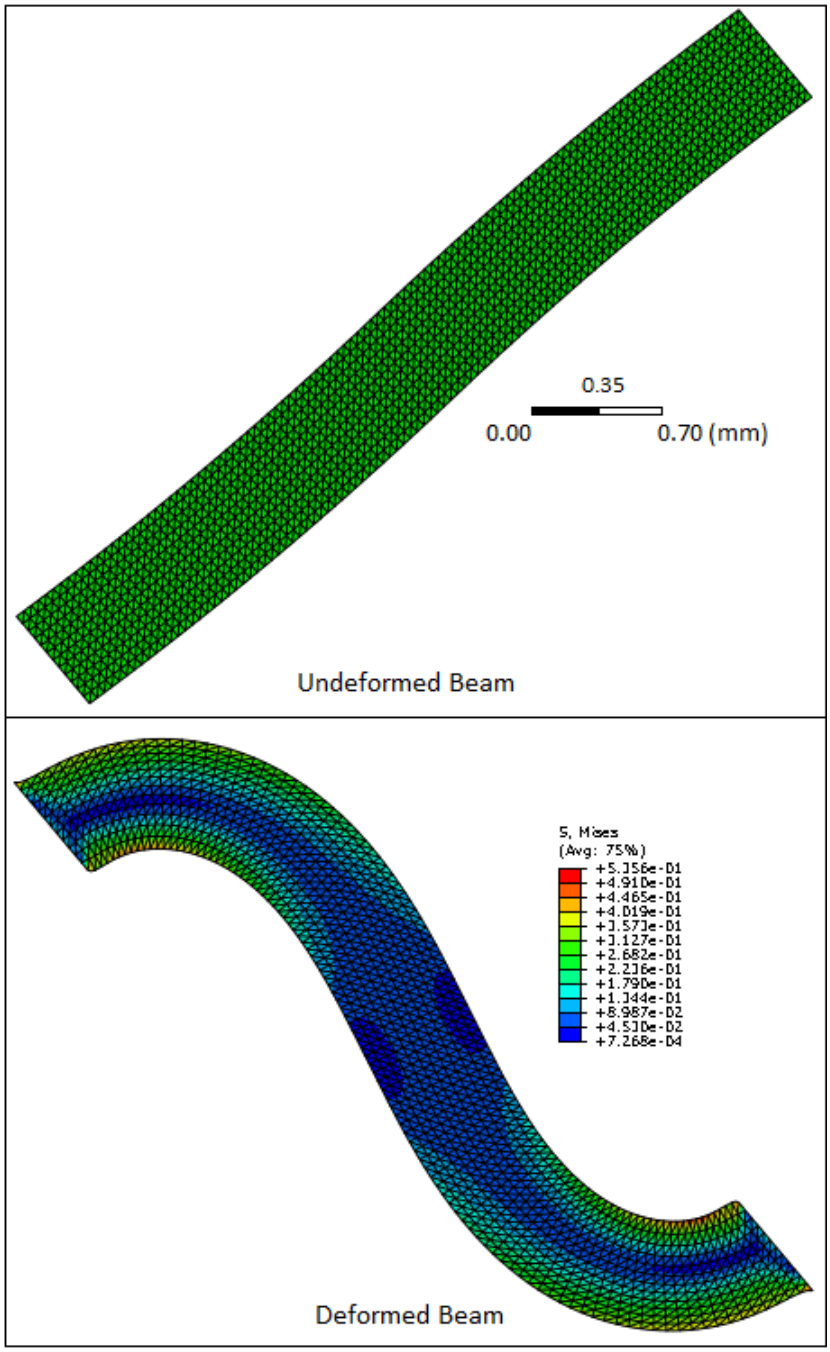

Figure C.7: Undeformed-deformed shape of the beam for *s-shape-r20*

C.8 Images Taken from the Curved Beam Analysis Named *S-Shape-R6*

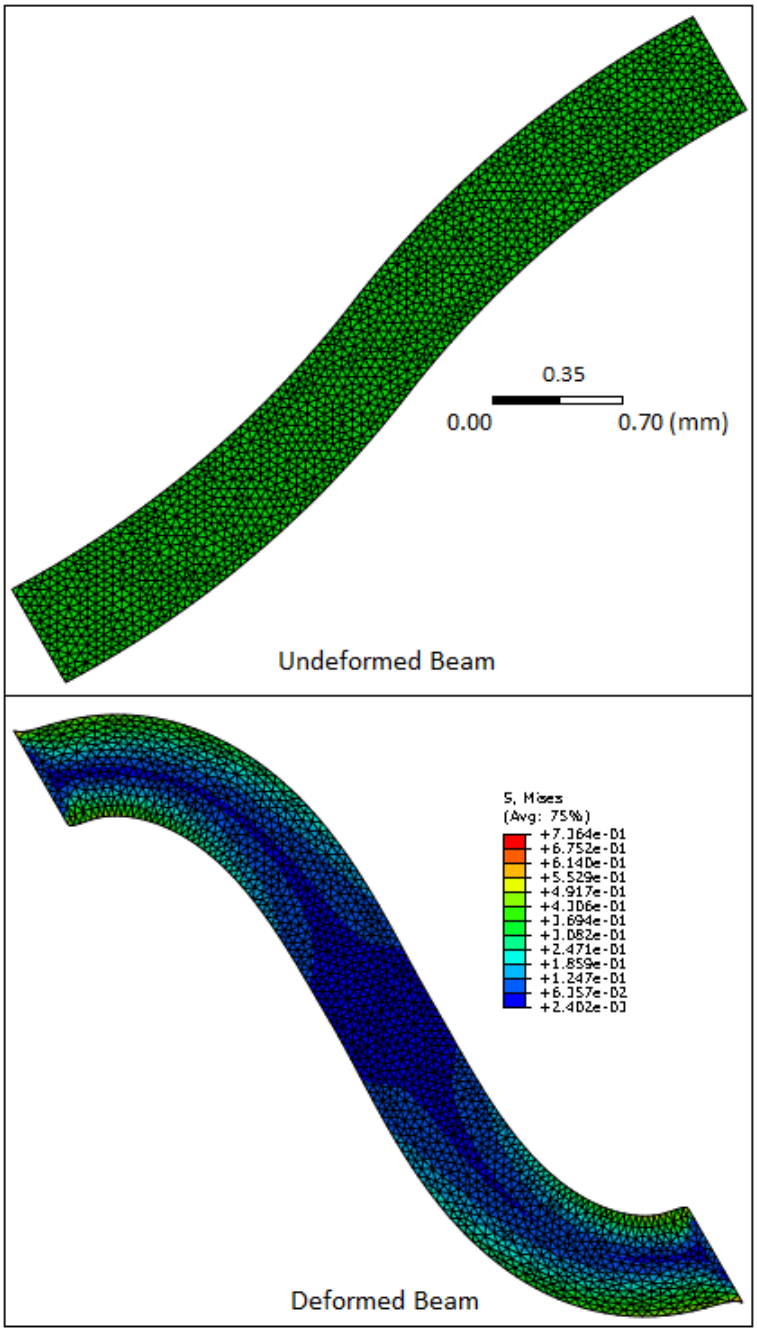

Figure C.8: Undeformed-deformed shape of the beam for *s-shape-r6*

C.9 Images Taken from the Curved Beam Analysis Named *S-Shape-R5*

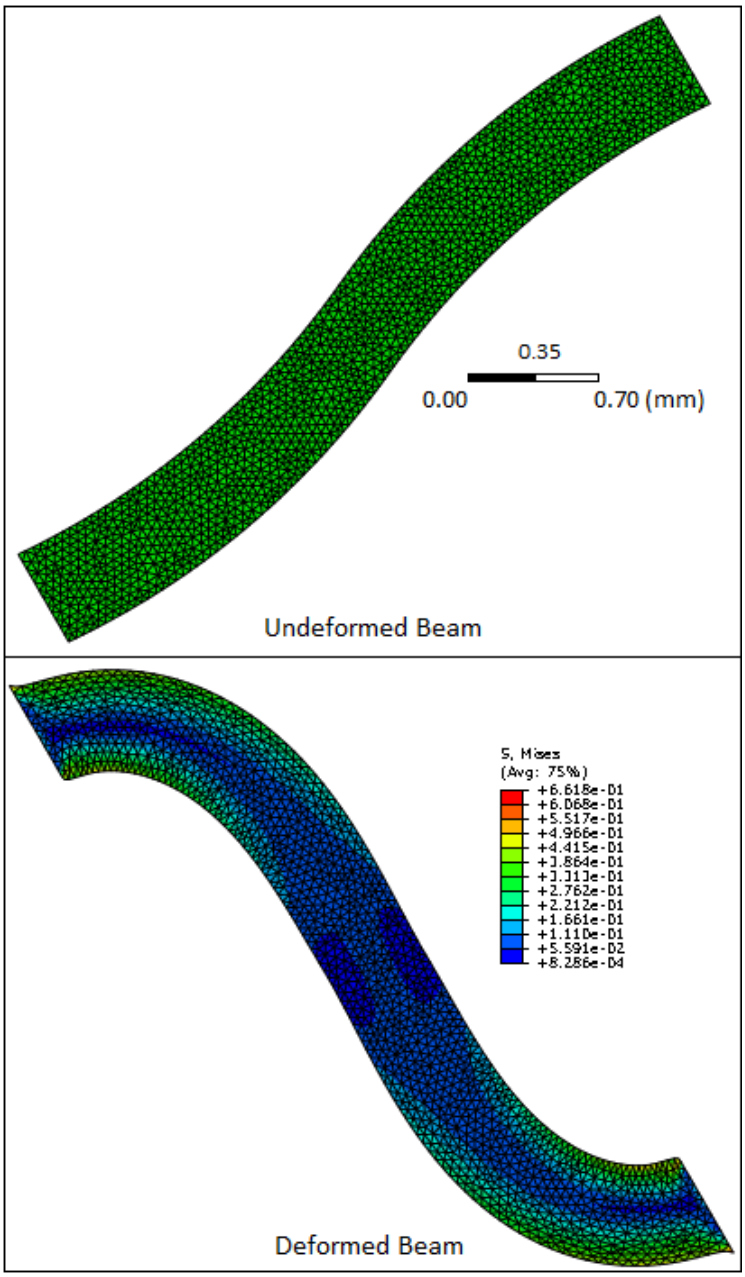

Figure C.9: Undeformed-deformed shape of the beam for *s-shape-r5*

C.10 Images Taken from the Curved Beam Analysis Named *S-Shape-R4* (Crashed)

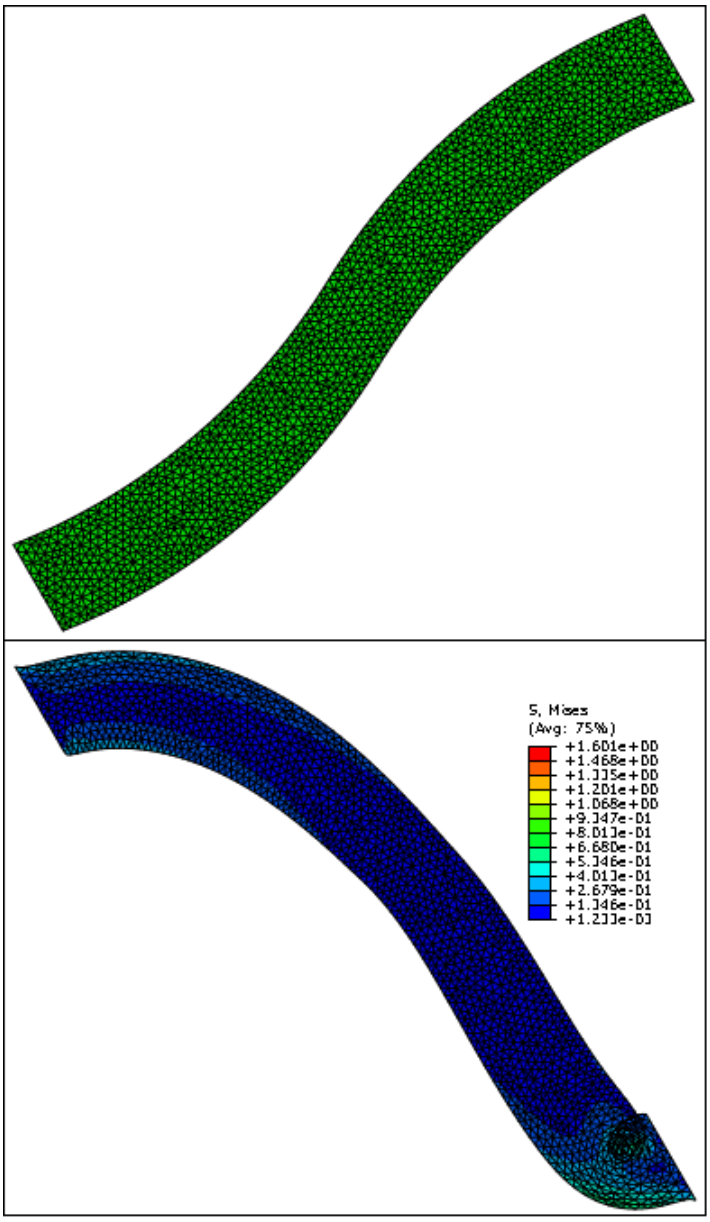

Figure C.10: Undeformed-deformed shape of the beam *s-shape-r4* which crashed when radius of its both concave and convex arcs is reduced from 5 mm to 4 mm

APPENDIX D

DEFORMED AND UNDEFORMED SHAPES OF THE CURVED BEAM NAMED S-SHAPE-R5 AT DIFFERENT TILT ANGLES

D.1 Images Taken from Analysis of *S-Shape-r5* for 30° Tilt Angle

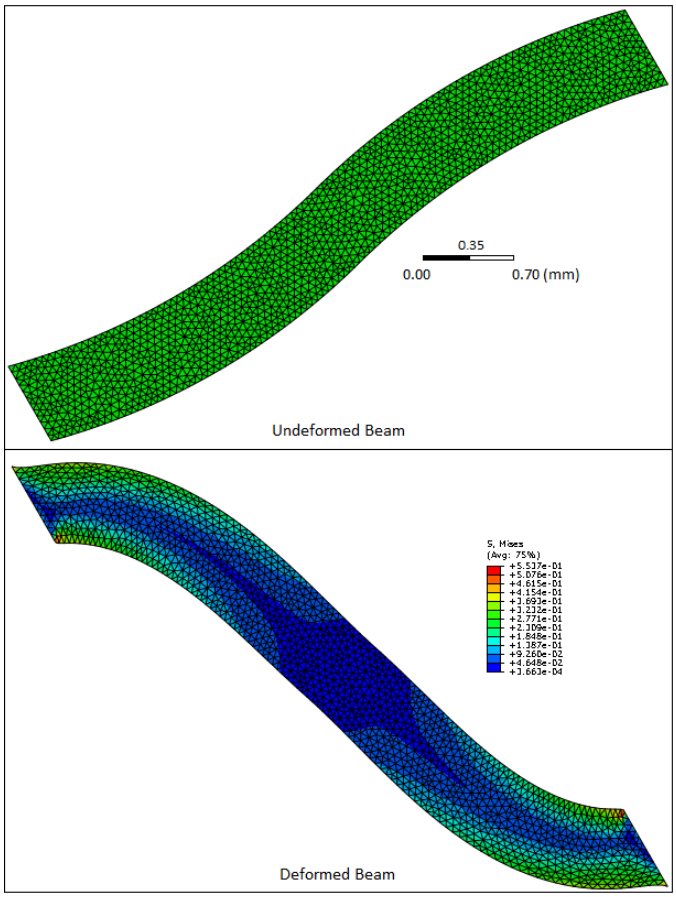

Figure D.1: Undeformed-deformed shape of the beam *s-shape-r5* for 30° tilt angle

D.2 Images Taken from Analysis of *S-Shape-r5* for 35° Tilt Angle

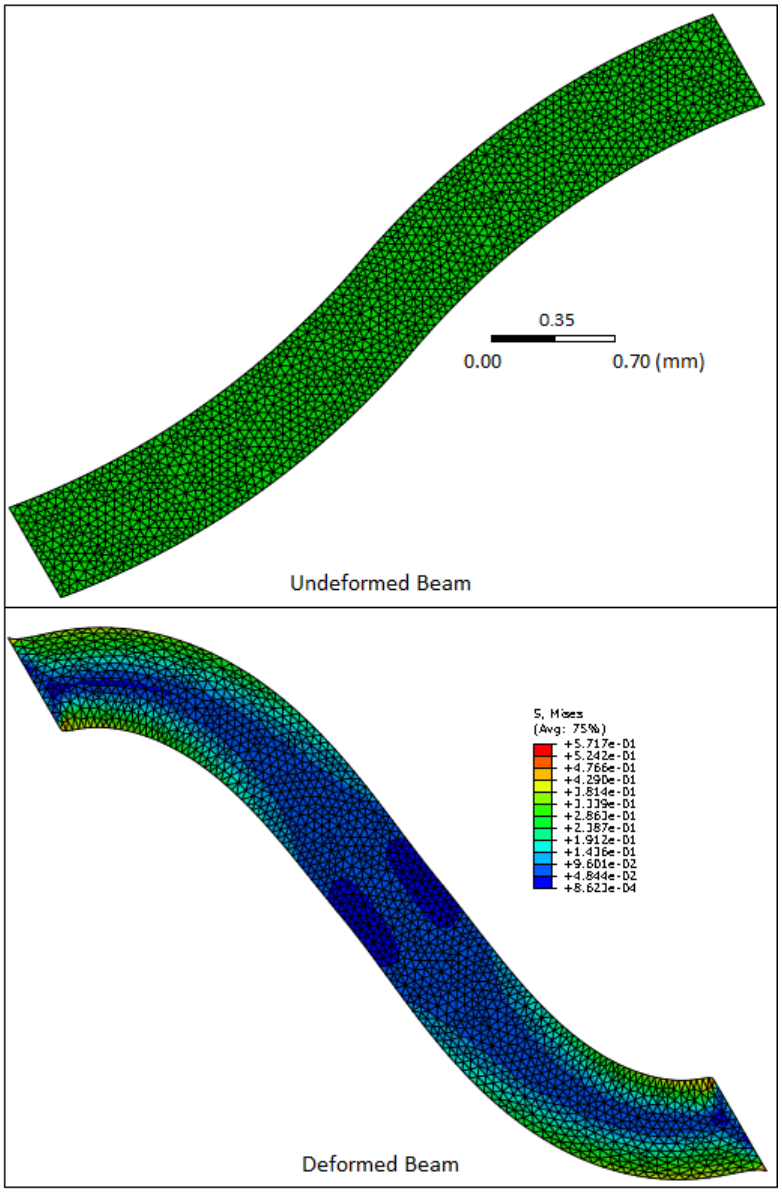

Figure D.2: Undeformed-deformed shape of the beam *s-shape-r5* for 35° tilt angle

D.3 Images Taken from Analysis of *S-Shape-r5* for 40° Tilt Angle

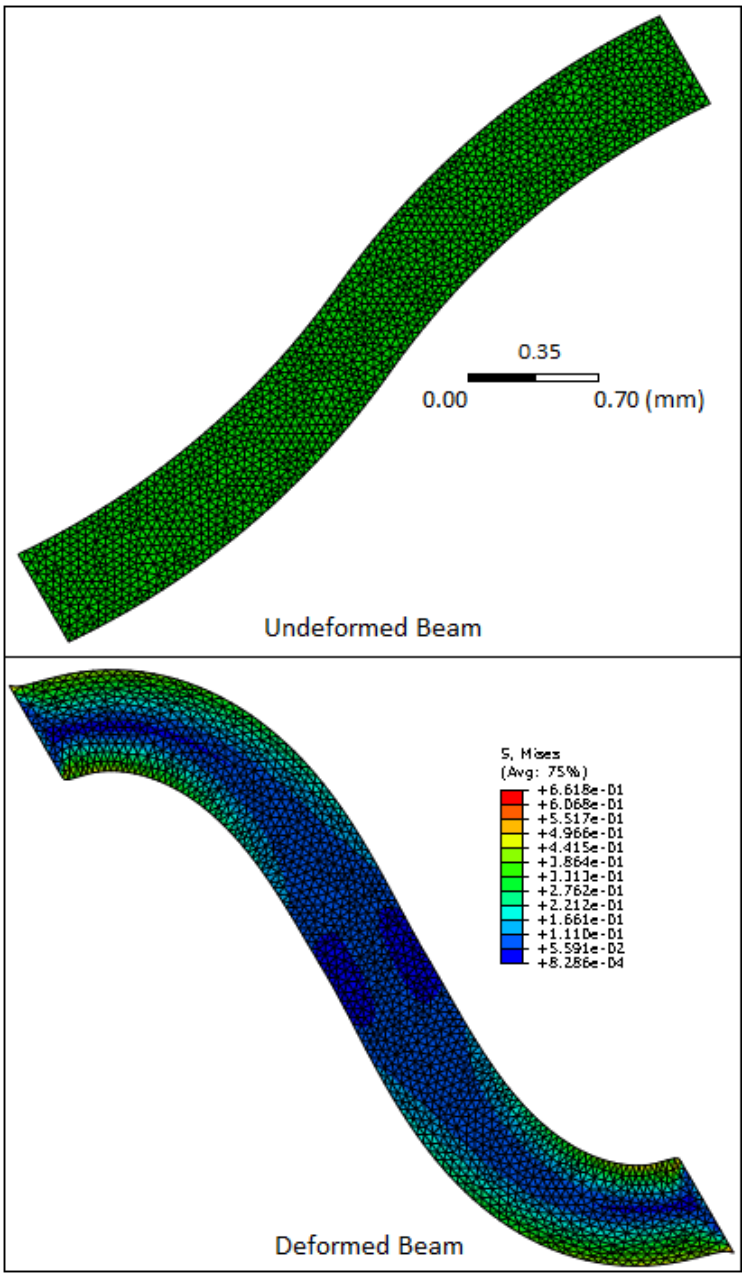

Figure D.3: Undeformed-deformed shape of the beam *s-shape-r5* for 40° tilt angle

D.4 Images Taken from Analysis of *S-Shape-r5* for 45° Tilt Angle

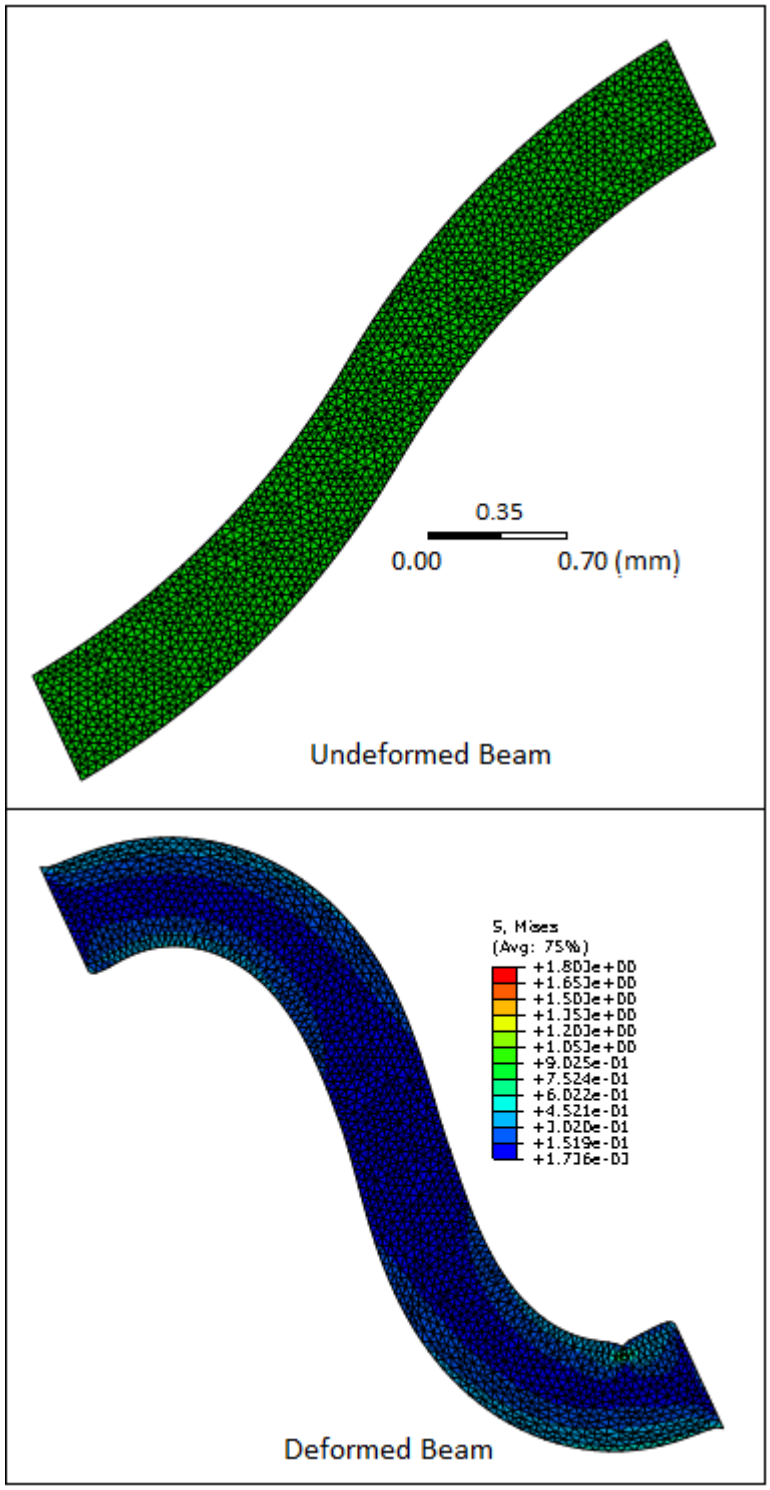

Figure D.4: Undeformed-deformed shape of the beam *s-shape-r5* for 45° tilt angle

D.5 Images Taken from Analysis of *S-Shape-r5* for 45° Tilt Angle (Showing Self Contact Occurred During the Analysis)

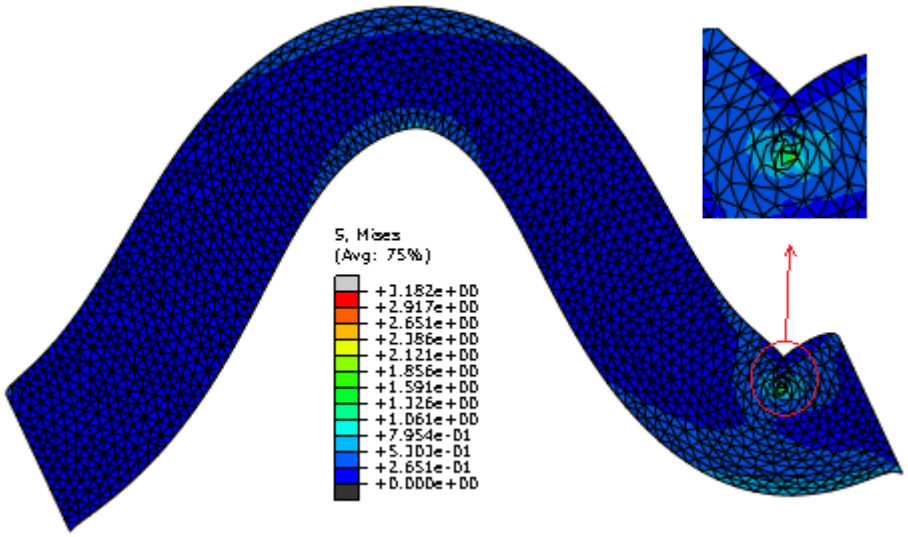

Figure D.5: Deformed shape of the beam *s-shape-r5* with self contact occurred at about 3 mm vertical displacement of its upper end for 45° tilt angle

D.6 Images Taken from Analysis of *S-Shape-r5* for 50° Tilt Angle

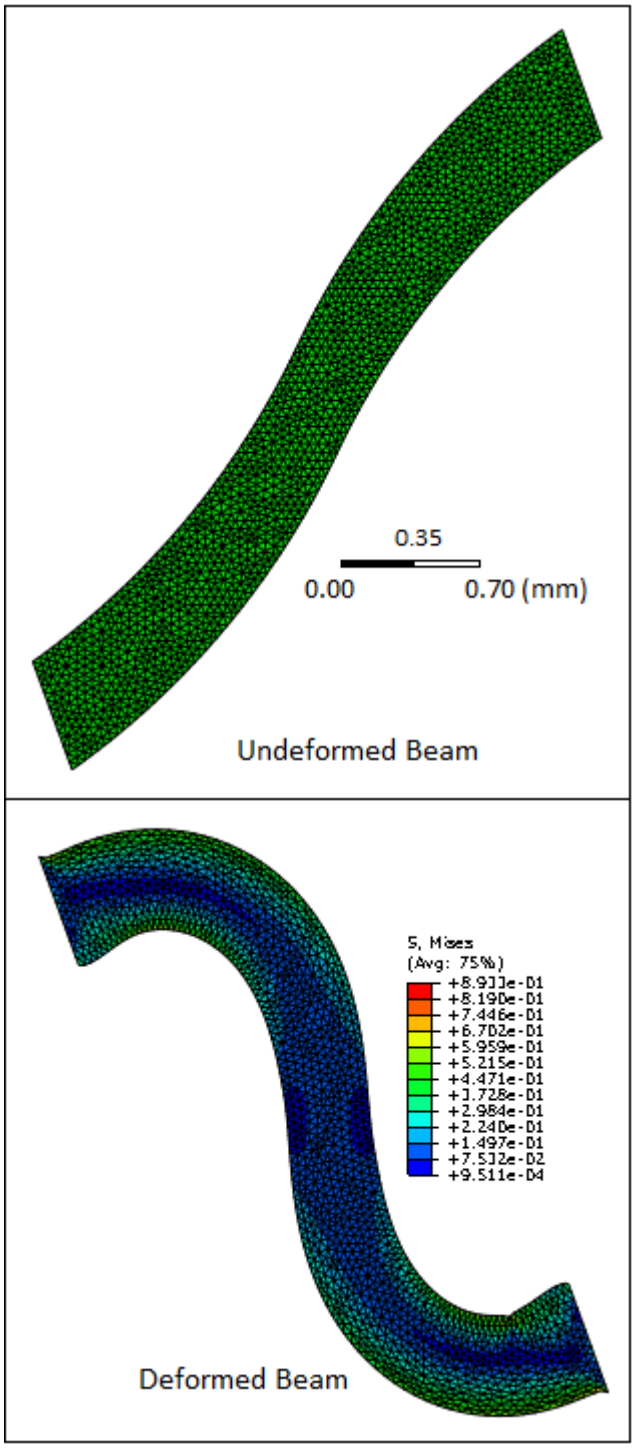

Figure D.6: Undeformed-deformed shape of the beam *s-shape-r5* for 50° tilt angle

D.7 Images Taken from Analysis of *S-Shape-r5* for 50° Tilt Angle (Showing Two Self Contacts Occurred During the Analysis)

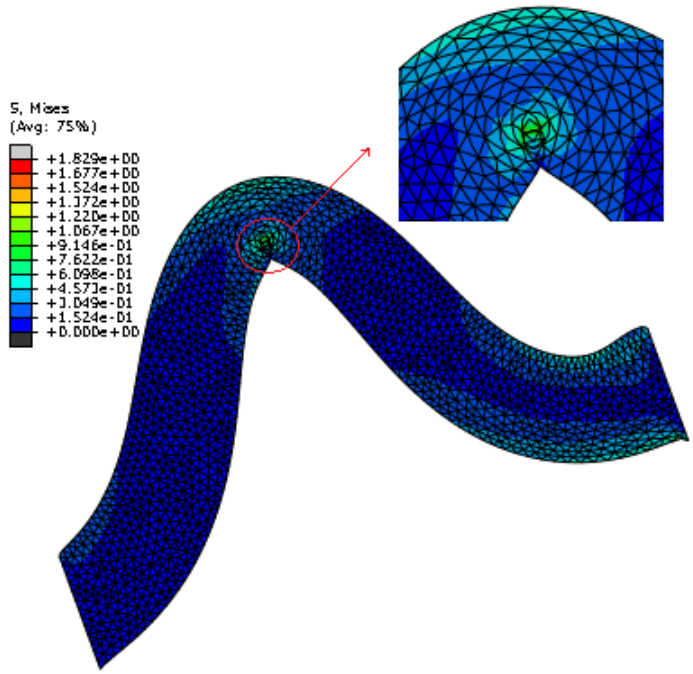

Figure D.7: Deformed shape of the beam *s-shape-r5* with self contact occurred at about 2 mm vertical displacement of its upper end for 50° tilt angle

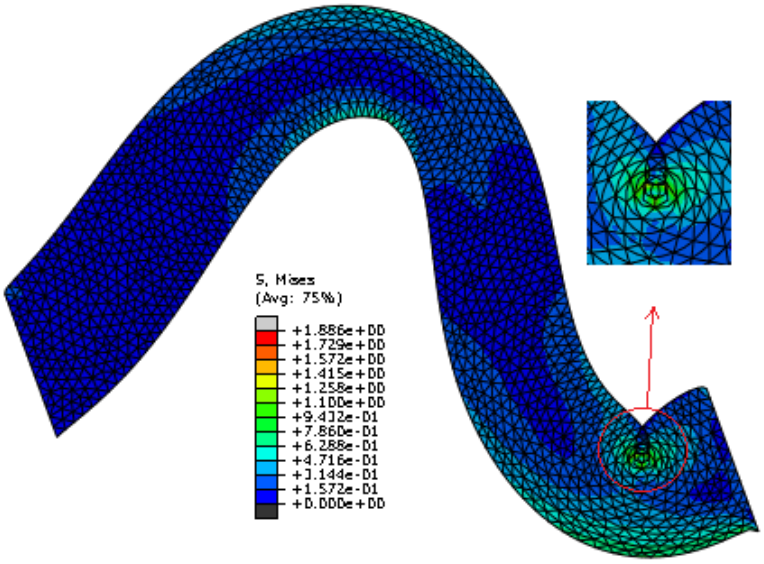

Figure D.8: Deformed shape of the beam *s-shape-r5* with self contact occurred at about 3.5 mm vertical displacement of its upper end for 50° tilt angle

APPENDIX E

DEFORMED AND UNDEFORMED SHAPES RELATED TO ASPECT RATIO STUDY OF THE CURVED BEAM S-SHAPE-R5

E.1 Images Taken from Analysis of the Curved Beam S-Shape-r5 with L5 % ↑, t5 % ↓

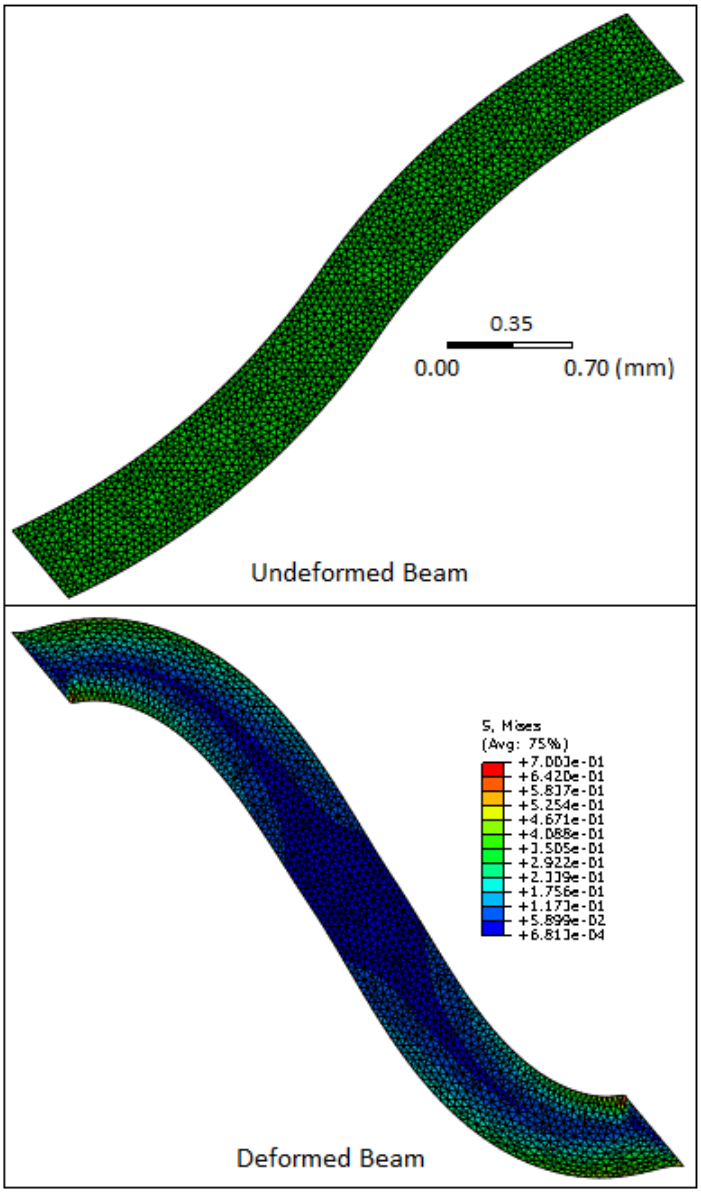

Figure E.1: Undeformed-deformed shape of the curved beam s-shape-r5 for 5% increase in length, 5% decrease in width

E.2 Images Taken from Analysis of the Curved Beam S-Shape-r5 with L10 % ↑, t9 % ↓

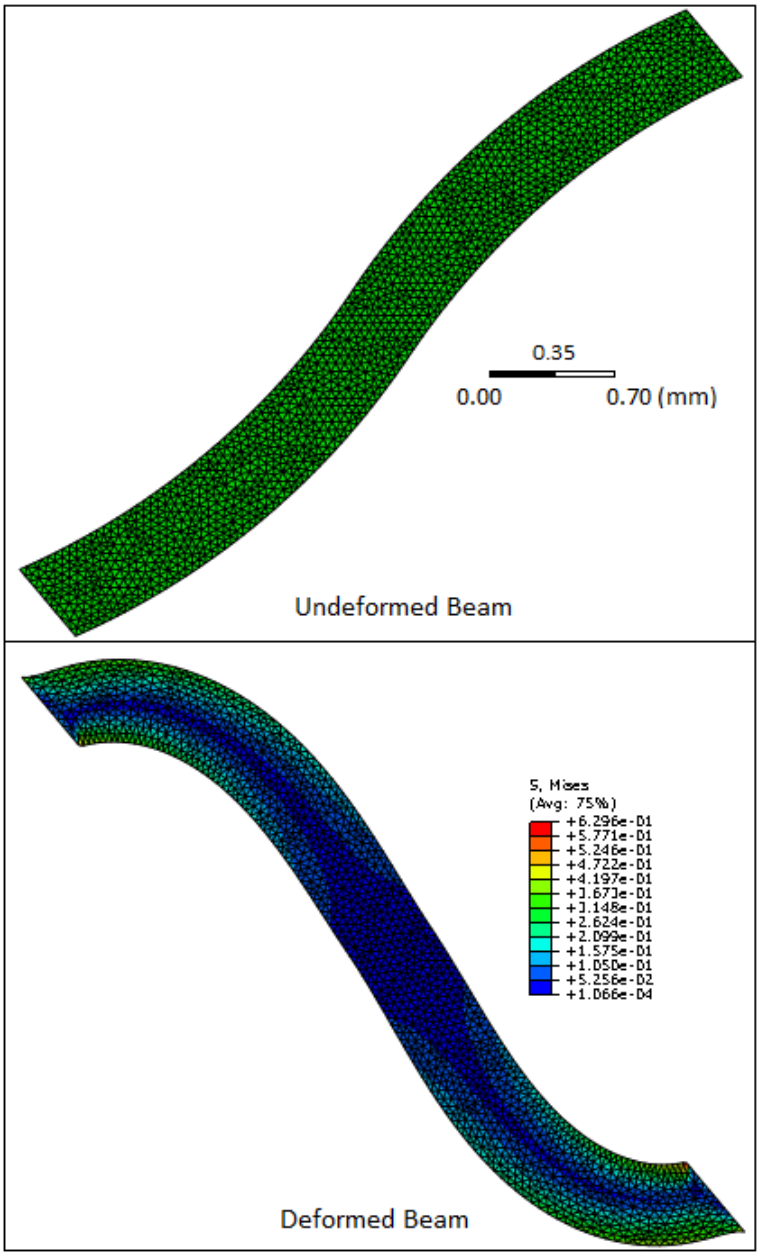

Figure E.2: Undeformed-deformed shape of the curved beam s-shape-r5 for 10% increase in length, 9% decrease in width

E.3 Images Taken from Analysis of the Curved Beam S-Shape-r5 with L5 % ↓, t5 % ↑

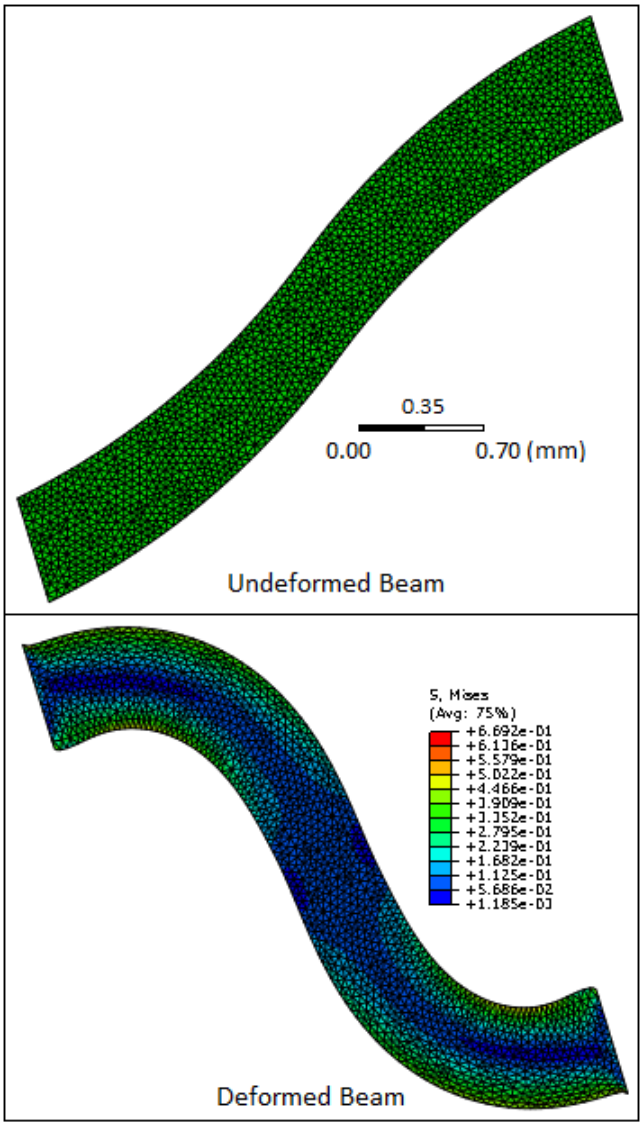

Figure E.3: Undeformed-deformed shape of the curved beam s-shape-r5 for 5% decrease in length, 5% increase in width

E.4 Images Taken from Analysis of the Curved Beam S-Shape-r5 with L10 % ↓, t11 % ↑

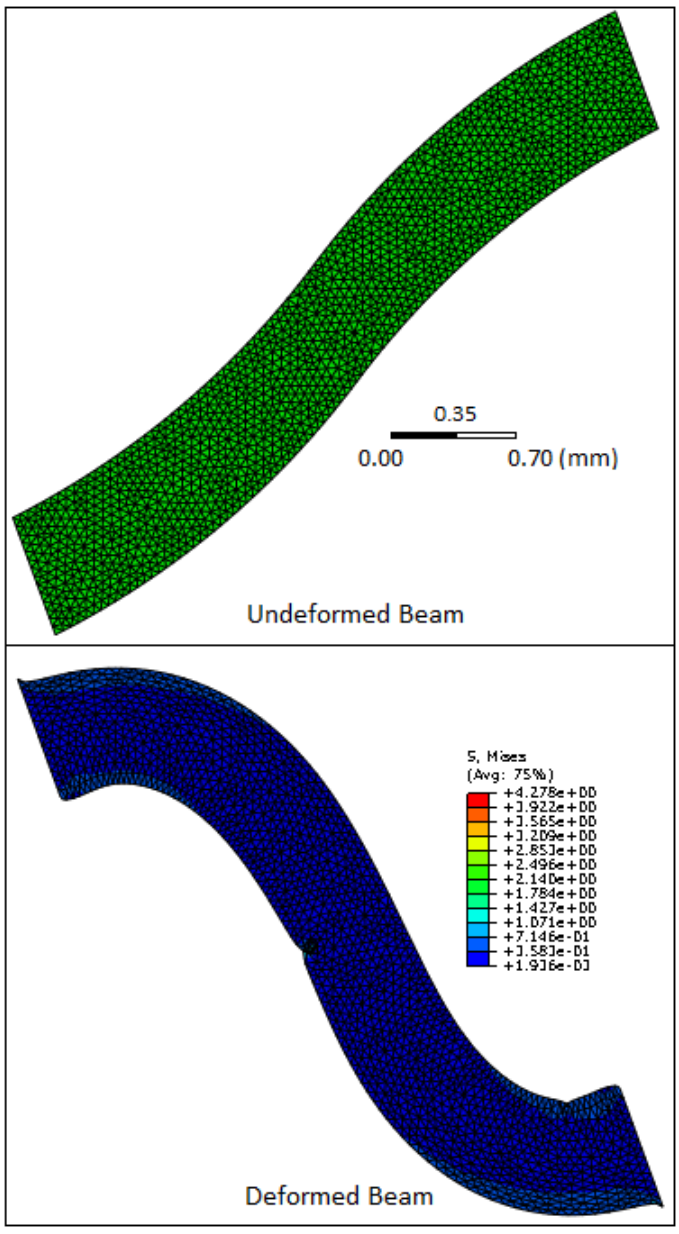

Figure E.4: Undeformed-deformed shape of the beam for 10% decrease in length, 11% increase in width

E.5 Images Taken from Analysis of the Curved Beam S-Shape-r5 with L10%↓, t11%↑ (Showing Self Contact Occurred During the Analysis)

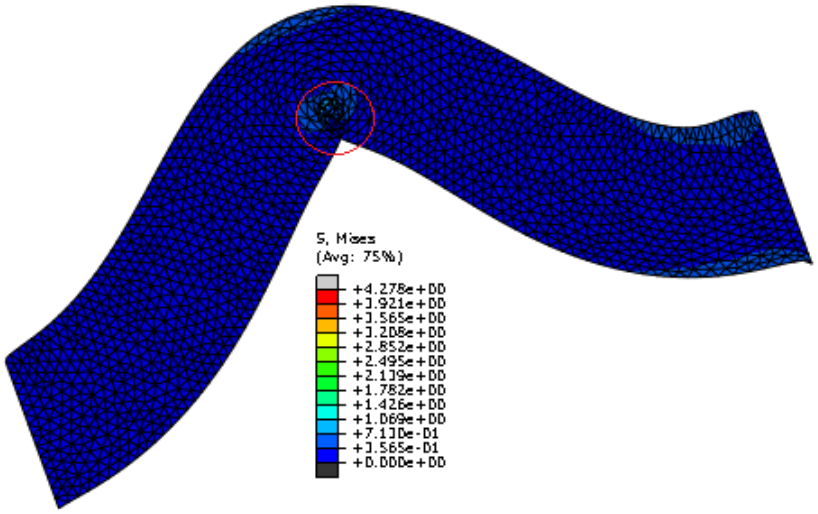

Figure E.5: Deformed shape of the curved beam s-shape-r5 with 10% decrease in length showing self contact occurred at about 1,8 mm vertical displacement of its upper end

APPENDIX F

DEFORMED AND UNDEFORMED SHAPES OF A STRAIGHT MODEL CONSISTING OF TWO BEAMS

F.1 Undeformed Shape Images Taken from Analysis of the Constructed Model Consisting of Two Reference Beams

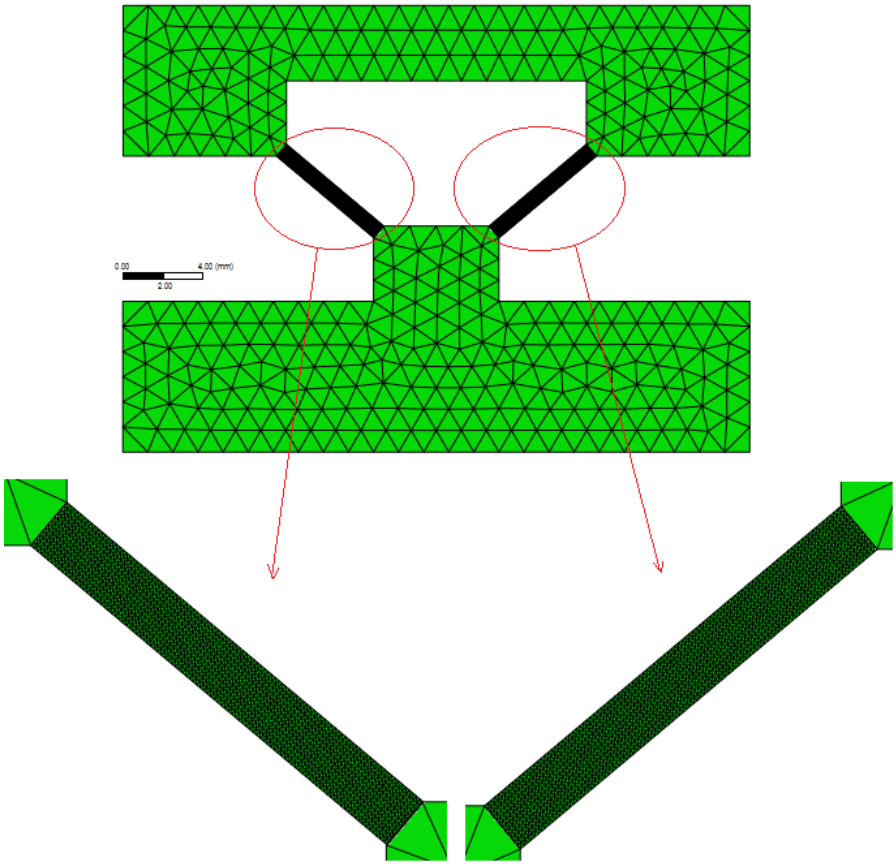

Figure F.1: Undeformed shapes of the constructed model consisting of two reference beams

F.2 Deformed Shape Images Taken from Analysis of the Constructed Model Consisting of Two Reference Beams

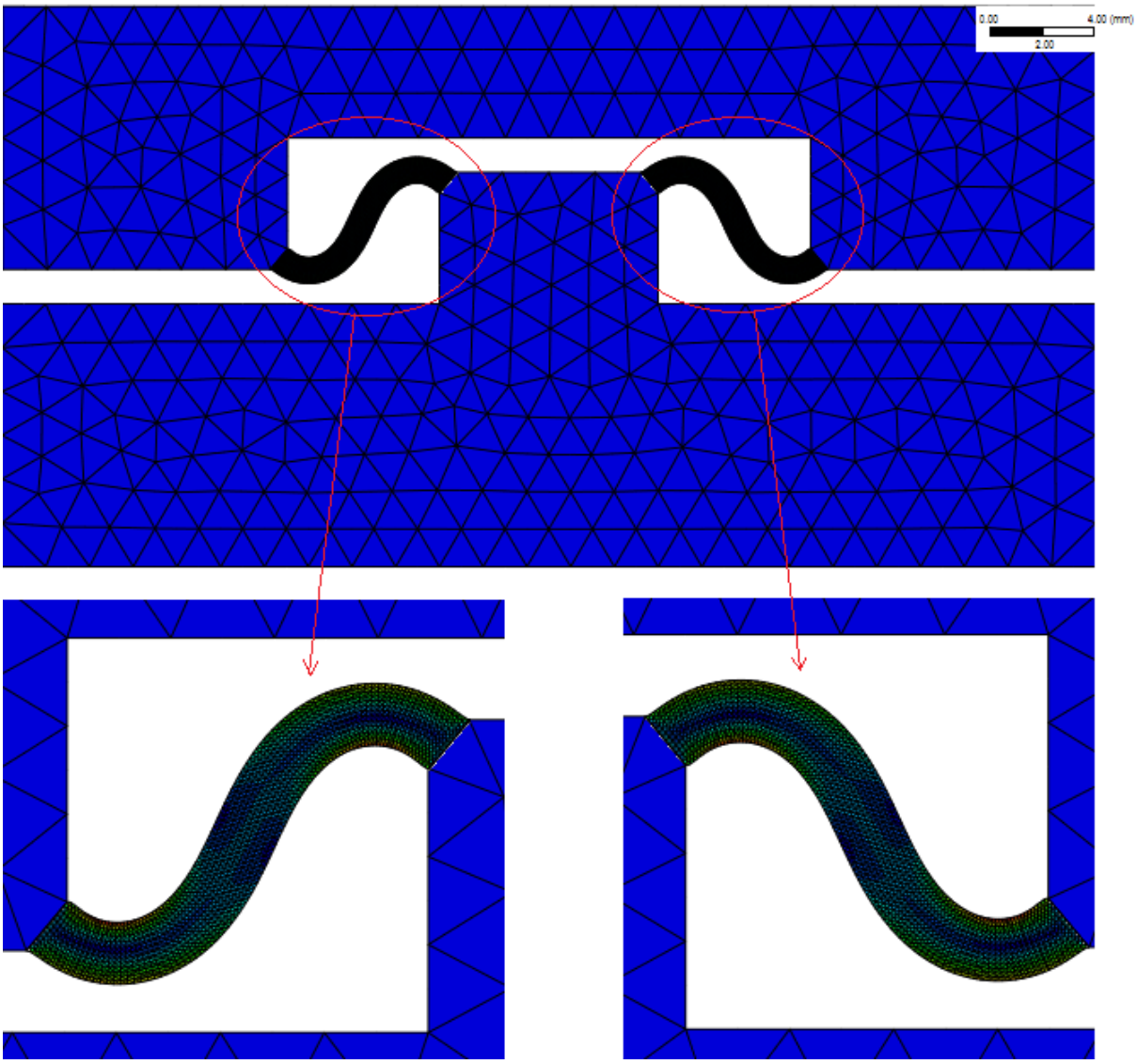

Figure F.2: Deformed shapes of the constructed model consisting of two reference beams